MULTI-ORGAN-ON-A-CHIP FOR CANCER DRUG TESTING

A Thesis Submitted to
The Graduate School of Engineering and Sciences of
İzmir Institute of Technology
in Partial Fulfillment of the Requirements for the Degree of

DOCTOR OF PHILOSOPHY

in Bioengineering

by
Abdurehman Eshete MOHAMMED

May 2022
İZMİR

ACKNOWLEDGMENT

I am grateful and happy to thank my esteemed advisor Prof. Devrim Pesen Okvur for accepting me into her lab, supervision, encouragement, help, and patience during my Ph.D. education. I want to thank my co-advisor, Prof.Dr. Esra Erdal Bağriyanik for her cell line support. I am thankful for Turkish government scholarship (YTB) for granting me a full scholarship to study here in Turkey.

I am delighted to thank my thesis committee members Assoc. Prof. Özden Yalçın Özuysal and Assit. Prof. Yavuz Oktay for their invaluable and constructive comments, suggestions, and guidance during my thesis progress.

I am glad to thank my friends and lab mates Eyüp Yöndem, Özge Nur Belli, Yağmur Ceren Unal, Hussein Getaneh, Fetiya Bahiru, Müge Bilgen, Ismail Tahmaz, Aslı Kısım, Begüm Gökçe, Ali Can, Ali Yetgin, Gizem Batı, Güncem Ocak, Deniz Cemre Turgut, Helin Giriş, Ceylan Demir, Dilan Sakinci, Mahmut Çetin and housemates for their help and support during my Ph.D. education.

My special thanks go to my mother, Zewudie Bushira; she was a strong and wonderful mother. If she were alive and saw this day, I would be delighted, but not. I am grateful to thank my brother Kassahun Eshete for his care, guidance, and encouragement throughout my education, starting from elementary school until now. You are the kindest and most special brother to me. I want to thank my sister Fatuma Eshete for her assistance and inspiration in my life. Lastly, I am happy to thank my queen Ekram Ahmed Mohammed for her unlimited love, support, and encouragement throughout my education.

ABSTRACT

MULTI-ORGAN-ON-A-CHIP FOR CANCER DRUG TESTING

Cancer is one of the devastating and fatal severe diseases worldwide that kills millions of people every year. Globally cancer is the second leading cause of death after cardiovascular disease and was responsible for 10 million deaths in 2020. Breast cancer is one of the predominant cancers in females and is the cause of more than half a million females death each year. The primary cause of cancer patients' death is cancer metastasis. Triple-negative BREAST cancer (TNBC) is mainly treated by chemotherapy.

In the current drug discovery and development processes, the efficacy and toxicity of chemotherapies identify using 2D and animal testing but not simulating the in vivo microenvironment. This research designed multiorgan-on-a-chip with liver and breast cell line compartments, and drug PKPD modeling was done by Monolix software. In this research, a unique multiorgan-on-a-chip (MOC) was designed and fabricated, generated experimental PK and PD data using the new MOC device, and modeled and simulated PK and PD using the experimental data.

To conclude, we developed a new multiorgan-on-a-chip (MOC) platform used for PKPD modeling and PKPD simulations that would be helpful in the preclinical research to evaluate the effectiveness and toxicity of drugs. In the future, using calceinAM, a fluorescent cell viability dye, generating PD data for each cell type and determining side effects of doxorubicin in each cell line is essential. Adding more organs to the MOC, such as heart tissue, to study the cytotoxicity of doxorubicin in different organs gives more efficient data for PKPD modeling.

ÖZET

KANSER İLAÇ TESTİ İÇİN ÇOKLU-YONGA-ÜZERİ-ORGAN

Kanser, dünya çapında her yıl milyonlarca insanı öldüren yıkıcı ve ölümcül ciddi hastalıklardan biridir. Küresel olarak kanser, kardiyovasküler hastalıklardan sonra ikinci önde gelen ölüm nedenidir ve 2020'de 10 milyon ölümden sorumludur. Meme kanseri, kadınlarda en sık görülen kanserlerden biridir ve her yıl yarım milyondan fazla kadının ölümüne neden olmaktadır. Kanser hastalarının ölümünün birincil nedeni kanser metastazı. Üçlü negatif MEME kanseri (TNBC) esas olarak kemoterapi ile tedavi edilir.

Mevcut ilaç keşif ve geliştirme süreçlerinde, kemoterapilerin etkinliği ve toksisitesi, 2D ve hayvan testleri kullanılarak belirlenir, ancak in vivo mikro ortamı simüle edilmez. Bu araştırma, karaciğer ve göğüs hücre hattı bölmeleri ile çip üzerinde multiorgan tasarladı ve ilaç PKPD modellemesi Monolix yazılımı tarafından yapıldı. Bu araştırmada, benzersiz bir çip üzerinde çoklu organ (MOC) tasarlandı ve üretildi, yeni MOC cihazı kullanılarak deneysel PK ve PD verileri oluşturuldu ve deneysel veriler kullanılarak PK ve PD modellendi ve simüle edildi.

Sonuç olarak, ilaçların etkinliğini ve toksisitesini değerlendirmek için klinik öncesi araştırmalarda yardımcı olacak PKPD modellemesi ve PKPD simülasyonları için kullanılan yeni bir çip üzerinde çoklu organ (MOC) platformu geliştirdik. Gelecekte, bir floresan hücre canlılığı boyası olan calceinAM'ın kullanılması, her hücre tipi için PD verilerinin üretilmesi ve her hücre hattında doksorubisinin yan etkilerinin belirlenmesi esastır. Doksorubisinin farklı organlarda sitotoksisitesini incelemek için kalp dokusu gibi MOK'ye daha fazla organ eklemek, PKPD modellemesi için daha verimli veriler sağlar.

TABLE OF CONTENTS

LIST OF FIGURES

Figure **Page**

Figure **Page**

LIST OF TABLES

Table **Page**

ACRONYMS AND ABBREVIATIONS

2D Two-dimensional

3D Three-dimensional

5-FU 5-Fluorouracil

AB Alamar blue

ABC ATP-binding cassette

AIC Akaike Information Criteria

APTES 3-Aminopropyl) triethoxysilane

BIC Bayesian Information Criteria

BICc Corrected Bayesian Information Criteria

CA Compartmental analysis

CO Cardiac output

DAPI 4′,6-diamidino-2-phenylindole

DMEM Dulbecco's Modified Eagle's medium

DNA Deoxyribonucleic acid

DOX Doxorubicin

ECM Extracellular matrix

EDTA Ethylenediaminetetraacetic acid

ER+ Estrogen positive

FDA U.S Food and Drug Administration

FRET Förster or fluorescence resonance energy transfer

HER2+ Human epidermal growth factor receptor two positive

HGF Hepatocyte growth factor

HMFs Human mammary fibroblasts

HPLC High-performance liquid chromatography

HPLC High-performance liquid chromatography

LOD Low limit of detection

LOQ Low limit of quantification

MOC Multiorgan-on-a-chip

NCA Non-compartmental analysis

NIH National Institute of health

OOC Organ-on-a-chip

PD Pharmacodynamics

PDX Patient-derived xenograft

PK Pharmacokinetics

PR+ Progesterone positive

RPM Revolution per minutes

RT Residence time

TNBC Triple-negative breast cancer

UV Ultraviolet

VPC Visual predictive check

CHAPTER 1

INTRODUCTION

1.1. Cancer

Cancer is a collection of diseases that can affect any part of the body. It arises from transforming normal cells into cancerous cells in a multistage process that generally progresses from a pre-cancerous lesion to a malignant tumor[1]. Causes of cancer are genetic changes, hereditary from parents, or starting during the individual's lifetime due to mistakes that appear during cell multiplication or damage to the deoxyribonucleic acid (DNA) caused by other factors.one of the characteristics of all types of cancer is uncontrolled proliferation and disseminating to secondary organs[2]. These changes result from the interaction between a patients genetic factors and the three types of carcinogens[1].

Cancer is a devastating disease caused by genetic variability and the buildup of numerous molecular variations[3]. Cancerous cells can grow without stopping to form tumors. The eight hallmarks of cancer that have a direct influence on cancer development and progression are sustaining proliferative signaling, evading growth suppressors, resisting cell death, enabling replicative immortality, inducing angiogenesis, activating invasion and metastasis, deregulating cellular energetics and metabolism, and avoiding immune destruction[4] (Figure 1.1).

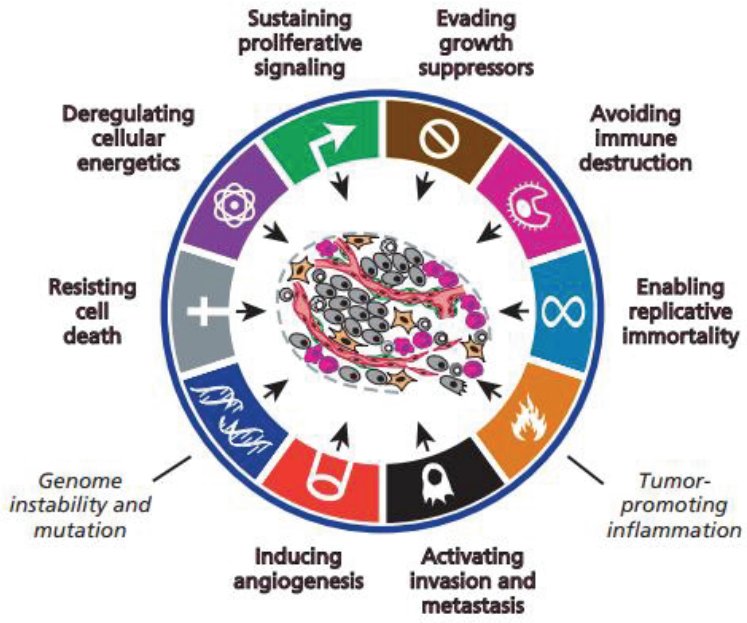

Figure 1. 1. The eight hallmarks of cancer [4]

A tumor is a large number of cancer cells in the body. It results from the uncontrolled proliferation of cells and unexpected longevity of cell life. The two kinds of tumors are benign and malignant. Benign tumors do not disseminate to secondary sites, either the regional site or distant body sites, and they remain in the primary site. In contrast, malignant tumors can invade other secondary sites of the body[5]. Malignant tumors can disseminate to nearby tissues or distant secondary organs through the blood circulation or the lymphatic system and create new cancer away from the primary cancer and termed metastases[2].

1.2. Cancer metastasis

Metastasis is the dissemination of the cancer cells secondary areas of the body either near the primary tumor (regional metastasis) or away from the leading tumor site (distant metastasis)[6]. The tumor microenvironment, such as extracellular matrix (ECM), growth factors, chemokines, and metalloproteinases, has a significant impact on tumor metastasis, and 90% of cancer mortality is due to metastasis[7].

The main steps in cancer metastasis are an invasion, intravasation into the blood circulation or lymphatic system, extravasation from the circulatory system or lymphatic system, and colonization of a new site. The same name calls the secondary tumors like the primary tumor, not by the name of the affected secondary organ[6]. Breast cancer can

spread to any part of the body. The main sites of the body where breast cancer metastasize are bone, regional lymph node, liver, and brain. The breast cancer metastasizes to the above organs, termed stage IV breast cancer[8] (Figure 1).

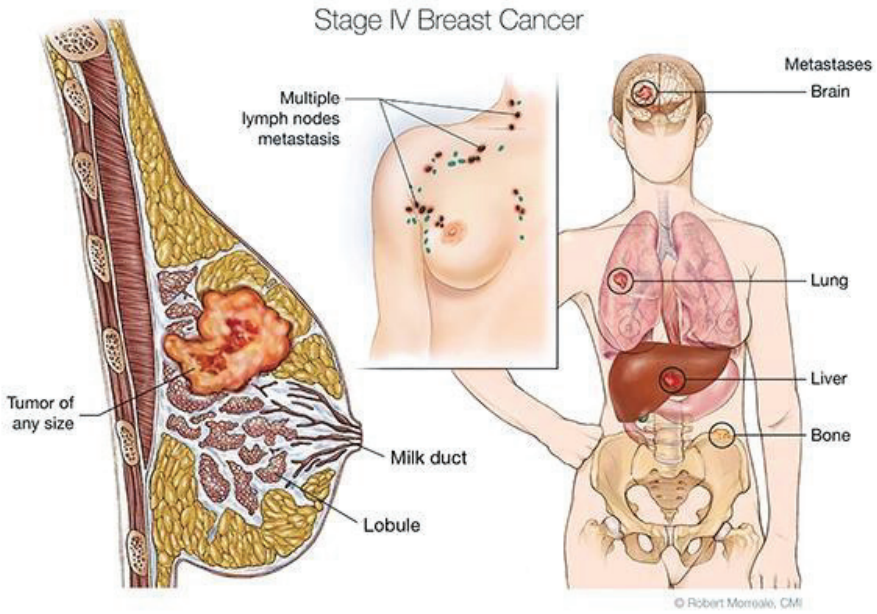

Figure 1. 2. Metastatic breast cancer [9]

1.3. Statement of the problem

Cancer is one of the most complicated and severe diseases that kill many people globally. It is the leading cause of morbidity and mortality in developed and developing countries. Cancer is the second leading cause of death worldwide after heart disease and was responsible for 10 million deaths in 2020. One in six deaths in the world is due to cancer. Despite cancer in both developed and developing countries, most cancer deaths occur in developing countries due to a lack of health facilities and treatment [1, 10-12].

The United Nations report showed that the current world number of humans is 7.7 billion, and this number will be increased to 8.6 billion (2030), 9.8 billion(2050), and 11.2 billion (2100)[13]. For the increment of cancer cases, the rapid growth of the world population may directly influence[14]. In 2020, there were 19.3 million confirmed new cases of cancer worldwide[10].

In 2020, breast cancer was the most dominant cancer case, followed by lung, colorectal, prostate, stomach, and liver cancer. In contrast, lung cancer was the leading cause of cancer deaths, followed by colon and rectum cancer[1].

The most frequent cancer among women is breast cancer, with 2.3 million new cases in 2020, and most cancer-related deaths of women worldwide are due to breast cancer[1].

In women's life span, 1 out of 12 women will be affected by breast cancer. Also, it is the primary reason for cancer-related death in women. In 2020, nearly six hundred eighty-five thousand women died because of breast cancer. The effect of cancer on morbidity and mortality is higher in emerging countries [15]. The laboratory and imaging techniques to diagnose breast cancer are improved, but the somatic cell genetic variation is another problem in cancer management[16]. Most of the world's cancer cases occur in emerging continents. Seventy percent of cancer is reported from emerging countries[17]. In Turkey, cancer is the leading cause of death after heart disease. Predominant cancer in male Turkish is lung cancer, but for female Turkish, breast cancer is the predominant[18].

Despite advanced knowledge in biological sciences and diagnosis instruments, cancer cases are increasing from time to time[19, 20]. Furthermore, cancer drug resistance is another problem that makes many chemotherapies useless[21]. Different treatment options are available to decrease the disease and death of cancer. From these, chemotherapy is the best option for triple-negative breast cancer (TNBC). MDA-MB-231 is a triple-negative breast cancer cell line with estrogen, progesterone, and E-cadherin negative and characterized by mutated p53 tumor suppressor protein. Additionally, MDA-MB-231 cells lack the growth factor receptor human epidermal growth factor receptor two positive **(**HER2)[22].

Different types of cancers affect the human being, and cancer classification relies on the type of cell and tissue that is primarily affected[3]. One of such cancer types is breast cancer. The classification of breast cancer cells based on receptor status is estrogen positive (ER+), Progesterone positive (PR+), HER2+, and triple-negative (HER2-, ER-, and PR-negative). Among these, triple-negative breast cancer has the poorest outcome. The best option to treat these types of breast cancer is chemotherapy[23]. The route to anti-cancer chemotherapy may be intravenously, directly into the bloodstream, or by mouth ingestion. After the drug administration, the drug uses the blood circulation to reach the targeted cancer cells in the body. In a few cases, chemotherapy may inject into the spinal fluid. The adjuvant and neoadjuvant chemotherapy of breast cancer drugs mainly used are doxorubicin, epirubicin, paclitaxel, docetaxel,5-fluorouracil, Cyclophosphamide, and Carboplatin[24].

Different types of treatment options are present to treat cancer. Some cancers are treated only by chemotherapy; one of the breast cancer types treated by chemotherapy is triple-negative breast cancer. The significant problem in chemotherapy drugs is drug[25]. For advanced cancer (metastasized), there is no hundred percent effective cancer treatment. The tumor genetic difference and patient variations are the leading causes of cancer drug resistance[26]. If cancer causes resistance to most conventional cancer drugs and increases drug resistance, it leads the scientific community to further research new anti-cancer drugs [27]. The techniques used for cancer drug testing in pre-clinical research are two-dimensional (2D) cell culture and animal testing.

Organs-on-chips are microfluidic cell culture systems with controlled, dynamic conditions that directly emulate the physicochemical microenvironment of tissues in the human body[28]. The central concept of multiorgan-on-a-chip (MOC) is to mimic the internal tissue environment, such as blood flow, three-dimensional architectures, cell-cell interaction, and concentration gradients[29].

Multiorgan-on-a-chip is one of the new techniques that may be useful for discovering and developing drugs. Despite this, the drugs discovered and developed by conventional drug testing show unexpected toxicity and drug efficacy problems, accounting for about 50% of the drug development failures. About 23% of the drug candidates failed at the final stage of drug development after much money was spent[30]. Moreover, the drug failure rate in clinical research is about 90%[31].

1.4. Animal model, 2D, 3D cell culture, and MOC

Animal models and human clinical trials are crucial parts of drug development. The models are expensive, and it needs much time to conduct the research, which may cause the drug discovery and development process costly. Furthermore, using animals for drug toxicity testing have ethical concern from local and international society[32]. Due to ethical concerns, Russell W et al. recommend using non-animal methods to overcome the suffering of animals in experiments[33].

The available therapy selection models are in vitro and patient-derived xenograft cancer models. Due to their complex internal environments, mice are mainly used for the efficacy testing of many therapeutic drugs. Contrary to their complex internal microenvironment, there are many limitations in using animals for drug testing and translating the result directly to humans. Some of the differences between animals and

humans are physiology, metabolism, tumor cell interaction with the natural immune system, proliferation, dissemination of cancer to other sites, and the nature of the cell themselves. In patient-derived xenograft cancer models, patient biopsies are engrafted in immune-compromised mice, and after the growth of the tumor, the drug will give to the mice, and the appropriate drug is selected for the patient. However, this procedure is complex and needs much time, and the data that is generated in this method is not appropriate for clinical decision-making [34].

Testing drug effects in vitro by cell culture techniques started more than a hundred years ago. Despite the long age, the in vitro culturing technique still does not simulate most of the internal biological systems of the living things. The cell culture technique's architecture, blood flow, and signaling pathways are not recapitulating with the in vivo microenvironment [35].

Using patient-derived biopsies in the two-dimensional cell culture technique gives faster results than the animal model in predicting drug response. However, the result gained in this method has its limitations, such as a rapid selection of proliferating cells than inactive cells, surface-attached and uncontrolled differentiation of cancer cells[36].

The three-dimensional cell culture technique uses extracellular matrix (ECM) to simulate the internal architecture and is the advanced way of the 2D cell culturing technique. The 3D cell culture technique is better than the 2D cell culturing technique in many aspects by simulating the internal microenvironment. The ECM has many components, and it influences cell polarity, metabolism, and migration of cells. The advantage of the 3D cell culture technique is the formation of a cluster of cells, lumen formation, reduced proliferation, and differentiation than the 2D cell culture technique. In the 2D cell culture technique, the normal and malignant breast epithelial cells sometimes show the same morphology and doubling times. However, in 3D cell culture techniques, the normal and malignant cells show different morphology of the breast epithelial cells[37, 38].

Malignant tumor cells cultured in the 3D cell culture technique embedded in ECM form disorganized and proliferative spheroids, and the breast cancer biopsies give a 3D spheroid that produces milk-secreting channels. Sung et al. researched human mammary fibroblast cells cultured in 2D and 3D culturing techniques to investigate the effects of invasive phenotype transition of breast cancer cells. The fibroblasts culture in 3D showed a more invasive phenotype of the breast cancer cells than the fibroblasts cultured in the 2D culturing technique[34].

The other advantage of culturing human mammary fibroblasts in 3D is the production of signaling molecules. The signaling molecule produced in 3D induces the progression of non-invasive breast cancer cells to an invasive phenotype. The above function of the 3D cell culture technique suggests that 3D culturing with ECM is better than 2D and somewhat simulates the internal microenvironments [34].

The tumors' invasiveness and detailed cancer biology are characterized by tumor samples cultured in vitro either in 2D or 3D culturing techniques. The gold standard in vitro culturing of cells is the two-dimensional culturing technique. The two-dimensional cell culture technique is used in many cellular assays to investigate the metastatic property and cytotoxicity. Despite this, the 2D culturing technique cannot simulate the 3D architecture of the internal microenvironment, the property of ECM (biophysical and biochemical), and the cell-to-cell interaction of human tumors. In addition, cellular signaling, cell cycle, and drug response are different in cells cultured in 2D and 3D cell culture techniques[39].

The conventional way of evaluating a new drug in the pre-clinical stage of the drug development stage is performed in two-dimensional cell culture technique and animal testing. The drug is applied to the cell culture in the two-dimensional cell culture models, and the drug's toxicity is evaluated. However, it does not mimic the internal microenvironment of the body. In vivo, after administration, the drug undergoes “absorption, distribution, metabolism, and excretion (ADME)” processes in a time-dependent manner. However, in two-dimensional cell culture, the above processes are not present. Due to this, the interaction of organs in the body may cause unpredicted toxicity and lack of efficacy[40, 41].

The advantage of cultivating cells in 3D cell culture is using small samples and reagents and constructing in vivo like physiologically relevant in vitro microenvironment[42]. Three-dimensional cell cultures are better than two-dimensional cell cultures in many aspects. However, testing the drug in single 3D cell culture does not give results like the in vivo microenvironment. In a single organ-on-a-chip, there is no multiorgan interaction and paracrine signaling. The major shortcoming of the experiments in the conventional multiwell plate and a single 3D cell culture is the lack of multiorgan interactions.

Multiorgan-on-a-chip mimics the dynamic in vivo microenvironment by empowering cell-to-cell communications in microfluidic co-culture devices to better understand the diverse dynamics in cellular interactions. Different cells can be cultured

in a separate chamber and connected with channels that mimic blood flow. Also, there might be paracrine communication among the cultured cells[42, 43]. Furthermore, the multiorgan-on-a-chip can be used to model the body reaction to the drug and the reaction of the drug to the body, understand different biological responses, better mimic the complex internal micro-climate, and identify unwanted adverse drug reactions[44].

1.5. Drug discovery and development processes

The drug development processes are "discovery and development, pre-clinical research, clinical research (phase I-III), U.S Food and Drug Administration (FDA) review, and FDA post-market safety monitoring" (Figure 1.3). After discovering and developing the new drug, preclinical research is conducted before human binges. During the pre-clinical stage, information about dosing and toxicity is gathered and evaluated. Based on the pre-clinical research result, the investigators decide whether to continue the phase one clinical trial on humans or not. Currently, pre-clinical research is done in vitro and in animals [45].

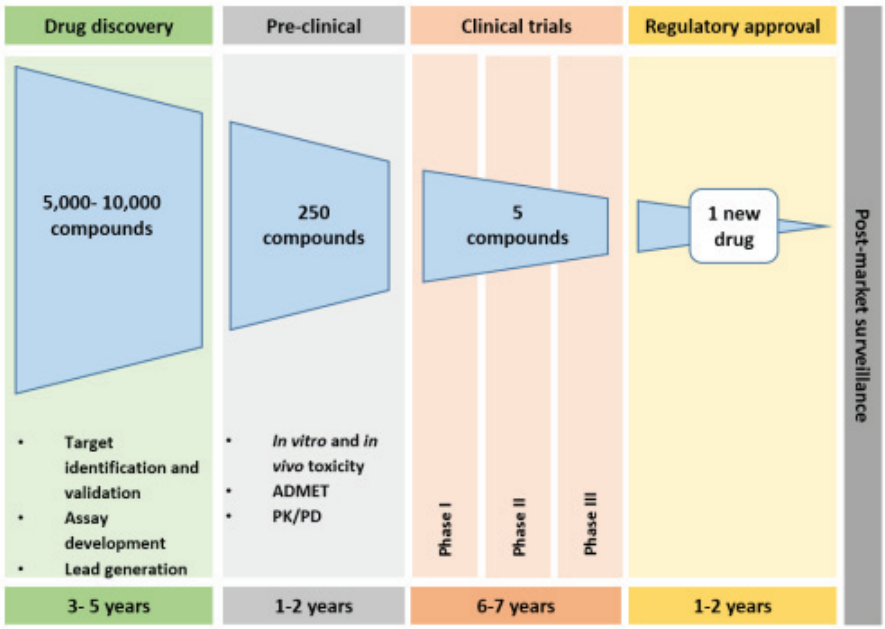

Figure 1. 3. Drug discovery and development timeline[46]

Drug development is challenging in terms of cost and time, and roughly only one in ten drugs entering clinical trials finally becomes approved as a drug[47]. The leading cause for the low achievement to get a new drug in clinical trials is the lack of efficacy,

which is not recognized until the final stage of the clinical trial after most of the drug development costs are spent[48]. The side effects of the drug cause approximately 5% of hospital admission. The cost of having a new cancer drug needs $648 million, and it takes lots of years of experiments in both in vivo and in vitro environments. From 1980 to 2009, 15% of drugs that show efficacy in phase two clinical trials create unexpected side effects in different vital organs[49, 50].

Predicting the drug's toxicity in the pre-clinical stage may save most resources. A little success of the drug candidates in animal and human clinical trials shows the current drug toxicity testing methods have to improve [51].

Drug discovery is a multi-stage process that needs the interaction of different scholars, and it takes a lot of time and money. Due to high cost and time, the pharmaceutical industries face challenges in the drug discovery and development process[52].

From 1969 to 2002, the FDA recorded 2.3 million drugs effects from 6000 registered compounds. Seventy-five drugs were removed from the market due to lack of efficacy, and a further eleven were given special attention[51]. A large amount of drug that gives good result in pre-clinical research might show a lack of efficacy or toxicity when given to human beings. The low success rate of compounds at the final stage of clinical trials affects the development of new drugs[51].

1.6. Pharmacokinetics and pharmacodynamics

Pharmacokinetics **(**PK**)** is the analysis of "absorption, distribution, metabolism, and excretion (ADME)" of the drug by different organs in vivo, and pharmacodynamics **(**PD**)** is the analysis of the effects, either the therapeutic effect or adverse drug reaction of the drug to the body after administration. Modeling of PKPD was used to evaluate the relationship of dose-concentration- response. The drug's pharmacological effect and the drug's time-dependent concentration were investigated, and modeling of pharmacokinetics and pharmacodynamics was made [53, 54].

The PK and PD of drugs can be evaluated by mathematical equations[54, 55]. "Pharmacokinetics (PK) refers to the concentration profiles of a drug in the body after administration, whereas pharmacodynamics (PD) refers to the pharmacological effect". In physiological-based pharmacokinetic modeling, different organs are cultured in a

separate compartment, the compartments are connected each other by using media to create multiorgan interactions[54].

1.7. Doxorubicin

Doxorubicin (Figure 1.4) is antibiotic chemotherapy classified under the drug class of anthracycline, which has a wide range of anticancer activity and is extracted from Streptomyces peucetius var. caesius bacterium[56]. The drug is administered intravenously. In humans, fifty percent of doxorubicin is excreted unchanged in stool via biliary excretion. In vivo, doxorubicinol is the primary metabolite, and it may cause cardiac toxicity depending on the amount of dose. The effectiveness of doxorubicinol is under doxorubicin, but it can affect the cardiac muscle calcium pump[57, 58].

1.7.1. Doxorubicin mechanism of action

After doxorubicin enters the cytoplasm of the cancer cell reacts with a few enzymes such as Xanthine oxidase (XDH), Nitric oxide synthase 3 (NOS3), and NAD(P)H dehydrogenase (NQ01)", producing doxorubicin semiquinone. When the doxorubicin semiquinone is reduced back to doxorubicin produces reactive oxygen species (ROS). The ROS causes oxidative stress to the cancer cell and provokes cell death. Moreover, ROS damages the DNA of the cancer cell. The entrance of doxorubicin to the cell's nucleus from the cell cytoplasm is via the help of proteasomes and intercalates with the base pairs of the double helix DNA and causing disruption of DNA replication and affecting the function of the Topoisomerase II enzyme. The two-electron reduction of doxorubicin with Carbonyl reductases and Aldo-keto reductases produces the cardiotoxic doxorubicinol (Figure 1.5)[59].

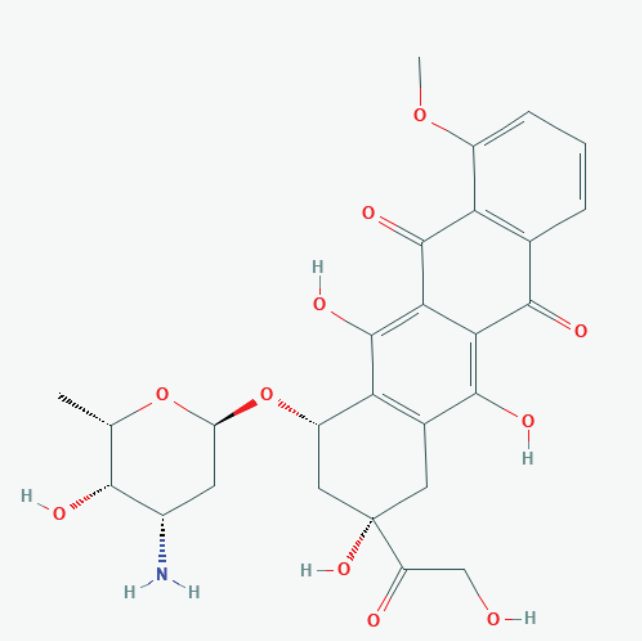

Figure 1. 4. Chemical structure of Doxorubicin [56]

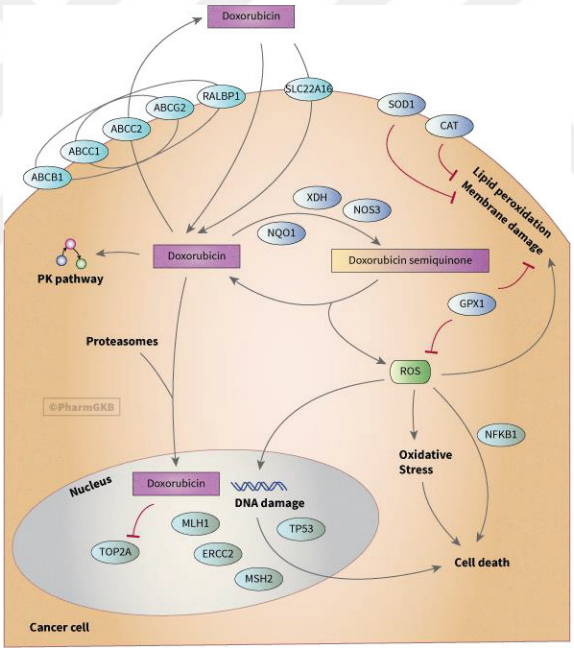

Figure 1. 5. Doxorubicin pathway, pharmacodynamics[59]

1.7.2. Doxorubicin pathway, pharmacokinetics

Doxorubicin follows three main mechanisms for metabolism. The three mechanisms are two-electron reduction, one-electron reduction, and deglycosidation. Around fifty percent of doxorubicin is excreted from the body unchanged; the rest follows the above three mechanisms. The two-electron reduction mechanism produces the major doxorubicin metabolite doxorubicinol. The enzymes that participate in two-electron

reduction pathways are “carbonyl reductase 1 (CBR1), carbonyl reductase 3 (CBR3), Aldo keto-reductase 1A1 (AKR1A1), and Aldo-keto reductase 1C3 (AKR1C3)[59]” (Figure 3). Doxorubicinol has low efficacy than doxorubicin; instead, it creates cardiotoxicity[60].

One-electron reduction doxorubicin metabolism mechanism creates DOX semiquinone. The enzymes involved in this mechanism are “xanthine oxide (XDH), Nitric oxide synthase 1-3 (NOS 1-3) NADPH dehydrogenase (NQO1) NADH dehydrogenase”. DOX semiquinone is an unstable metabolite and re-oxidized back to doxorubicin and produces reactive oxygen species (ROS). The transporters that participated in doxorubicin metabolism are Solute carrier family 22 members 16 (SLC22A16 importer) and ATP-Binding Cassette Sub-Family B Member 1 (ABCB1), ATP Binding Cassette Subfamily C Member 1 (ABCC1), ATP Binding Cassette Subfamily C Member 2 (ABCC2), ATP Binding Cassette Subfamily G Member 2 (ABCG2) and RalA Binding Protein 1 (RALBP1 exporter)[59] (Figure 1.6). The ABC transporters transport doxorubicin from the cancer cell and involve cancer drug resistance mechanisms[61].

The third doxorubicin metabolism mechanism is Deglycosidation; only 1-2% of doxorubicin is metabolized in this method. There is a reduction in the production of Deoxyaglycone metabolite and hydrolysis to produce hydroxyaglycone metabolites. The two metabolites, deoxyaglycone and hydroxyaglycone produced by reduction and hydrolysis processes, respectively[59] (Figure 1.6).

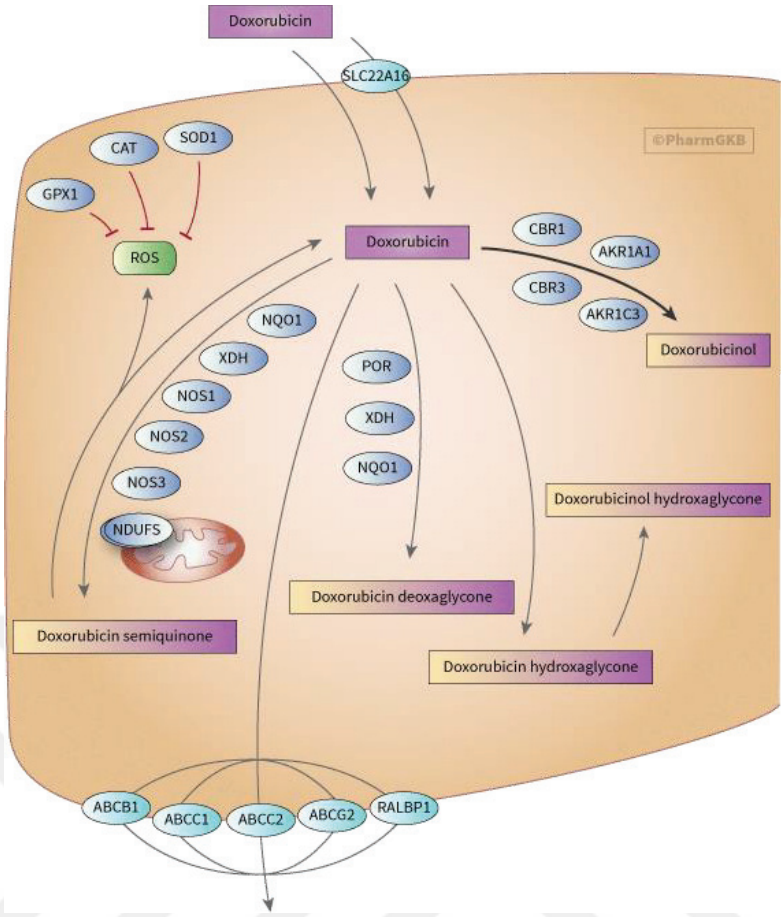

Figure 1. 6. Doxorubicin pathway, pharmacokinetics[62]

1.8. Determining PKPD model from the literature

Few scholars researched multiorgan devices such as gut-liver[63], liver-fat-blood vessel[64], liver-tumor-bone marrow[52], lung-liver-fat tissues[65], and liver-skin[66] and some of them prepared the PKPD model. Moreover, few researchers prepared PKPD model for different drugs and metabolites. Lee et al. prepared the PKPD model of Luteolin in MOC containing two compartments of the liver (HepG2) and tumor (HeLa) cells. Both Luteolin and its metabolite Diosmetin have anti-cancer activity[29]. The equations for PKPD modeling are as follows:

PK model

Luteolin in Liver

$$V_L.\frac{dCLT,L}{dt}=Q_L*C_{LT,\,B}-Q_L*C_{LT,\,L}-\frac{Vm,LT*CLT,L}{Km,LT+CLT,L}*V_L$$

Luteolin in Tumor

$V_L.\frac{dCLT,L}{dt}=Q_T*C_{LT,\,B}-Q_T*C_{LT,\,T}$

Luteolin in Blood

$V_B.\frac{dCLT,B}{dt}=Q_L*C_{LT,\,L}+Q_T*C_{LT,\,T}-Q_L*C_{LT,\,B}-Q_T*C_{LT,\,B}$

Diosmetin in Liver

$V_L.\frac{dCDM,L}{dt}=Q_L*C_{DM,\,B}-Q_L*C_{DM,\,L}-\frac{Vm,DM*CDM,L}{Km,DM+CDM,L}*V_L$

Diosmetin in Tumor

$V_L.\frac{dCDM,L}{dt}=Q_T*C_{DM,\,B}-Q_T*C_{DM,\,T}$

PK parameters

A. The volume of organ i (Vi)
B. A flow rate of organ i (Qi)
C. Concentration of drug in organ i (C drug i)
D. The maximum rate of drug in organ i (Vmax i)
E. Michaels-Menten kinetic constant for drug in organ i (Km i)

PD model

$\frac{dCS}{dt}=K_g*C_S\,(1-\frac{CS}{CSS})-K_{sr}*C_S+K_{rs}C_R-K_{LT}*C_S-K_{LTG}*C_S$

$\frac{dCR}{dt}=K_{sr}*C_S-K_{rs}*C_R-K_d*C_R$

$K_{LT}=\frac{KmaxLT*LT}{EC50LT+LT}$

$K_{LTG}=\frac{KmaxLTG*LTG}{EC50LTG+LTG}$

PD parameters

A. Number of cells **(**C)

B. Number of sensitive cells (CS)

C. Number of resistance cells (CR)

D. Maximum cell number that can be reached (CSS)

E. Cell growth rate (Kg)

F. Cell death rate (Kd)

G. Maximum cells kill rate (Kmax)

H. Saturation constant (EC50 of drug**)**

I. Concentration of drug

J. Rate of a change cell population from sensitive to resistant group (Ksr) and

K. Rate of change of cell population from resistant to sensitive group (Krs)

A second study conducted by Sung JH et al. prepared a PKPD model for 5-fluorouracil (5-FU). Uracil is combined with 5-FU to increase the pharmacological activity of the primary drug. This study used three separate compartments that have liver, tumor, and marrow cells. The cell culture chamber and the channel layers are separately placed. The channel layer is placed above the cell culture. Moreover, they used a sub-compartment of a chip for each cell, and the evaluation of the PKPD model follows the sub-compartmental equations as follows(Sung, Kam, and Shuler, 2010).

Equations for PD modeling

$$\frac{dC1}{dt} = Ks*C1\left(1-\frac{C1}{CSS}\right)-C4*C1-Kd*C1$$

$$\frac{dC2}{dt} = \frac{\frac{Kmax*FU}{KC50+FU}-C2}{tau}$$

$$\frac{dC3}{dt} = \frac{C2-C3}{tau}$$

$$\frac{dC4}{dt} = \frac{C3-C4}{tau}$$

The third study that models the PKPD of chemotherapy was done by Sung et al. They used 5-FU to describe the cancer cell growth effect. The cell-cycle specific model equation developed by these researchers is presented [40].

PD model

$$\frac{dCs}{dt} = Kg*Cs\ (1-Cs/Css) - Ksr*Cs + Krs\ CR - KC_S$$

$$\frac{dCR}{dt} = Ksr*Cs*Krs*CR - kd*CR$$

$$K_{5\text{-}FU} = Kmax,_{5\text{-}FU} *_{5\text{-}FU} / EC50,_{5\text{-}FU} +_{5\text{-}FU}$$

1.9. Long term goal

To develop a multiorgan-on-a-chip that can be used in the drug discovery and development process at the preclinical stage.

1.9.1. Specific aims

A. To determine the models for doxorubicin's pharmacokinetic (PK) and pharmacodynamics (PD) for breast cancer cells (MDA-MB-231), normal human mammary epithelial cells (MCF-10A), and liver cells (HePG2).
B. To realize PDMS based MOC according to the determined PKPD model
C. To assess the PD and PK in MOC.
D. To simulate the selected PKPD model.
E. To compare different dosing regimens.

CHAPTER 2

MATERIAL AND METHODS

2.1. Multiorgan-on-a-chip design and fabrication

The liver and breast chips were designed with a scale-down factor of 1:50000[63]. The single organ-on-a-chip and MOC chips were designed by the AutoCAD 2020 software student version, and the molds of the organ-on-a-chip and MOC were printed by Formlabs Form 2 3D printer.

2.1.1. Physiological parameters for chip design

The physiologic parameters that are used for chip design are the cardiac output of the human liver 25%, which is a multiplication result of heart rate and stroke volume and expressed as percentages [67, 68], and the volumetric blood flow of human (Female) 4.7 liter/minute[69], which is the amount of blood that is pushed by the heart per minute, the residence time of blood in human for each organ, which is the amount of time the blood stays in the organ, the residence time of blood in the chip, the volumetric blood flow of chip which is scaled down from human volumetric flow based on a scaling factor of 1:50,000 such that 4.7 L/minute divided by 50000 gave us 9.4 $*10^{-5}$L/minute)[70]. When the scaling factor is less than 50000, the volume of chips will increase, and it needs more reagents and chemicals. However, when the scaling factor is increased from 50000, the volume of chips will decrease, and fewer reagents and chemicals are needed for experiments. We think that the 50000 scale factor gives a reasonable scale, and we use the 50000 scaling factors in our experiments.

The blood flow of single liver and breast chips was obtained by dividing the blood volume of organs by the residence time of organs. The residence time of blood in the liver and breast was 1.08 and 2.68 minutes, respectively[71].

2.1.2. Liver chip parameter calculations and design

The volume of liver chips in MOC was calculated by dividing the female liver volume, which is 1398 ml[72], by the scale factor 50000, and it gave us 28 µl of liver chip volume. The blood volume of the liver chip was calculated as follows.

Blood volume of liver chip=Blood volumetric flow of chip* Cardiac output of chip* Residence time of chip

$= 9.4*10^{-5}$ L/min*0.25 *1.083 minutes

$=25.45*10^{-6}$ L

=25.5 µL

=26 µL

Blood flow for liver chip=$\frac{25.5uL}{1.083\ mimutes}$=23.5 ul/min = 24 µl/minute

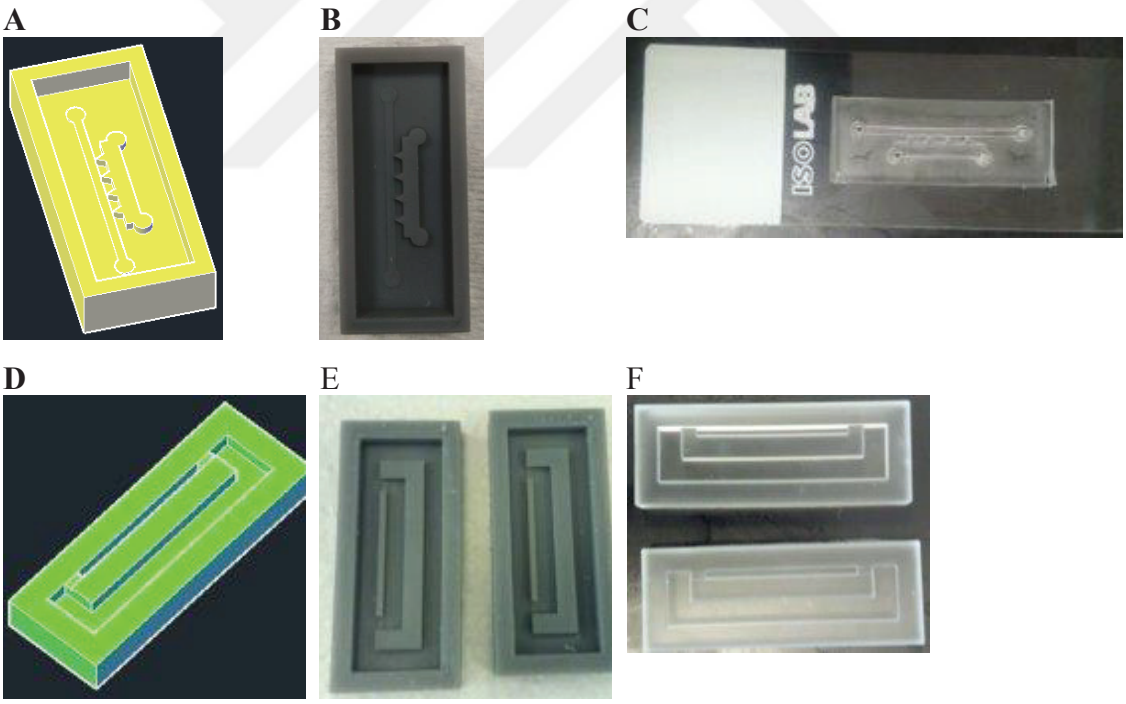

Figure 2. 1. Liver organ-on-a-chip design and fabrication.

(A) AutoCAD design of liver organ-on-a-chip (B) 3D printed mold of liver organ-on-a-chip. (C) Microscopic slide bonded liver organ-on-a-chip. (D) AutoCAD design of open-top liver organ-on-a-chip. (E) 3D printed mold of open-top liver organ-on-a-chip. (F) Open top liver organ-on-a-chip.

2.1.3. Breast chip parameter calculations and design

The mean breast volume of the left and right breasts are 642 and 643mL, respectively[73]. The sum of the breast volume is 1285mL (1285g). The blood flow of breast cancer and normal breasts is 0.32 mL/min/g and 0.06 mL/min/g [74]. If the tumor and some surrounding tissues are removed (lumpectomy) by surgery, the average tumor-to-breast ratio is 6%. Nevertheless, in removing all the breasts by surgery (mastectomy), the average tumor-to-breast ratio is 30%[75].

A single breast chip volume was calculated by dividing the female breast volume(643ml)[73] by the scale factor 50000, which gave us 13 µl of single breast chip volume. The blood flow of a single normal breast was calculated by multiplying the blood flow (mL/minute/g) with the single breast volume.

Total normal breast blood flow=0.06mL/minute/g*643g (single breast)

=38.58mL/minute

Cardiac output of normal breast= Total normal breast blood flow/Total cardiac output

=38.58mL/min/4700 mL/minute

=0.82%

Total breast cancer blood flow = Blood flow (mL/minute/g) * the single breast volume

Total breast cancer blood flow = 0.32 ml/min/g * 643 g

=205.76 ml/min

Cardiac output of breast cancer = Total breast cancer blood flow/ Total cardiac output

=205.76 ml/min / 4700 ml/min

=4.37%

The blood volume of breast cancer chip (MDA-MB-231) =Blood volumetric flow of chip* Cardiac output of chip* Residence time of chip

= $9.4*10^{-5}$ L/min*0.043778*0.5 minute

=2.057 µL

Blood flow for breast cancer chip= Breast cancer chip blood volume/Residence time

=2.057 µL/0.5 min

=4.11 uL/min

The blood volume of the normal breast (MCF-10A) = Blood volumetric flow of chip* Cardiac output of chip* Residence time of chip

=$9.4*10^{-5}$ L/min*0.0082*2.683 minute

=2.07 uL

Blood flow for normal breast chip= Normal breast chip blood volume/Residence time

=2.07 uL/2.683 minutes

=0.77 uL/min

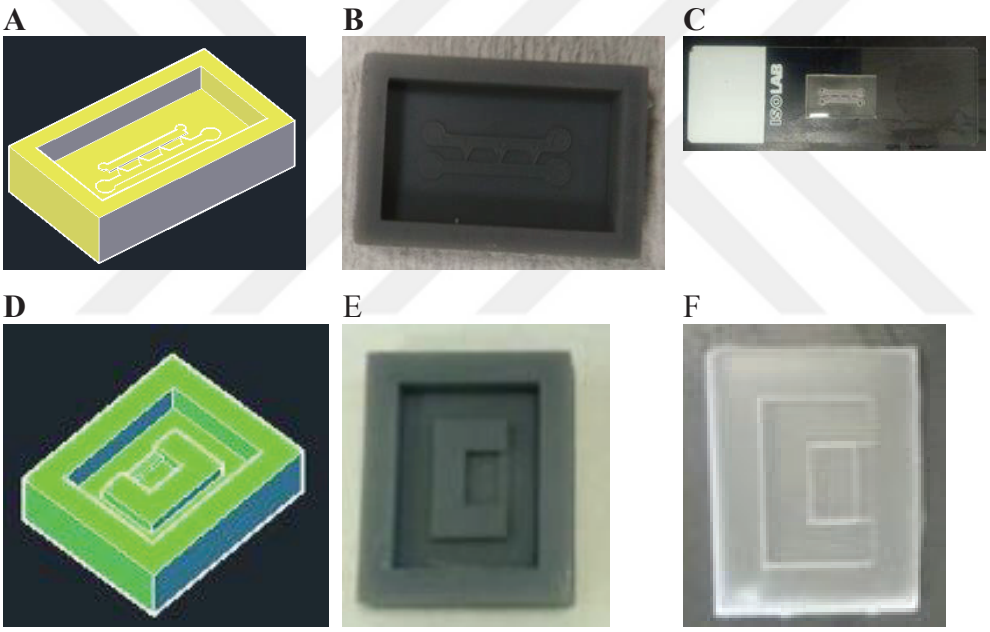

Figure 2. 2. Breast organ-on-a-chip design and fabrication

(A) AutoCAD design of breast organ-on-a-chip (B) 3D printed mold of breast organ-on-a-chip. (C) Microscopic slide bonded breast organ-on-a-chip. (D) AutoCAD design of open-top breast organ-on-a-chip. (E) 3D printed mold of open-top breast organ-on-a-chip. (F) Open top breast organ-on-a-chip.

2.1.4. Multiorgan-on-a-chip design and fabrication

In the MOC, the liver and breast were designed side by side to allow the diffusion of chemicals and molecules to realize organ communications. The dimension of the liver compartment of the MOC is 0.4mm (height), 6.99mm (width) and 10mm (length) and the dimension of breast compartment in the MOC is 0.4 mm (height), 3.2125mm (width) and 10mm (length). We keep equal height for both liver and breast compartment to have the same matrix thickness, convenient for confocal microscopy. The MOC is open-top and does not need bonding to a microscopic slide.

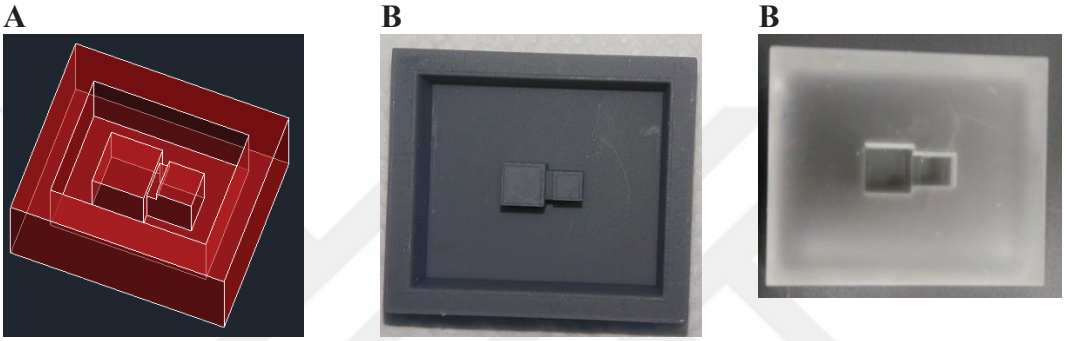

Figure 2. 3. Multiorgan-on-a-chip design and fabrication

(A) AutoCAD design of Multiorgan-on-a-chip (B) 3D printed mold of Multiorgan-on-a-chip. (C) Multiorgan-on-a-chip PDMS

2.1.5. Mold processing after 3D print

After printing of molds by 3D printer, the molds are removed from the printer's platform and processed in Isopropyl alcohol (IPA). The molds are put in an IPA container, pattern face up in new isopropyl alcohol, and the isopropyl alcohol container shakes for 2 minutes to remove the remaining resin from the molds. After shaking for 2 minutes, the molds transfer to the second Isopropyl alcohol container, and the molds are put inside face down without touching the pattern of the mold, put magnetic stirrer and stir for five minutes, agitate the molds during the five-minute string time to facilitate the removing of resin from the molds. After the first washing is finished, a five-minute wash with string is continued with isopropyl alcohol in a new container. During magnetic stirring, move up and down the mold container to facilitate the cleaning of resin. Also, avoid touching molds each other during stirring. Remove the molds from the second stirring and rinse

the molds with isopropyl alcohol to remove the remaining resin from the molds. After rinsing, place the molds face down on filter paper for a few minutes and put the molds vertically on the filter paper, and place them in the laminar hood overnight to dry the molds. After the overnight laminar hood exposure, the molds are put in Form Cure for 30 minutes to make permanent bonds. For larger molds, 60-70 minutes of UV exposure are recommended. The IPA that is used in the first shaking procedure was removed as dirty. A total of 15 minutes is enough for mold IPA processing. Moreover, cleaning the jar with tissue paper is mandatory before adding the new IPA. After UV curing, the molds are ready for mold washing and PDMS casting.

2.1.6. Mold washing and demolding

The molds are put in a glass jar and sonicate with up water for 5 minutes (sonicator at 50%), followed by up-water washing. Then, the molds were sonicated with 70% ethanol for 2 minutes; the 70% ethanol-filled jar containing the molds was put on the bench for 2 minutes and washed with up-water. After washing is finished, the demolding solution is poured into a glass jar, and the inner part (pattern) of the molds is put face down into the demolding solution for a few seconds and removed from the demolding solution and dry the back of the molds with tissue paper. After the back of the molds were cleaned with tissue paper, the molds were put in the laminar hood for 20 minutes to facilitate drying the molds. Finally, the molds are transferred into an incubator (37 ^{O}C) for an hour for complete drying of molds, and PDMS casting follows.

2.1.7. PDMS casting

The polydimethylsiloxane (PDMS) prepared a 10:1 ratio of elastomer and curing agent. The PDMS solution was mixed well with a spoon until the mixture produced white foam in all solutions. The mixed PDMS solution was kept in a desiccator, and a vacuum was applied to remove the air bubbles from the solution. After removal of air bubbles, the PDMS solution was poured into the molds. After PDMS casting on mold had air bubbles, the air bubbles were removed by pasture pipette blowing. Finally, the PDMS cast molds were kept in an incubator at 37 ^{O}C for 24 hours for complete polymerization. If the PDMS was not sticky, the polymerization was completed, and the PDMS chips were ready to separate from the molds.

2.1.8. Chips cutting, punching, and cleaning

After the PDMS was completely polymerized, the chips were removed from the molds. If necessary, the unnecessary parts from the chips were cut and punched with a tissue puncher of the appropriate size. After punching the chips, the chips were cleaned with scotch tape, and the chips were placed in a glass jar pattern faces up and sonicated with up-water for 10 minutes. The chips were rinsed with up-water one time, sonicated with 70% alcohol for 5 minutes, waited for 5 minutes in 70% ethanol on a bench, and rinsed with up-water one time. After the chips cleaning was finished, the chips were put in autoclaved Petri dishes with Whatman papers, and the Petri dishes were placed in the incubator at 37 ^{O}C for 24 hours for complete drying of the chips. Chip punching was used for single liver and breast chips only. There was no punching procedure for multiorgan-on-a-chip (MOC) chips because the chips were open-toped, and punching was not needed.

2.1.9. Chip bonding

After washing and drying, the chips bonding with a microscopic slide were done. Before starting chip bonding, the hot plate was adjusted to 100 ^{O}C. The chips were cleaned with scotch tape, put on the microscopic slides pattern face upward, put inside the ultraviolet light (UV)/Ozone device, and applied UV/Ozone for 5 minutes. Functionality checking was necessary for both the UV light indicator (red) and power light indicator (green). The chips were bonded on microscopic glass slides by placing the pattern of the chips on the microscopic slides. After the bonding process was finished, the bonded chips were put on the hot plate, covered with aluminum foil, and waited for 15 minutes. The chips were put in a clean Petri dish and treated with UV for 30 minutes in a laminar flow hood. After UV was finished, chips were put in Petri dishes, and the chips were ready for an experiment.

2.2. Cell culture

This study used MDA-MB-231, HePG2, and MCF-10A cell lines for experiments. The MOC experiment contains MDA-MB-231, HePG2, and MCF-10 cell lines. The breast compartment was composed of MDA-MB-231 and MCF-10A cell lines in the MOC experiment in a 1:1 ratio. The cells were cultured in Petri dishes and incubated at 37^{o}C, complementing 5% CO_2. When there was confluency of around 90%, the passage

was done according to the procedure. Prior to the experiment in the 3D-cell culture, the chips were coated with (3-Aminopropyl) triethoxysilane (APTES) to decrease the PDMS's hydrophobicity and facilitate the attachment of the cells in the chip. In the MOC chip, the matrix area is at the bottom of the chip, and a medium is added from the top of the Matrigel-cells interface to facilitate the diffusion of the medium. The single liver and breast bonded chips separated the Matrigel cells and media compartments.

The APTES coated chips were filled with Matrigel cell suspension and incubated at 37^{o}C for complete polymerization for 45 minutes. After the polymerization was complete, the chips were removed from the incubator, and the media compartment was filled with the appropriate cell culture media. In the MOC chip, the flow of fluid was by diffusion, and the time for cell-Matrigel incubation time was 45 minutes prior to the addition of media. Autoclaved ultra-pure water was placed inside the jar that contained the experiment chips to prevent evaporation. The final concentration of cells for MDA-MB-231, HePG2, and MCF-10A was 5 million cells per ml.

2.2.1. Organ-on-a-chip cell culture

After the design of the organ-on-a-chip (OOC) and MOC were completed, HePG2 and MDA-MB-231 cell lines were cultured in 2D culturing techniques. When the cells became confluent in the 2D cell culture, the cells were transferred to organ-on-a-chip (OOC) to evaluate cell viability and test the drug. In the OOC, after 24 hours of experiment, 10 μM doxorubicin was added, and after 48 hours of incubation cell viability test was done. Each experiment in the OOC had at least four chips: two chips for drug testing, one chip for 70% Ethanol as control, and one chip for methanol. The chips experiment used an equal amount of Matrigel (4 mg/ml) and cell suspension with 5 million cells per ml of final cell concentration. After the Matrigel cell suspension mixture was added to the chips and incubated for 15 minutes upward and 15 minutes downward to homogeneous cell distribution and to have the 3D structure of matrix and suspension. After 24 hours, the old media was removed from the chips and replaced by media that had doxorubicin (two chips) and methanol (one chip) and media only for the 70% ethanol control chip. After 48 hours of incubation, viability dyes were added to all four chips and incubated for one-four hours. 70% ethanol was added 30 minutes before adding dyes to kill the cells in the ethanol chip. After the incubation of the dyes was completed, confocal images were taken.

2.2.2. MOC cell culture

In one MOC experiment, twelve chips were required, six chips for drug testing, three chips for methanol as control, and three chips for 70% ethanol. The Alamar blue stain 70% ethanol-treated chips remain blue after incubation at 37 ^{O}C. All chips were incubated for 24 hours at 37 ^{O}C with a 5% CO_2 supplement, and the media was removed and replaced with media that had doxorubicin and methanol for the drug test and methanol chips, respectively. For drug testing, three different doxorubicin doses (2.59 μM, 25.86 μM, and 38.79 μM) were used in the MOC experiment. There were three-time points (24, 48, and 72 hours) for one dose. After 24, 48, and 72 hours of incubation of the drug, media was removed from the chips, collected in Eppendorf tubes, and stored at -20 ^{O}C.

2.2.3. MCF-10A cell line culture medium

The MCF-10A cell culture medium was composed of DMEM: F12 (Biological Industries), 5% donor horse serum, 1% L-glutamine, 1% Penicillin-Streptomycin, 20 ng/ml EGF, 0.5 ug/ml hydrocortisone, 100 ng/ml cholera toxin and 10 ug/ml insulin. Passage number 5-20 was used for experiments in MOC experiments. Trypsin EDTA-C was used for 17 minutes to reduce cell adhesion in cell suspensions and facilitate the cleavage power of trypsin and detachment of cells from the Petri dish's surface. After detaching the cells from the petri dish, an MCF-10A medium was added to neutralize the trypsin. The cell suspension was centrifuged at 3800 RPM for five minutes. After the centrifuge was completed, the supernatant was removed by vacuum pipetting, and MCF-10A medium was added to create cell suspensions for passage with a ratio of ¼ for full confluency in 2-3 days for experiments.

2.2.4. MDA-MB-231 and HePG2 culture medium

MDA-MB-231 and HePG2 cells culture media was composed of “DMEM High Glucose (Biological Industries), 10% fetal bovine serum, 1% L-glutamine, 1% Penicillin-Streptomycin”. The Petri dishes used for cell culture in this experiment were 60 mm Petri dishes. Passage number 6-30 was used in these experiments. Trypsin EDTA-C for the MDA-MB-231 cell line and EDTA-A for the HePG2 cell line are used to detach cells from Petri dishes. The incubation time of Trypsin-EDAT-C for MDA-MB-231 cell line and HePG2 cell lines are 4 and 5 minutes, respectively. After cell detachment was

completed and confirmed under a microscope, a cell culture medium was added to the petri dish to neutralize the trypsin solution and re-suspension the cells. The cell suspension of MDA-MB-231 and HePG2 was centrifuged at 3800 RPM for five minutes. After centrifugation, the supernatant solution was discarded, and a new medium was added for re-suspension of cells. The re-suspended cells were used for passage in a ratio of ½ or ¼ for 90-100% confluency in 2-3 days.

2.3. Cell viability testing

We used different DNA staining dyes to identify the live and dead cells. The Hoechst 33342(Sigma Aldrich), DAPI, and Blue (Molecular Probes) were used as all cell indicators. Because they stained all cells, both the live and dead cells. The NucRed Dead 647 Ready Probes (Thermo Fisher), DRAQ7™ (ab109202), and Green (Molecular Probes) were used to stain dead cells. The assumption here is that the dead indicator dye only stains dead cells. Additionally, we used Alamar blue dye for absorbance measurement and understanding of the viability of the cells in the MOC experiment.

2.4. Image analysis

After confocal imaging, image analysis was done by Image J/Fiji software. The channels were separated by Python code. The confocal images were analyzed manually or by using automated macros. The steps of manual image analysis with Image J/Fiji were stack formation (Image>Stacks>Image to stack), Zsum construction (Image>stacks>Zproject), subtracting background (Gaussian blur) (process>filters>gaussian blur), threshold (image>adjust>threshold) and despeckle (process>noise>despeckle) of the images, and finally, analysis to get the result and save it as an excel file. After stack formation, the image type changed to 8bit. The following are the macros that were used in the image analysis.

Zsum8bitGB macro

Used to create Zsum of images, Gaussian blur Zsum images and to change the type of the image to 8bit.

“macro "Z project folder" {

```
requires("1.33s");
dir = getDirectory("Choose a Directory ");
list = getFileList(dir);
setBatchMode(true);
for (i=0; i<list.length; i++) {
path = dir+list[i];
open(path);
}”
“run ("Images to Stack", "name=Stack title=[] use");
run ("Z Project...", "projection=[Sum Slices]");
run ("Conversions...", "scale");
run("8-bit");
save(path+"Zs8b.tif");
run ("Gaussian Blur...", "sigma=6");
save(path+"Zs8bGB.tif");
close ();
close ();
}”
```

Image calculator macro

Used to subtract gaussian blur from the Zsum stack to reduce background.

```
// @File (label="source directory X",style="directory") dirX
// @File (label="source directory Y",style="directory") dirY
// @File (label="destination directory",style="directory") dest
// get a list of all files in the two folders
listx = getFileList(dirX);
listy = getFileList(dirY);
```

```
// stop the macro if the number of images is not the same
if (listx.length != listy.length) {
exit ("number of images is not equal");
}
// set batch mode to not see the images when opened
setBatchMode(true);
// start a for loop to process all image pairs one by one
for (i=0; i<listx.length; i++) {
// get the paths to an image pair
incomingx = dirX+File.separator+listx[i];
incomingy = dirY+File.separator+listy[i];

// open the image at list position i and rename them
open(incomingx);
title = getTitle();
print ("now working on..." + title);
rename("XX");
open(incomingy);
rename("Y");

// subtract the images from each other
imageCalculator("Subtract create ", "XX", "Y");
rename("result");
// construct the output file name and path
outFile = dest +File.separator+ title + "C.tif";

// save the image
selectWindow("result");
saveAs("Tiff", outFile);
print("Done");
```

```
// close all open images
run ("Close All");
}
print (" ");
Print ("All done");
```

Threshold and despeckle macro

Used for creating threshold (black and white) and remove noise from the images.

```
“dir1 = getDirectory("Choose Source Directory");
dir2 = getDirectory("Choose Destination Directory");
list = getFileList(dir1);
setBatchMode(true);
for (i=0; i<list.length; i++) {
showProgress(i+1, list.length);
open(dir1+list[i]);”

“setAutoThreshold("Triangle dark");
setOption("BlackBackground", true);
run ("Convert to Mask");
run("Despeckle");
saveAs("D.tif", dir2+list[i]);
close ();
}”
```

2.5. Alamar blue cell viability assay

The Alamar blue dye was blue in the oxidized form and had more negligible fluorescence. The viable cells can reduce the Alamar blue to resorufin, which was red and has pink solid fluorescence. The dead cells had not the ability to reduce resazurin to resorufin, and the color of the dye remains blue.

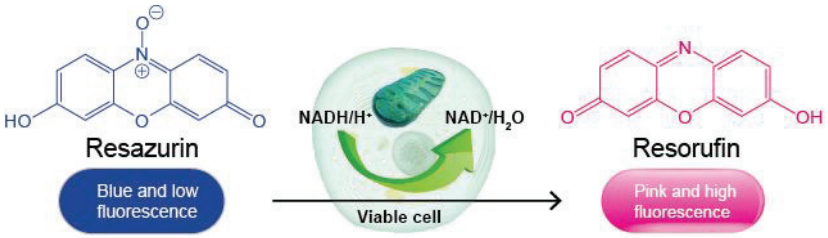

Figure 2. 4. Alamar blue cell viability assay principle [76]

In this study, cells were treated with 70% ethanol for 30 minutes as a positive control and stained with Alamar blue. We prepared four chips for the cell viability assay with Alamar blue, 2 MOC chips for cell viability assay treated with doxorubicin, one 70% ethanol-treated MOC chip, and one methanol-treated MOC chip. The cancer drug doxorubicin was dissolved with methanol, and we are using methanol as our negative control to rule out the effect of doxorubicin correctly. After adding Alamar blue to the MOC chips, the chips were incubated at 37 ^{O}C for 4 hours, and by Thermo Scientific Multiskan Spectrum spectrophotometer read the absorbance of the Alamar blue. In the 3D Alamar blue viability assay, cells may proliferate from time to time, and Alamar blue reduction increases than the initial value.

2.5.1. Alamar blue absorbance calculations

$$\text{Percent difference in reduction} = \frac{\text{A570} - (\text{A600} * \text{RO}) \text{ for drug well}}{\text{A570} - (\text{A600} * \text{RO}) \text{ Methanol well as control}} * 100$$

$$R_O = \frac{AO570}{AO600}$$

AO_{570} = Absorbance of oxidized form at 570nm

AO_{600} = Absorbance of oxidized form at 600nm

R_O is the correction factor; if we use it without this, we may get negative numbers.

2.6. Cell tracking

Cell Tracker Blue CMAC and cell Tracker Green CMFDA dyes were used. MDA-MB-231 cells were labeled with a blue cell tracker, whereas MCF-10 cells were labeled with a green cell tracker. Cells were washed with serum-free media, and cell trackers were prepared with serum-free media with the appropriate concentrations. The final concentration of the green and the blue tracker was 5uM and 25uM, respectively. Cells labeled with green cell tracker were incubated for 30 minutes at 37 ^{O}C supplement with

5% CO_2, whereas for cells labeled with blue cell tracker, the incubation time was an hour. After incubations, the cells were washed three times with serum-free media, and the cells' media was added to the petri dish and incubated overnight to overcome cell stress and were ready for experiments.

2.7. Cells counting using a hemocytometer

The correct final cell concentration of MDA-MB-231, HePG2, and MCF-10A cells for the 3D cell culture cells was counted with a hemocytometer. An equal amount of cell suspension and Trypan Blue were mixed (10 ul from each) and loaded into the hemocytometer. The dead cells took the trypan blue dye and looked blue, but the viable cells did not take the trypan blue dye and looked shining. After the cells settled in the counting chamber, the cells were counted in the 16 squares in the four corners of the hemocytometer. After the cells were counted, the average of the cells was used for further calculations.

2.8. High-performance liquid chromatography

High-performance liquid chromatography (HPLC) is an instrument that is used to separate a fluid mixture based on the affinities of molecules to the stationary phase. After preparation of the mobile phase with the correct P^H, the sample is injected automatically into the machine and the mobile phase solution, and the sample is mixed before reaching the column. The components mixed with the mobile phase have different characteristics and interact with the stationary phase according to their affinity inside the column. The affinity interaction is the base for the separation of molecules in HPLC. Molecules with a high affinity to the stationary phase reach the detector last. In the reverse phase of HPLC, the stationary is made from hydrophobic inert compounds, and the mobile phase is made of polar solvents. There is an application of high pressure to push the sample through the column. The retention time started from sample injection and finished when the sample reached the detector. The result is presented as a retention time versus intensity graph called a chromatogram. The solute concentration is calculated from under the curve of the chromatogram area [77, 78].

2.8.1. Chromatographic conditions

This study accomplished drug analysis using the Waters Symmetry C18 column maintained at 35 °C and a mobile phase consisting of acetonitrile and water (32:68, V/V; P^H=3). The flow rate was kept at 1 mL/min for isocratic elution, and the column effluent was monitored with an ultraviolet detector at 235nm. Waters Symmetry C18 Column-WAT045905 (4.6 * 150mm, 5um particle size, pore size 100Å, Waters) and gradient elution with 0, 15, 17, 19, and 25 were used to analyze the concentration of doxorubicin in the media.

2.8.2. HPLC sample preparation

After 24, 48, and 72 hours of drug incubation, the media was collected from the chips into the Eppendorf tube as HPLC samples. A 160 µL collected media and 900 µL of chloroform/ methanol (4:1) mixtures were added into the Eppendorf tube, mixed with vortex for 10 minutes, and centrifuged for 10 minutes at 10000 g. Then, the organic fluid was collected and placed under the hood overnight. After all the organic fluids were evaporated, 320 µL of mobile phase (Acetonitrile: ultra-pure water) was added, and the solid substances were dissolved and centrifuged for 5 minutes at 10000g. Finally, the supernatant fluid is collected and transported to the Biotechnology and Bioengineering Application and Research center IZTECH BIOMER , IYTE, with brown tubes for HPLC analysis [79].

2.9. Drugs and reagents

Doxorubicin Hydrochloride (D558000), Idarubicin Hydrochloride (1167000), Doxorubicinone (Doxorubicin aglycone) (D559070), Doxorubicinol Hydrochloride (>90%) (Mixture of diastereomers) (D558020), and Doxorubicinol (>90%) (D558025) were purchased from Toronto Research Chemicals, Canada. The chemicals used for HPLC mobile phase were acetonitrile, 85% Orthophosphoric acid, and ultra-pure water that IYTE Integrated Research Center supplies.

2.10. Data preparation for PKPD modeling

The samples collected from the MOC experiments were analyzed with HPLC to get concentrations of drugs. The concentrations of the drug obtained from HPLC analysis were used to model the pharmacokinetics (PK) of the drug. The data obtained from Alamar blue cell viability assay was used to model the pharmacodynamics (PD) of the drug. Also, the data obtained from Image analysis by image J/Fiji gave pharmacodynamics data. The PK data was imported to PKanalix software for non-compartmental analysis (NCA) and compartmental analysis (CA). Then, the PK data was exported to Monolix for population PK modeling. The cell viability data were imported to Monolix software for PD modeling. The Monolix software constructed the PKPD modeling, and different PKPD models were compared and evaluated using Sycomore software. After the best PKPD model selection, simulation of the drug was done by Simulx software.

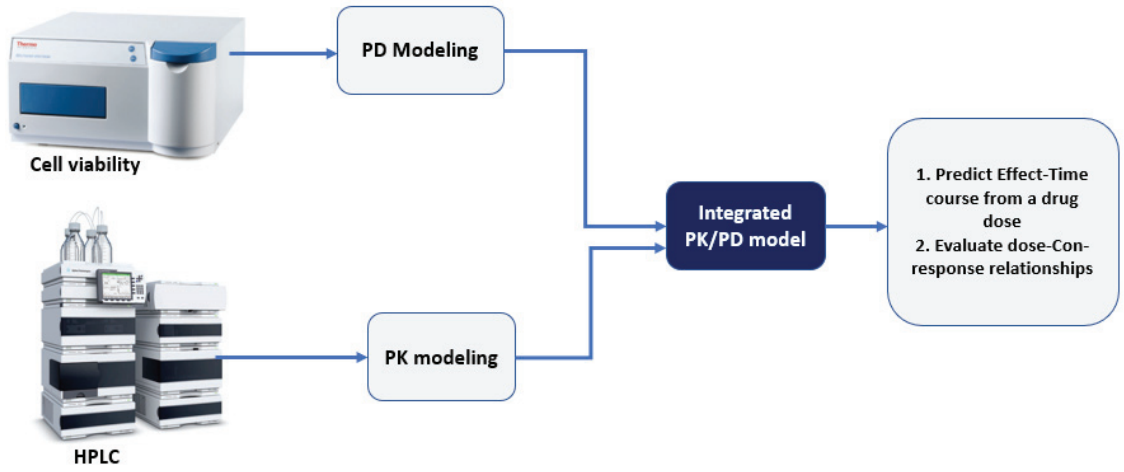

Figure 2. 5. Schematic diagram of PKPD modeling in Monolix.

CHAPTER 3

RESULT AND DISCUSSION

3.1. Cell viability assay in bonded organ-on-a-chip

The first experiment used an organ-on-a-chip bonded with a microscope slide in the cell viability assay. This organ-on-a-chip had separate matrix and media channels. The cell suspension and matrigel(4 mg/ml) were mixed in a 1:1 ratio. The final concentration of cells was 5 million cells per ml. After 24 hours of experiment in the 3D microenvironment, doxorubicin was applied to the chips and incubated for 48 hours. At the end of 48 hours of incubation, the media samples were collected for HPLC analysis, and the media channel was replaced by Hoechst and NucGreen cell viability dyes and incubated for 4 hours. Imaging of cells done with a confocal microscope. The Hoechst dye diffuses better than the green dye but does not wholly reach the edge of the opposite side of the post(Figure 3.1).

The confocal image showed that the NucGreen and Hochest dyes did not reach all the matrix areas. The dyes were diffused only through the post-open space from the media to the matrix channel. The media channel and the matrix channel were not connected side-by-side. We conducted a virtual cell (Vcell) simulation of the chips to prove the diffusion limitation. As seen in figure 3.2, the liver bonded organ-on-a-chip has diffusion limitations.

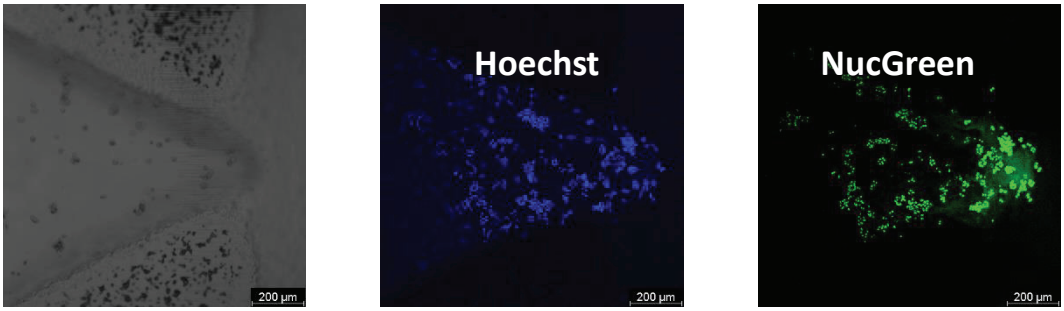

Figure 3. 1. HePG2 cells viability stained with Hoechst and NucGreen

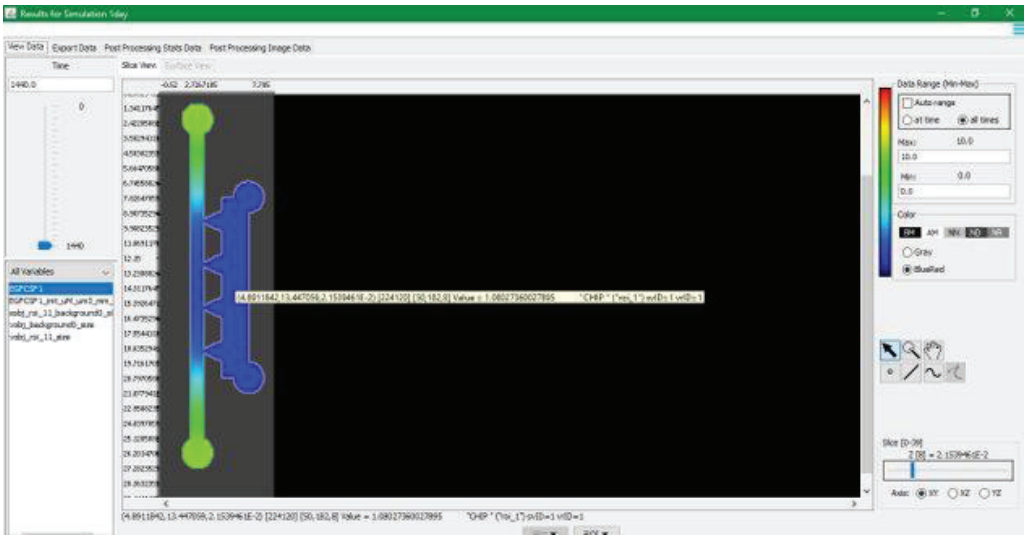

Figure 3. 2. Liver bonded organ-on-a-chip Vcell simulation

3.2. Cell viability assay in open-top organ-on-a-chip

To overcome the diffusion limitation in posted organ-on-a-chip open-top organ-on-a-chip was designed. After Vcell simulations, the open-top organ-on-a-chip had diffusion limitations, also confirmed with experiments (Figure 3.3).

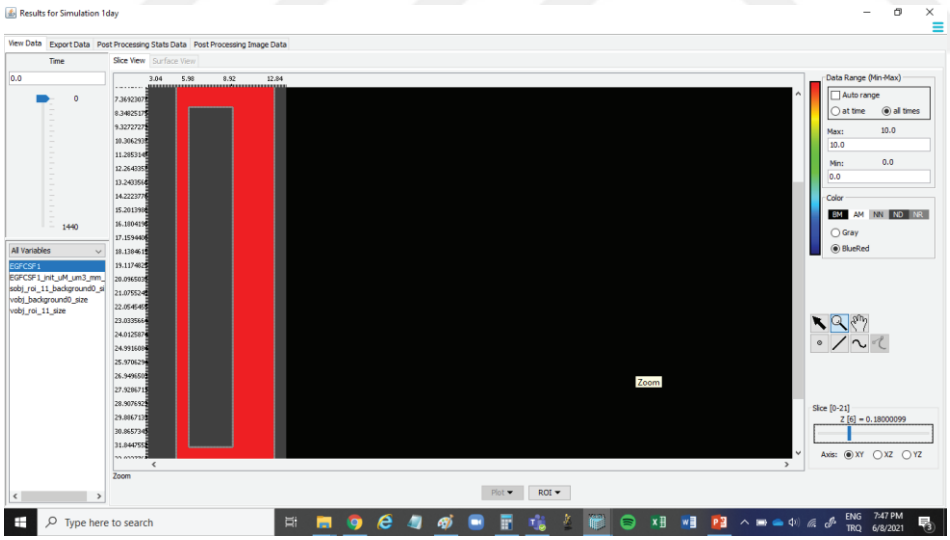

Figure 3. 3. Open-top liver organ-on-a-chip Vcell simulation

3.3. Cell viability assay in multiorgan-on-a-chip

The multiorgan-on-a-chip (MOC) had the liver and breast in the same chip to create a maximum matrix-medium interface. For liver and breast compartments, the matrix thickness was kept identical. The liver and breast compartments were designed

side by side, and media was poured to the top of the matrix to create an easy connection between the breast and liver compartments. The easy diffusion might facilitate organ interactions. The matrix-media interface might improve the paracrine signaling and exchange of molecules between the breast and liver cells. Hoechst/NucGreen, Hoechst/Dead647, NucBlue/NucGreen, DAPI/DRAQ7, and Alamar blue dyes were used for cell viability assessment in the MOC chip.

3.3.1. Cell viability assay in MOC with NucGreen dyes

Hoechst stained all cells in the cell viability assay (both alive and dead), and NucGreen stained only dead cells. The HePG2 70% ethanol chip was supplied with media for 96 hours and treated with 70% ethanol for 30 minutes before adding cell viability dyes to the chip. The Hoechst and NucGreen dyes stained the HePG2 cells properly(Figure 3.4 A-C). In the HePG2 methanol chip, the cells grew well. In the methanol chip, Hoechst and NucGreen cell viability dyes stained the cells properly in the methanol chip(Figure 3.4 D-F). Hoechst stained all cells excellently in the doxorubicin chip, but the doxorubicin chip stained with NucGreen showed almost no signal(Figure 3.4 G-I). One of the reasons for poor staining of the doxorubicin chip by NucGreen cell viability dye was that both the dye and doxorubicin bind DNA. The other possible reason might be the strong fluorescence of doxorubicin, and this fluorescence might interfere in two different ways. First, the emission from the drug would interfere with the NucGreen dye leading to an overlap of spectra. Secondly, the drug can interact with the green dye through fluorescence resonance energy transfer (FRET) because of the absorbance and emission profiles.

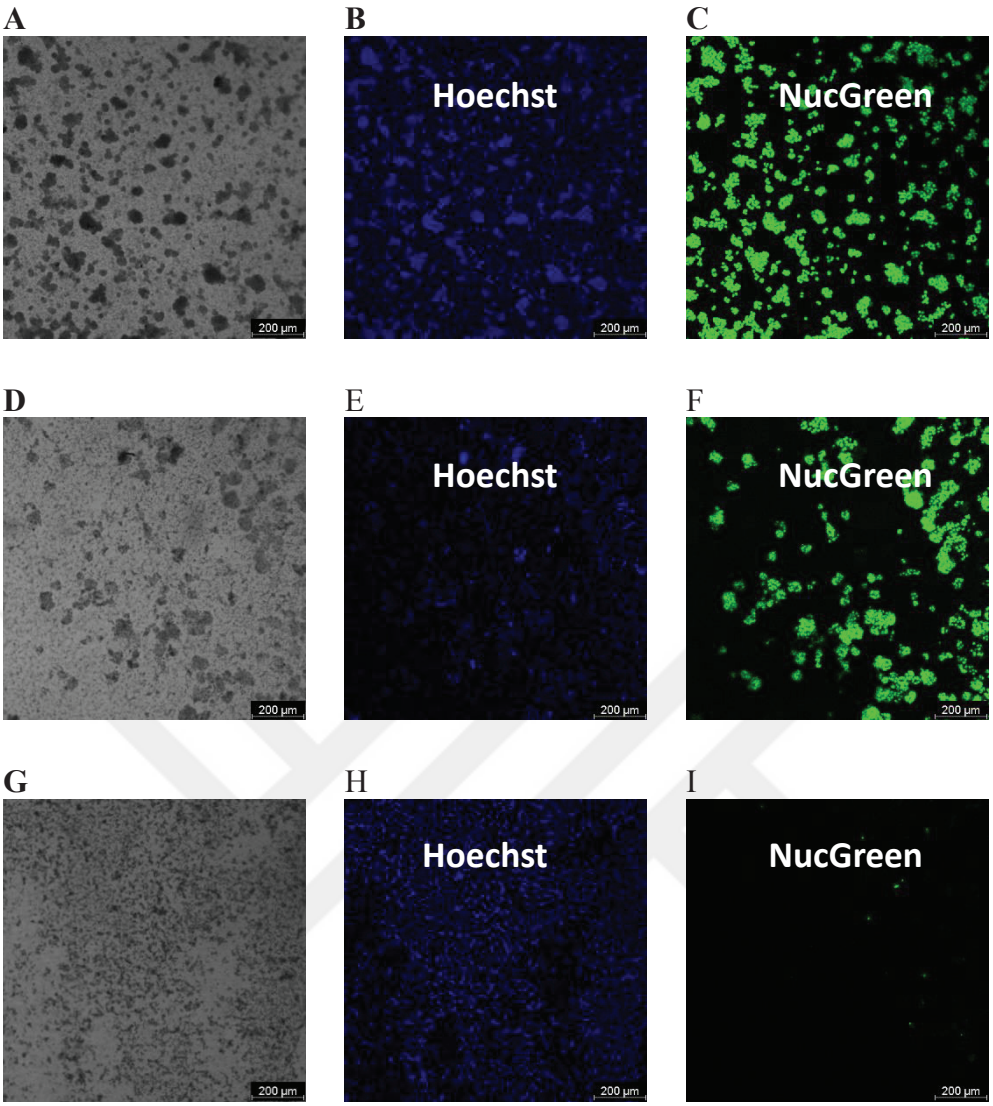

Figure 3. 4. Cell viability assay of HePG2 cells in MOC.(i) 70% ethanol chip(A-C) (ii)Methanol chip(D-F) (iii) Doxorubicin chip(G-I)

In the MDA-MB-231 cells, the Hoechst stained the cells properly in a 70% ethanol-treated chip, but the signal decreased in methanol and doxorubicin chips. In the doxorubicin chip, the signal of NucGreen was less when compared with the70% ethanol-treated chips. Both the doxorubicin-treated chips of HePG2 and MDA-MB-231 stained with NucGreen had weak signals (Figure 3.5 E-F). The poor signal might be that doxorubicin and NucGreen dye bind DNA, similar to HePG2 cells.

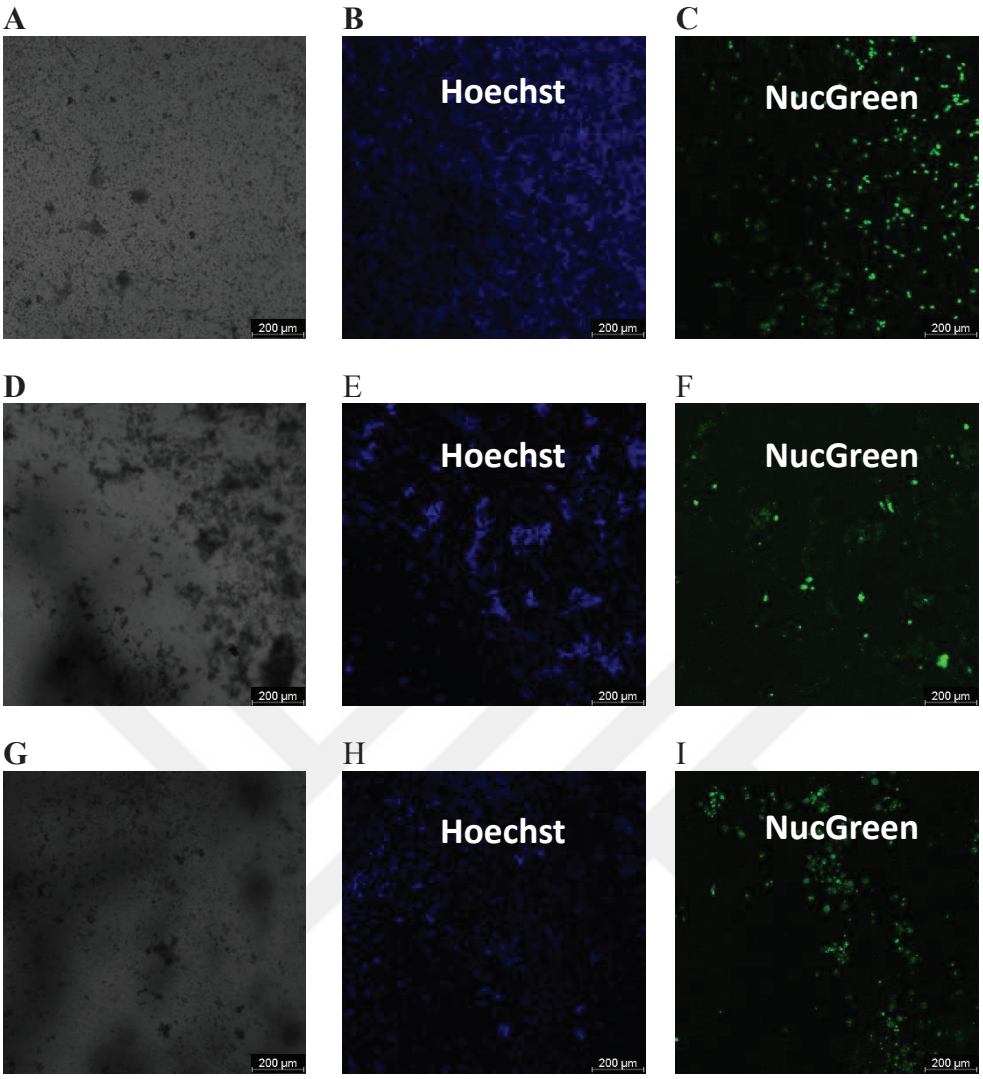

Figure 3. 5. Cell viability assay of MDA-MB-231 cells in MOC (i)70% ethanol chip(A-C), (ii)Methanol chip(C-D), (iii)Doxorubicin chip(E-F)

3.3.2. Cell viability assay in MOC with Nucred Dead647 dye

Hoechst and Dead 647 dyes used here.Both Hoechst and Nucred Dead 647 dyes stained the MDA-231 cells in 70% ethanol, methanol, and doxorubicin-treated chips(Figure 3.6 A-F). Once the dyes were diffused adequately to the cells, images took with a confocal microscope. After calculating the intensity of all cells(Hoechst) and dead cells(Nucred Dead647) by Image J/Fiji software, the intensity of dead cells became more than the intensity of all cells in almost all experiments. The image analysis evaluation showed that the Nucred Dead647 dye stained other molecules or substances presented in the media, and the intensity was more significant than the intensity of all cells (Figure

3.7). Usually, the intensity of dead cells had to be less than or equal to the intensity of all cells(70% treated chip).

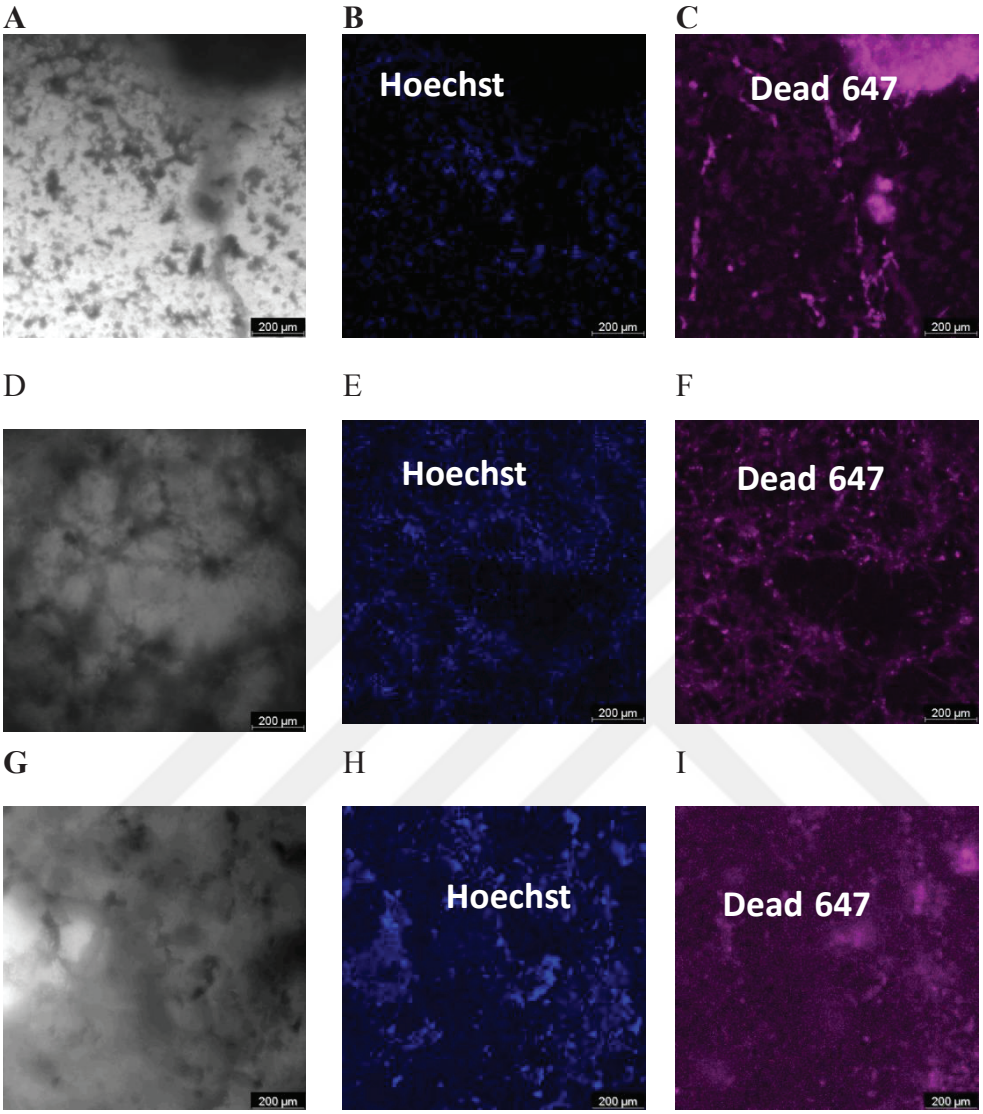

Figure 3. 6. Confocal image of MDA-MB-232 cells i) 70% ethanol chip (A-C), (ii) Methanol chip (D-F), (iii) Doxorubicin chip(G-I)

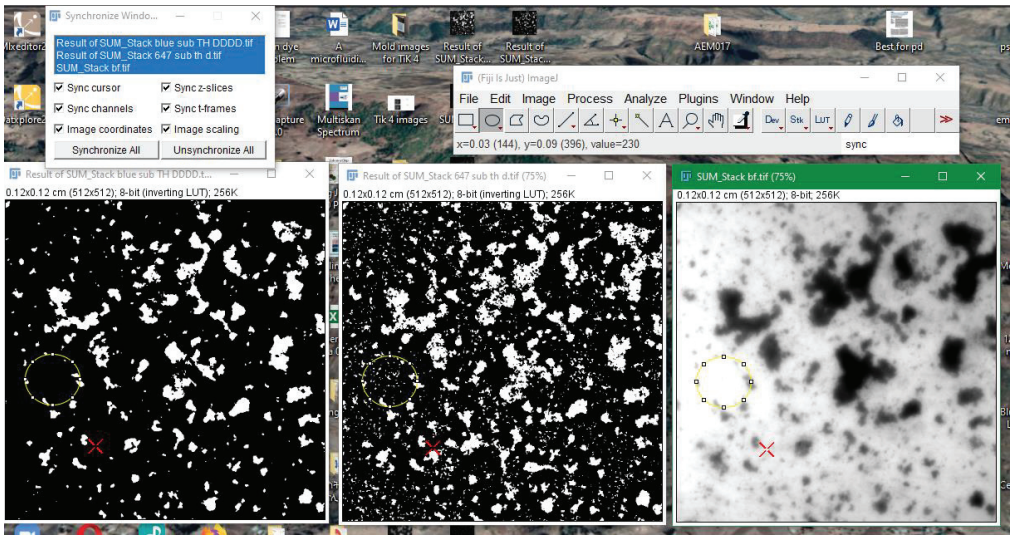

Figure 3. 7. Intensity comparison of cells stained with Nucred Dead647 and Hoechst

3.3.3. Cell viability assay in MOC with DRAQ7 dye

Here DAPI and DRAQ7 dyes were used. DAPI(4′,6-diamidino-2-phenylindole) dye was used to stain all cells (both viable and dead cells), whereas DRAQ7 dye was used only to stain dead cells. The DRAQ7 dye stained the 70% ethanol-treated chip well (Figure 3.8 C). Unfortunately, the DRAQ7 dye stained the methanol chip with a high signal. In the methanol chip, the ratio of dead cells might be less than in the ethanol-treated chip, but the signal of DRQA7 for both ethanol-treated chips and the negative control methanol was almost the same. The DRQA7 dye was not specific; it did not select only dead cells, but it stained all cells, including viable cells (Figure 3.8 C and F). This new dead cell dye was not working in this experiment. All the DNA staining cell viability dyes available in our laboratory were excluded from this experiment.

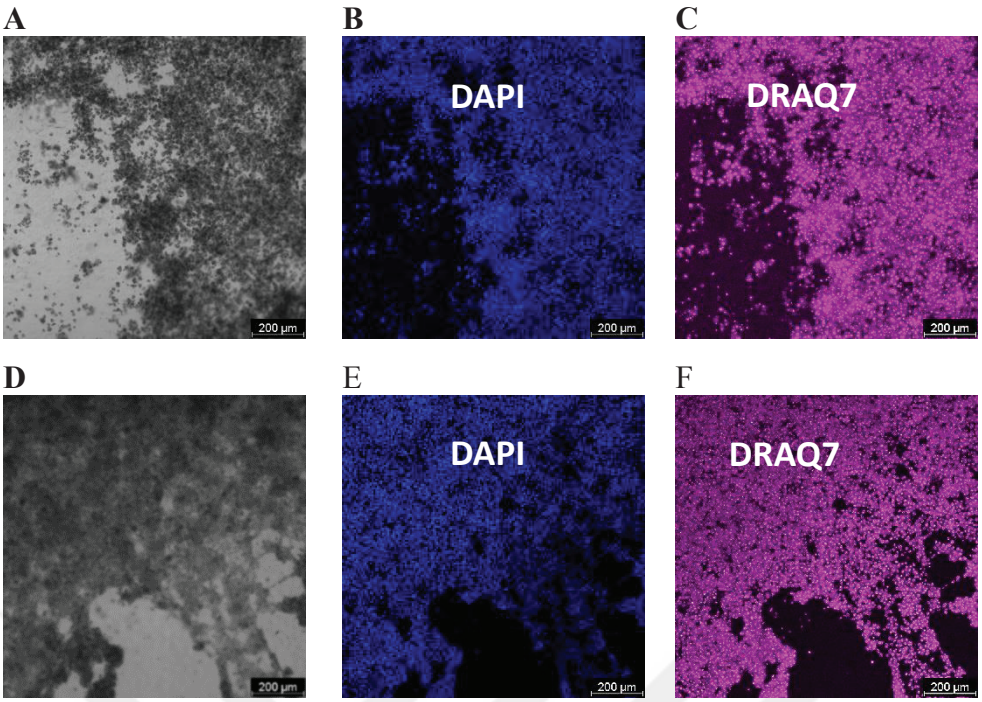

Figure 3. 8. Confocal image of HePG2 cells (i) 70% ethanol chip(A-C), (ii) Methanol chip(D-F)

3.3.4. Alamar Blue staining

After excluding the DNA staining dyes from this experiment, the choice of cells viability assay was Alamar blue cell viability assay. After incubating the cells for 24, 48, and 72 hours with the drug, the media were collected for HPLC analysis from the chip and substituted with Alamar blue dye diluted with complete media in a 1:7 ratio. Alamar blue absorbance was measured at 570 and 600nm. Alamar blue absorbance calculation for the 25.86 uM dose is presented in the following table(Table 3.1).

Table 3. 1. Percent difference reduction calculation

25.86 uM DOX Well plate no.	Samples	Abs 570nm	Abs 570nm-Abs Media	Abs 600nm	Abs 600nm-Abs Media
H2	AB + media	0.864809		0.796518	
H3	Media	0.28078		0.108905	
H7	Methanol	0.652159	0.371379	0.200112	0.091207
H5	DOX 1	0.730536	0.449756	0.303223	0.194318
H6	DOX 2	0.719713	0.438933	0.303793	0.194888
	Abs (AB + Media)-Media	0.584029		0.687613	
	$RO=AO_{570}/AO_{600}$	0.849357			
24 hours		% diff in reduction			
	DOX 1	96.86965			
	DOX 2	93.02254			
48 hours					
	DOX 1	58			
	DOX 2	64			
72 hours	DOX 1	28			
	DOX 2	19			

Percent difference in reduction = (A570-(A600*RO) for drug well/(A570-(A600*RO) for Methanol well) *100

3.4. HPLC analytical results

The collected media were protein precipitated with chloroform-methanol 4:1 ratio and transfered to IYTE Tümleşik Araştırma Merkezleri for HPLC analysis. The analyzed drugs were doxorubicin hydrochloride, Idarubicin Hydrochloride, doxorubicinol, and doxorobicinone. Doxorubicinol and doxorubicinone were the metabolites of doxorubicin. We used the drug Idarubicn as an internal control in HPLC analysis.

3.4.1. Standard calibration curve of drugs

The standard calibration curve for each drug and metabolites was prepared using the drug's concentrations on the X-axis and the peak area on the Y-axis. The slope, Y-

intercept, and standard error of the Y-intercepts were extracted from the regression line. The Y = SlopeX + Y-intercept formula was used to calculate the concentrations of the drugs after HPLC analysis[80]. In the calculations, y was used as the Peak area, and X was used as unknown drug concentrations. The retention time of each drug and metabolites was compared with the media used as control, and the retention time for different concentrations of the same drug was in the same place. The retention time of drugs were 6.3, 5.6, and 9.05 minutes for doxorubicin, Idarubicin Hydrochloride, and doxorubicinol. In other papers, the retention time of doxorubicin was reported as 3.5minutes[81] and 12 minutes[82]. The mobile phase chemicals used, the P^H, the protein precipitation chemicals, types of detector, and types of samples are not the same in all papers. The difference in the above parameters gave different retention times for doxorubicin in different papers. The calibration curve of doxorubicin hydrochloride, doxorubicinol, and idarubicin hydrochloride was presented in figure 3.9 A-C, and the R^2 of the doxorubicin calibration curve was 0.9958. Figure 3.9 D shows the peaks of each drug and their retention time. Figure 3.9 E showed multiple runs of the same drug to see the method's reproducibility.

A

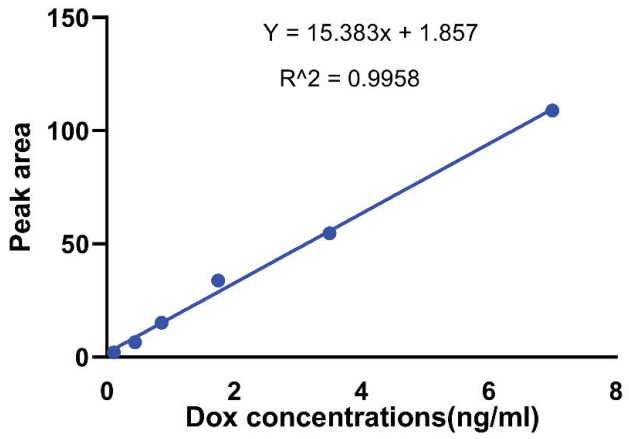
Y = 15.383x + 1.857
R^2 = 0.9958
Peak area
150
100
50
0
0
2
4
6
8
Dox concentrations(ng/ml)

B

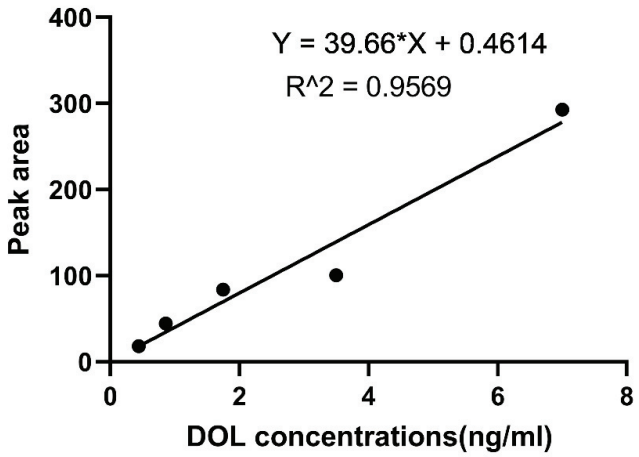
Y = 39.66*X + 0.4614
R^2 = 0.9569
Peak area
400
300
200
100
0
0
2
4
6
8
DOL concentrations(ng/ml)

C

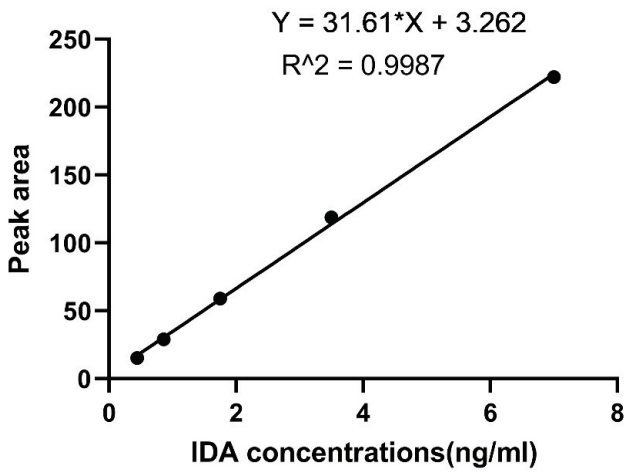
Y = 31.61*X + 3.262
R^2 = 0.9987
Peak area
250
200
150
100
50
0
0
2
4
6
8
IDA concentrations(ng/ml)

D

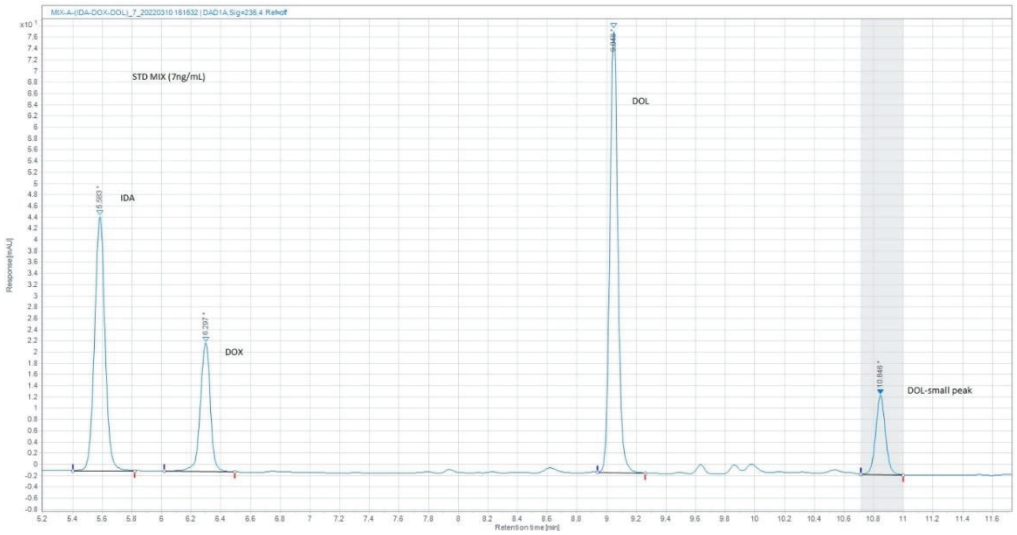

E

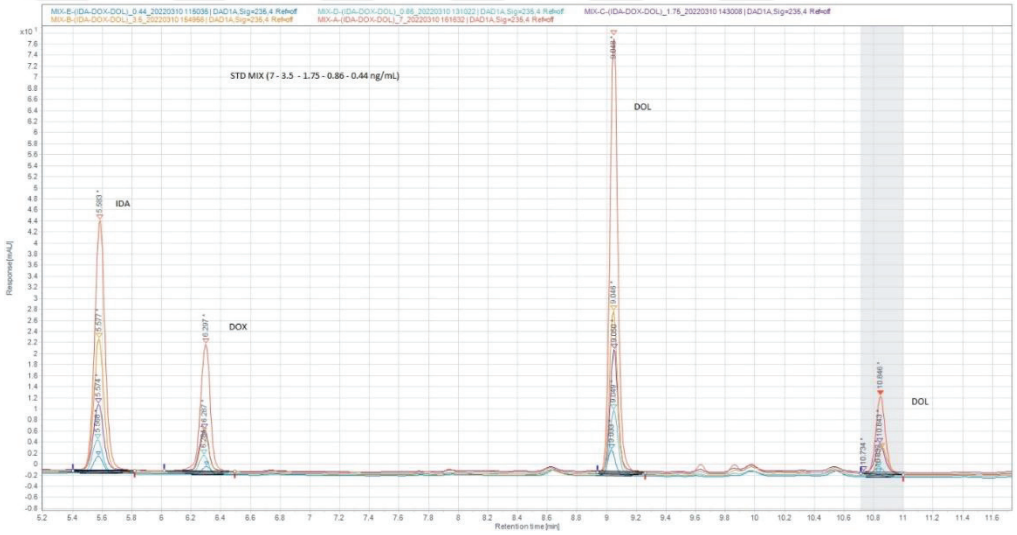

Figure 3. 9. Standard calibration curve for drugs

3.4.2. Low limit of detection and low limit of quantification

The formula calculated the low limit of detection(LOD) and low limit of quantification(LOQ), "LOD=(3.3*Standared Error of Y-intercept)/Slope and LOQ = (10* Standard Error of Y-intercept)/Slope, respectively[80]". The LOD were 0.35, 0.40 and 0.07 ng/ml for doxorubicin, doxorubicinol and idarubicin respectivelly. The LOQ of doxorubicin, doxorubicinol, and idarubicin was 1.07, 1.23, and 0.21 ng/ml, respectively. Different authors report different values for the LOQ for doxorubicin, for instance, 1.3 ng/ml[83], 5 ng/ml[84], 2 ng/ml[85, 86], and 1 ng/ml[87]. The values of LOQ were different in

different studies because of differences in methods. The only authors who analyzed doxorubicin from cell culture media reported the LOD as onepoint five nanogram per ml and LOQ as five nanogram per ml[86].

3.5. Pharmacokinetics analysis of doxorubicin

The non-compartmental analysis(NCA) and compartmental analysis(CA) of PK are used to examine how therapeutic drugs interact with different organs in the body and clear out of the body by the liver and kidney in a quantitative manner[88]. The NCA and CA of PK were analyzed by Pkanalix software, part of the Monolix suite. The CA considered the body interconnected organs and homogeneous fluid mixtures inside the body[89, 90]. The NCA uses mathematical equations to estimate PK parameters[91]. Both NCA and CA describe the status of the drug in a time-dependent manner. The first PK analysis in NCA and CA was the concentration versus time.

Figure 3.10 showed that after administration of doxorubicin, there was a significant decrease in the concentration at the 24 hours time point. At the 48 hours time point, the concentrations of doxorubicin increased slightly more than the 24 hours concentrations.

Furthermore, at 72 hours, the concentration of doxorubicin increased more than the 24 and 48 hours time points. During the first 24 hours, the cells took the doxorubicin, and the concentration decreased dramatically, but after 24 hours, the doxorubicin concentration increased than the 24 hours time point. The possible reason for the increment of concentration might be the ATP-binding cassette (ABC) transporters of the cancer cells[92]. Once the drug was steady-state, the drug's concentration decreased because of excretion from the body by the liver and kidney[93, 94]. There was no way to remove waste substances from the chip in the MOC, and the increment of drug concentration was possible.

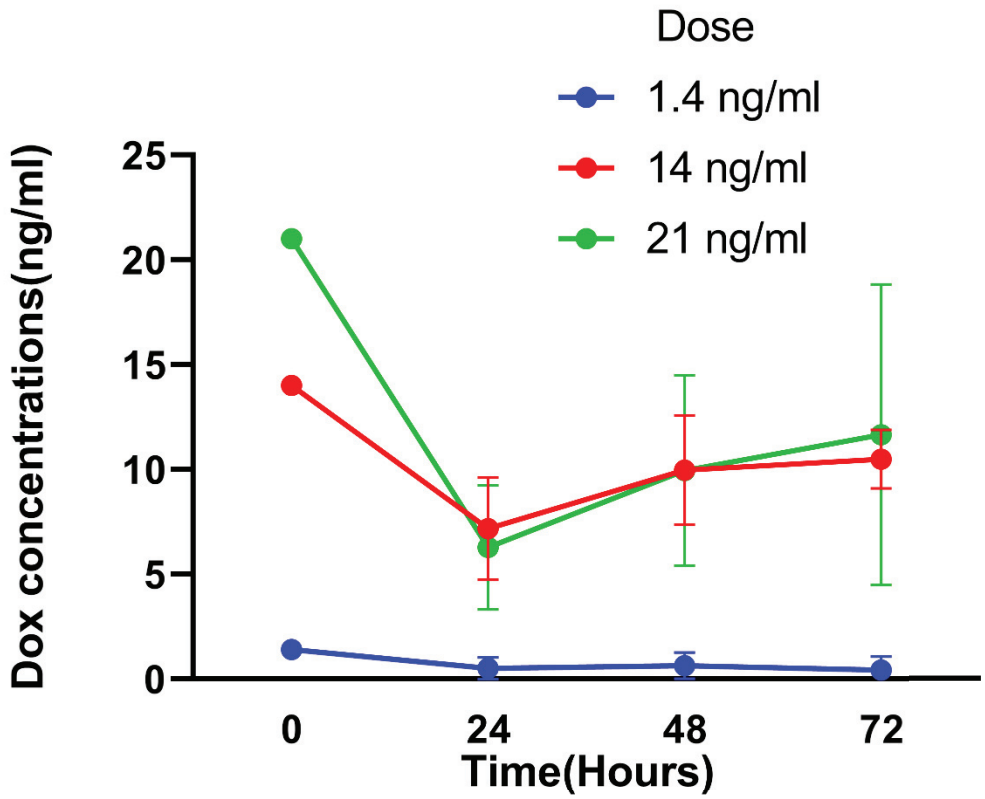

Figure 3. 10. Doxorubicin pharmacokinetics

The NCA used the lambdaZ regression to calculate the individual fits, but the CA used the observed data to calculate the individual fits. The R-square and adjusted R-square values were 87 and 77% in the non-compartmental analysis. The result indicated that the individual fits were estimated well in the NCA(Figure 3.11 and Table 3.2).

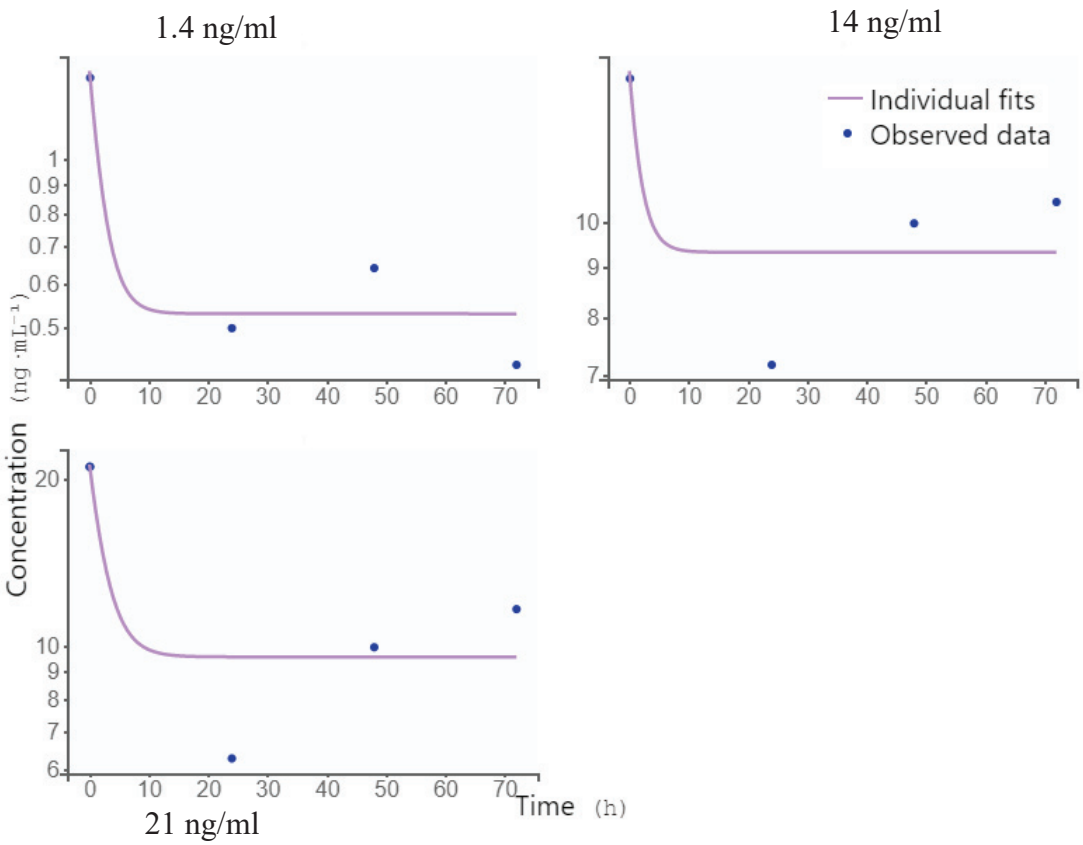

Figure 3. 11. Non-compartmental analysis of individual fits estimations.

The non-compartmental analyses calculated in this experiment were R-square, adjusted R-square, Area under the curve(AUC), Cmax, and Tmax(Table 3.2).

Table 3. 2. Non-compartmental analysis of PK

	MIN	Q1	MEDIAN	Q3	MAX	MEAN	SD
Rsq	0.79	0.8	0.82	0.95	0.99	0.87	0.11
Rsq_adjusted	0.59	0.62	0.73	0.93	0.99	0.77	0.21
AUClast (h·ng·mL^{-1})	49.36	213.48	705.82	763	782.06	512.41	402.82
Cmax (ng·mL^{-1})	1.4	4.55	14	19.25	21	12.13	9.93
Tlast (h)	72	72	72	72	72	72	0
Cl_obs (mL·h^{-1})	0.0046	0.007	0.014	0.017	0.018	0.012	0.007
Cl_pred (mL·h^{-1})	0.0048	0.0074	0.015	0.018	0.019	0.013	0.0075
Vz_obs (mL)	0.69	0.78	1.03	1.14	1.18	0.97	0.25
Vz_pred (mL)	0.74	0.82	1.08	1.21	1.26	1.03	0.26

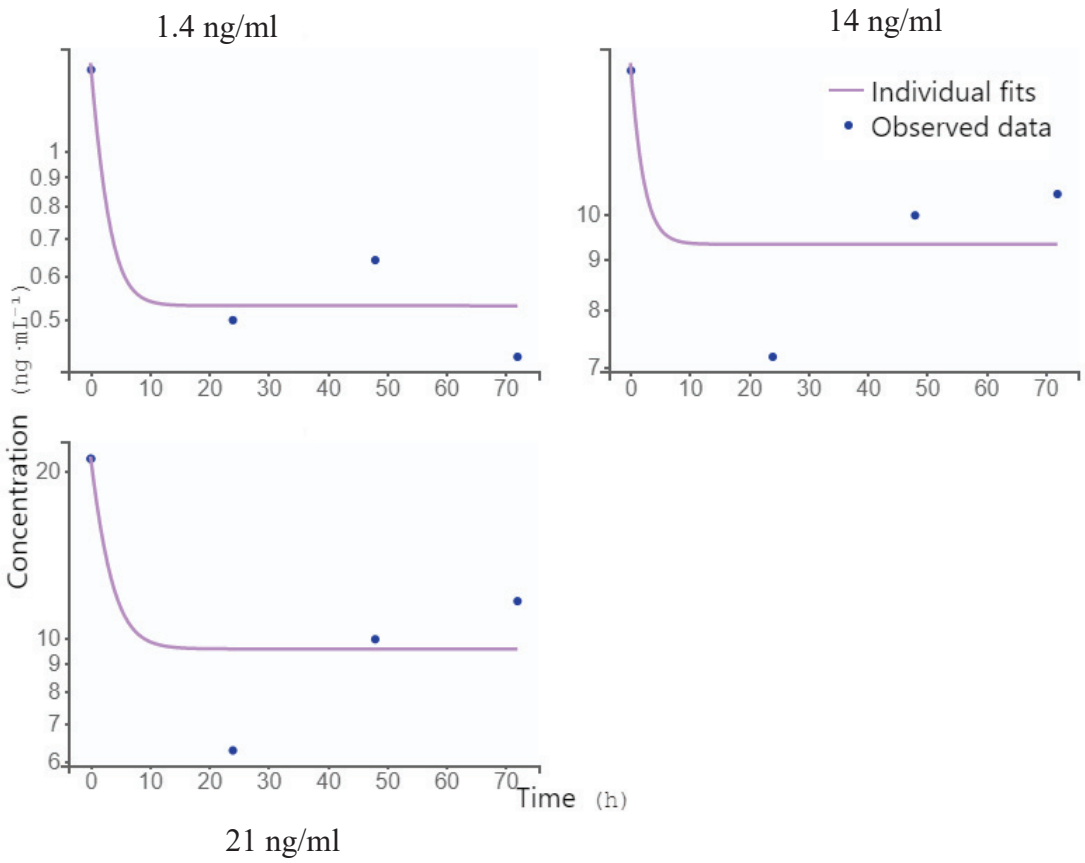

Figure 3. 12. PK compartmental analysis of individual fits estimations

In the compartmental analysis, the volume of distribution in the main compartment(V1), the volume of distribution in the second compartment(V2), intercompartmental clearance(Q), and maximum elimination rate (Vm), and Meachels-Menten constant were calculated. The mean intercompartmental clearance was (0.44±0.1, mean ± SD) ml/h.

Table 3. 3. Summary of the compartmental analysis of PK

	MIN	Q1	MEDIAN	Q3	MAX	MEAN	SD
V1 (mL)	1.94	1.95	1.96	1.98	1.98	1.96	0.018
Q (mL·h⁻¹)	0.36	0.37	0.4	0.52	0.56	0.44	0.1
V2 (mL)	1.04	1.38	2.41	3.1	3.33	2.26	1.16
Vm (ng·h⁻¹)	3.4E-10	3.5E-06	0.000014	0.000023	0.000026	0.000013	0.000013
Km (ng·mL⁻¹)	1.6E-07	0.02	0.078	0.089	0.093	0.057	0.05

3.6. PKPD Modeling

The data obtained from HPLC analysis was used for PK modeling, and the data obtained from the cell viability experiment was used for PD modeling. The PKPD modeling was done by Monolix software. Different models were developed with the PK and PD data, and the best PKPD model was selected.

3.6.1. PK Modeling

After entering the PK data into the Monolix software, the first step was to select a structural model. PK modeling was started from a simple structural model based on the background information of doxorubicin. The first model for PK modeling was by using bolus administration, one compartment distribution, and Michaelis-Menten elimination. The next step was to adjust the initial estimates for PK to estimate the population parameters such as volume of distribution(V), intercompartmental clearance(Q), maximum elimination rate(Vm), and a drug concentration at which the rate of elimination is 50% of Vm(Km). The initial estimates were selected by putting random values and observing the change on the prediction line or using the auto-initiate button present in the software. After PK parameter initial estimation, the initial parameters were fixed, and the next step was adding the PKPD model to the modeling step. Then, the PD model initial estimates were done by strictly putting random numbers and controlling the prediction line. The more the prediction line was near the observed data, the initial estimates and the population parameter estimation would go smoothly(Figure 3.18).

The first information in PKPD modeling was bivariate data. The bivariate graph showed cell viability(PD) on the y-axis and drug concentrations(PK) on the x-axis. The red arrow in the bivariate data indicated the direction of time. When the drug concentration decreased, the viability of the cells increased and vice versa(Figure 3.13).

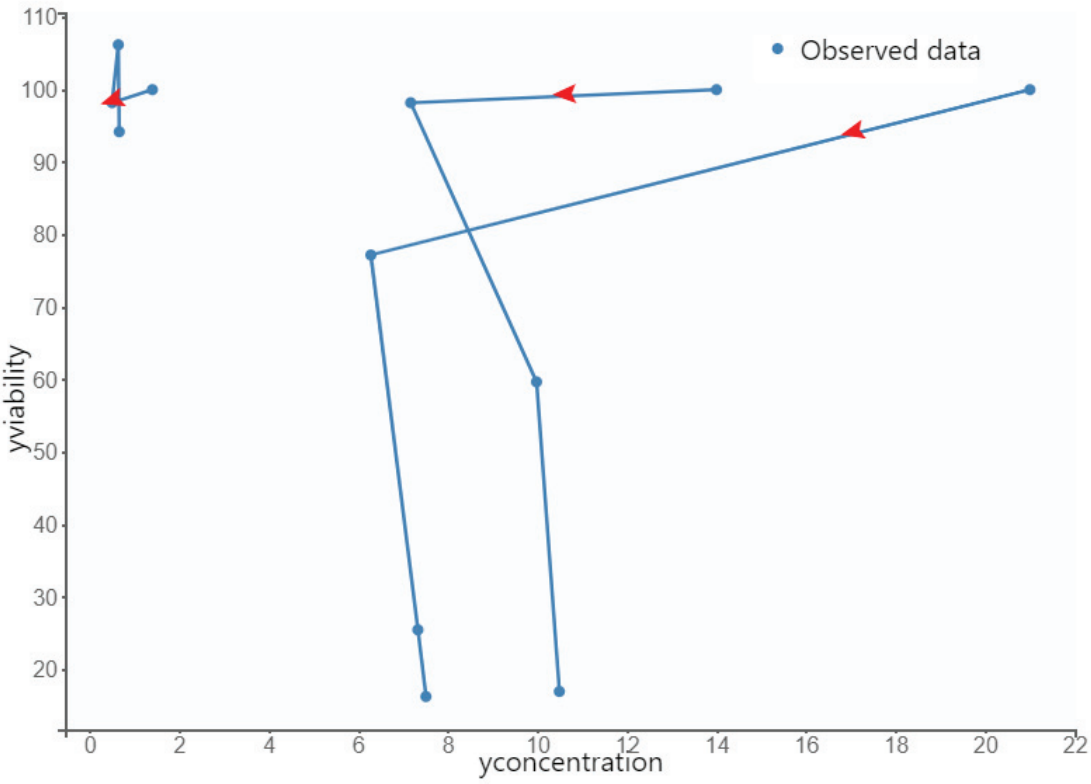

Figure 3. 13. Bivariate representation of PK and PD data

The individual fits graph was the concentrations vs. time graph. It had both the observed data and the predicted individual fits. The blue dots were the observed data of the PK model, and the pink line was the predicted individual fits after initial estimates(Figure 3.14).

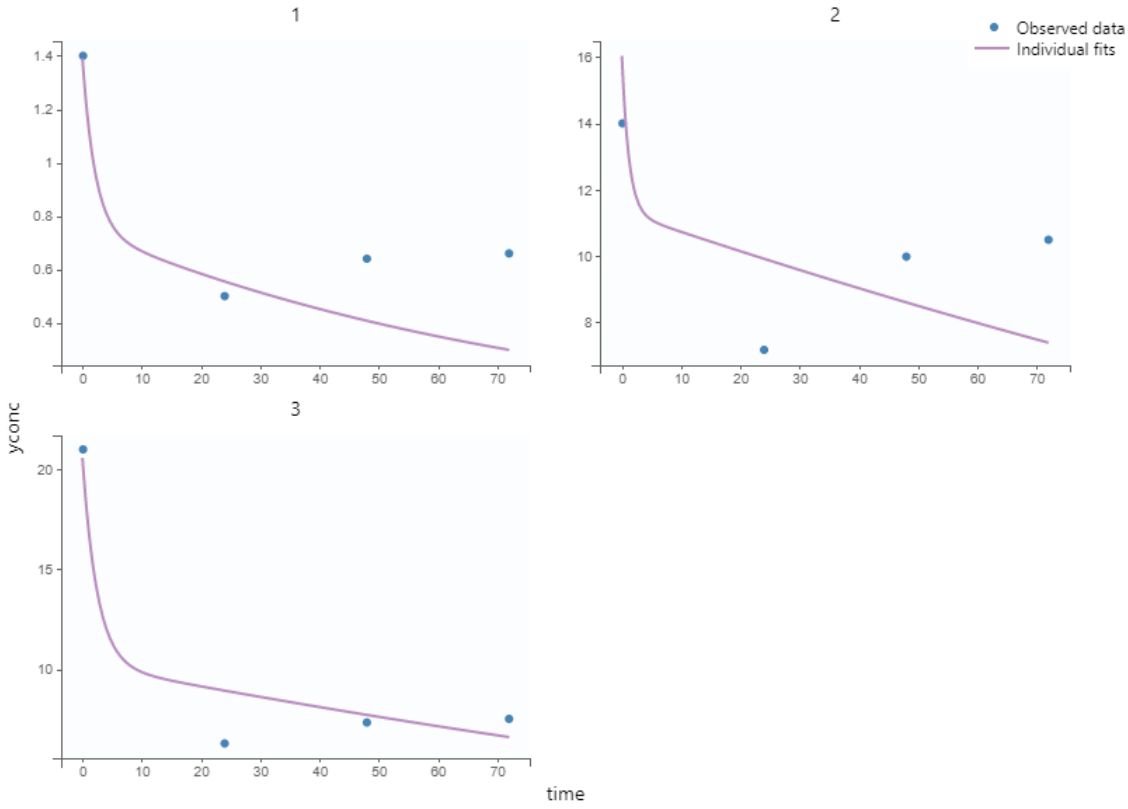

Figure 3. 14. Pharmacokinetics individual fits

One of the criteria for accepting the PK model was the critical examination of the observations to the individual predictions graph. Most of the observed data would be between the 90% prediction intervals, and the observed data had to or near the Y=X line.

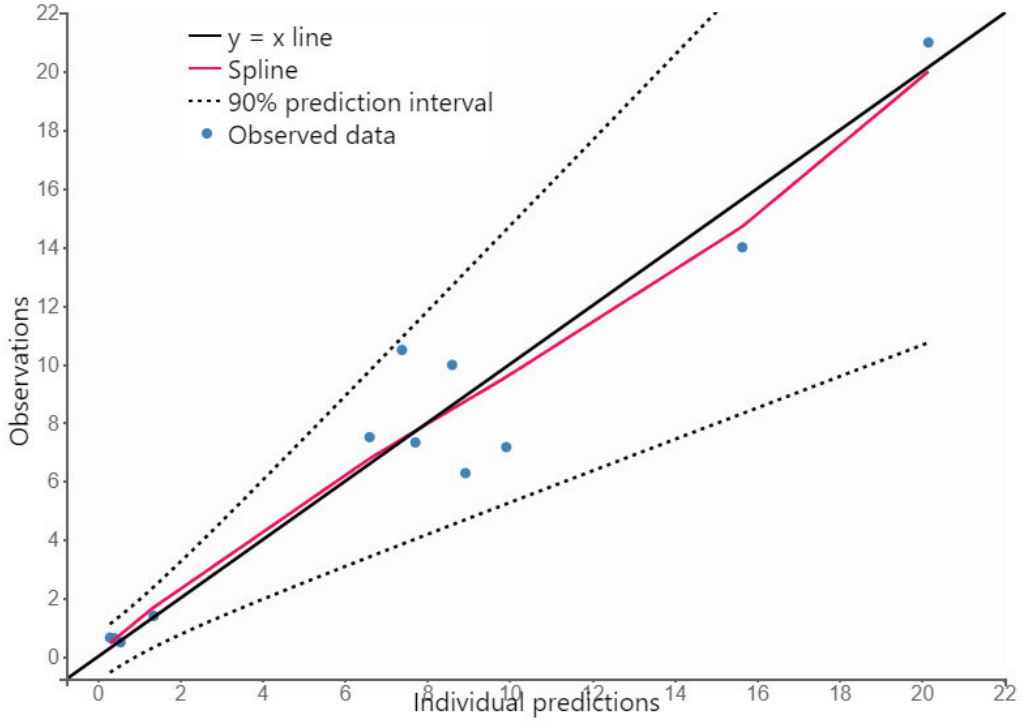

Figure 3. 15. Observations versus individual predictions of PK data

In the first PKPD model with bolus administration, one compartment, and Michaelis Menten elimination, most PK data were out of the 90% prediction interval. A total of seven PKPD models with different parameters were tried in the PKPD modeling. In the seventh PKPD model, the observed data were between 90% of the prediction interval(broken line) and near theY=X line(Figure 3.15). The visual prediction check(VPC) was another requirement for successful PK model predictions. The blue line indicates the empirical percentiles of doses, and the light blue and pink colors indicate the prediction interval. Most of the data in this experiment were between the prediction interval and two outlier data. The overall VPC indicates that the PK model was predicted well(Figure 3.16).

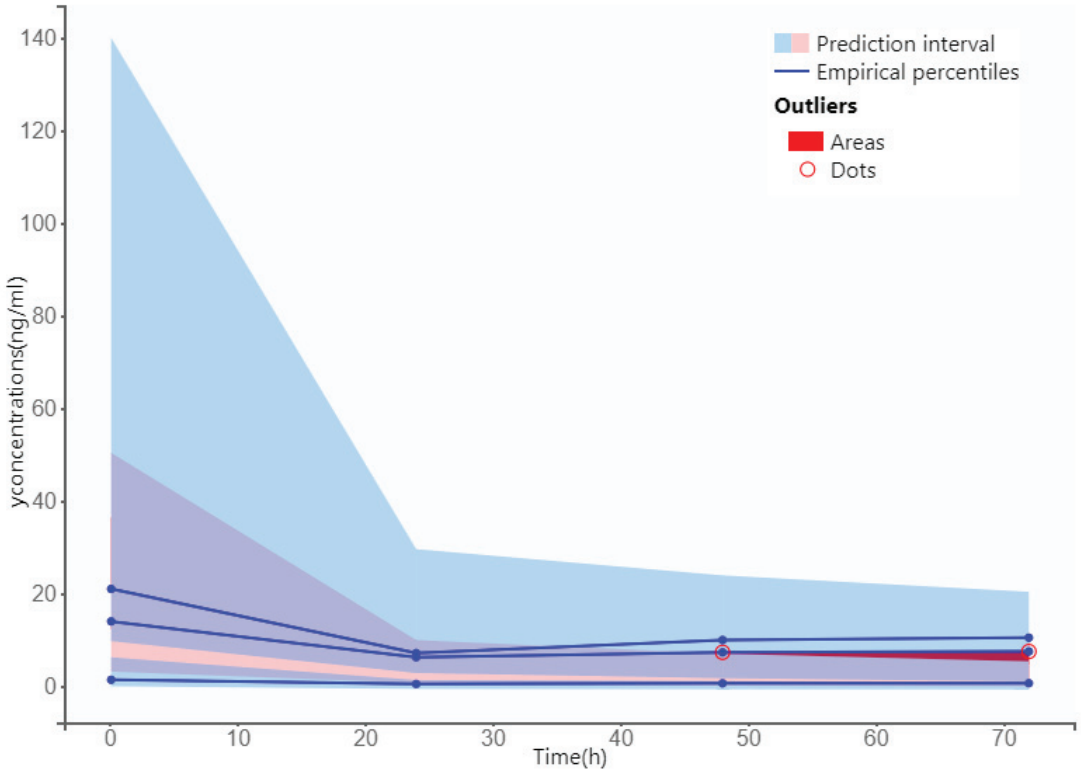

Figure 3. 16. The visual prediction check of the PK model.

3.6.2. PD modeling

The PD modeling used the cell viability data and expressed it as cell viability(response) versus dose. The figure showed that cell viability was decreased for the 14 ng/ml and 21 ng/ml doxorubicin doses at 48 hours. In all three doses, the cell viability was not affected after 24 hours of drug administration. Cell viability was not affected in the 1.4 ng/ml dose. At the 48 hours, the viability of cells for a 1.4 ng/ml dose increased a little bit; this was expected in a 3D cell culture because the cells proliferated, and at this time, cells might have more metabolic activity than the initial cells number and gave high absorbance during Alamar blue cell viability assay (Figure 3.17).

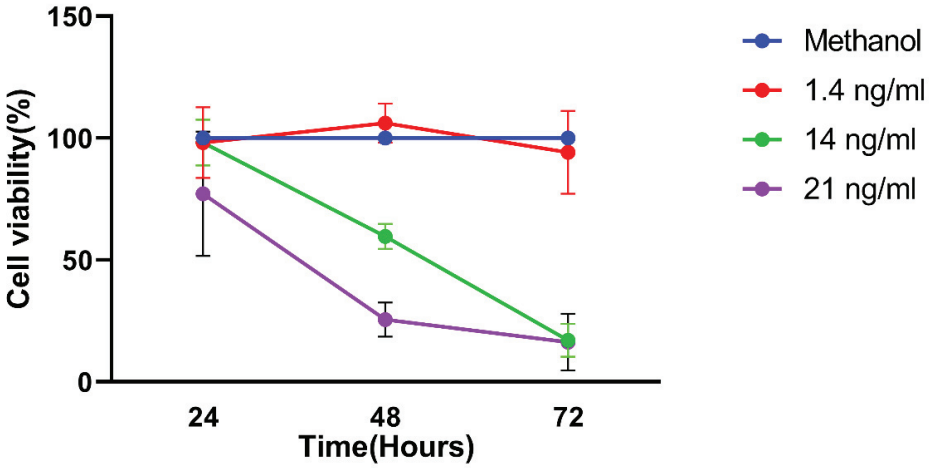

Figure 3. 17. Pharmacodynamic time-dependent profile

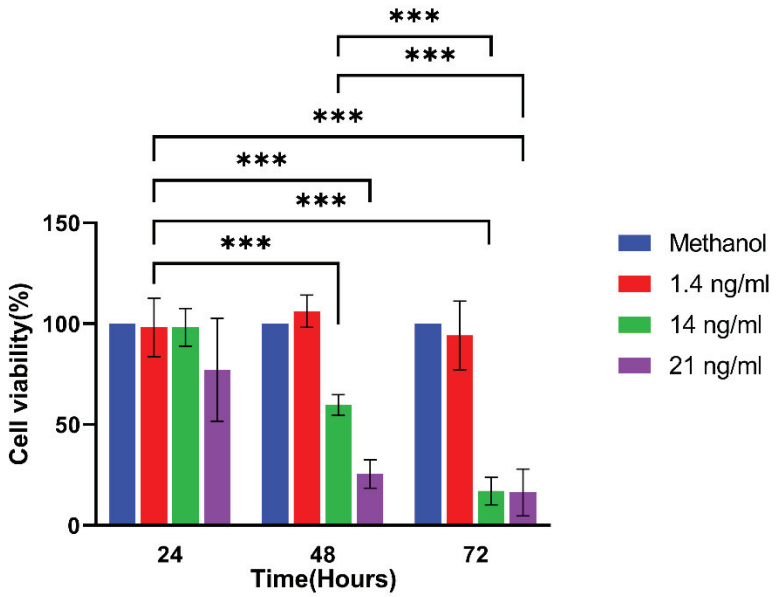

Figure 3. 18 Pharmacodynamics

Unpaired t-test , P<0.05*, P<0.01**, P<0.005*** were considered significant

The individual fits of PD data had blue dots as observed data and pink lines as predicted individual fits. The individual predictions and the observed data were fitted precisely for the 14 and 21 ng/ml doses. For 1.4 ng/ml dose, the effect was seldom on cell viability, and the line of individual fit did not precisely fit the observed data. The total individual fit of the PD data was pridicted well.

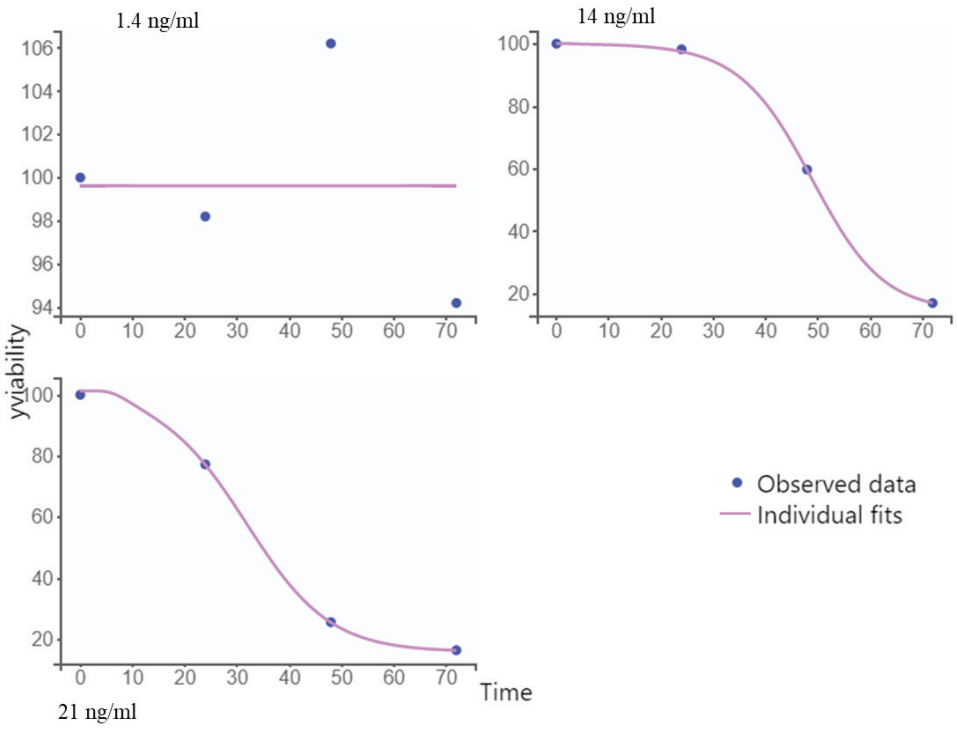

Figure 3. 19. Pharmacodynamics individual fits.

The observations versus individual predictions of the PD model were between the 90% prediction interval(broken line), and the observed data were closer to the Y=X line than the PK observed data. The observations versus individual predictions were one of the criteria for accepting the PD model(Figure 3.9).

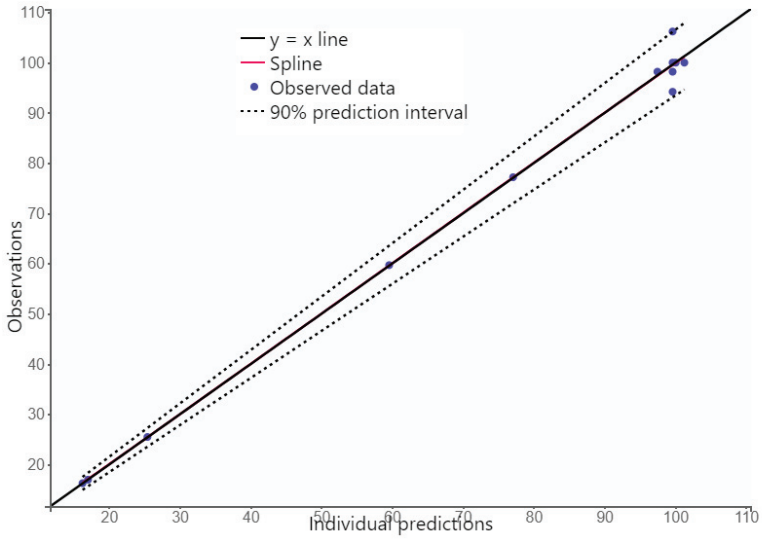

Figure 3. 20.Observation versus individual predictions of PD model

The other criteria for PD model acceptance were a visual predictive check(VPC). The empirical percentiles of most of the PD data were between the prediction interval, and there were two outlier data(Figure 3.20).

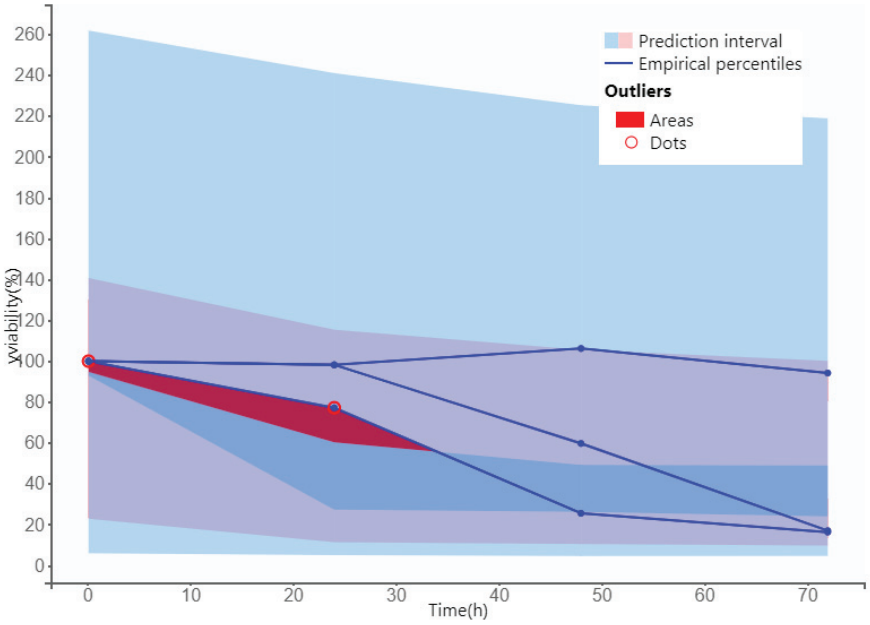

Figure 3. 21. The visual prediction check of the PD model

In assessing the correlation between random effects in the PD model, Km and Vm had positive correlations(correlation= 0.73). The individual fits, visual prediction check and observation versus individual predictions showed that the PD model predicted well.

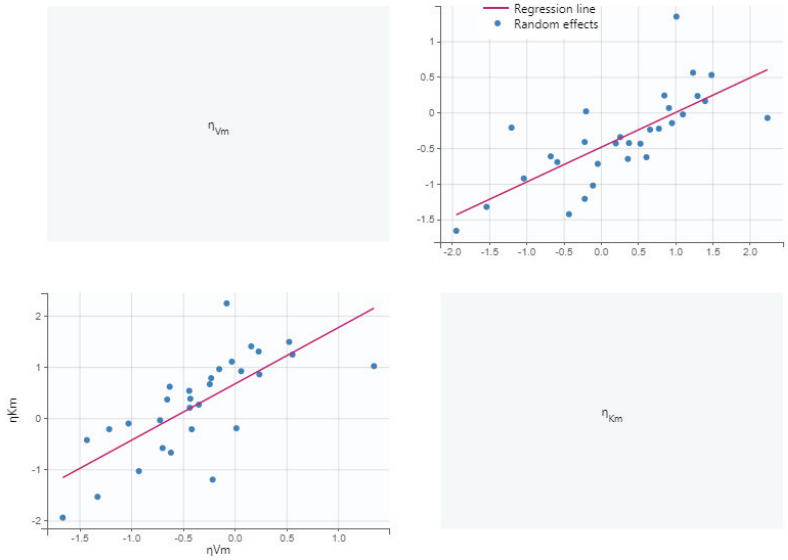

Figure 3. 22. Random effects correlation of PD model

3.6.3. PKPD structural model

DESCRIPTION

The PK data were tagged with the lowest observation id number value. The drug administration in this structural model is bolus. The PK model had a central compartment (volume V1), a peripheral compartment (volume V2), an intercompartmental clearance (Q), and a Michaelis-Menten elimination (Vm, Km). The PD model was a direct Emax model with baseline (baseline effect E0, maximal increase of effect Emax, and half-maximal effective concentration EC50). The parameter gamma accounts for the sigmoidicity of the drug effect.

"[LONGITUDINAL]

input = {V1, Q, V2, Vm, Km, gamma, E0, Emax, EC50}

EQUATION

ODE Type = stiff

PK:

;====== PK part of the model

; Parameter transformations

V = V1

k12 = Q/V1

k21 = Q/V2

; PK model definition

Cc = pkmodel (V, k12, k21, Vm, Km)

EQUATION

;====== PD part of the model

E = E0 + Emax * max (Cc,0) ^gamma/ (max (Cc,0)^gamma+EC50^gamma)

OUTPUT:

output = {Cc, E}”

3.7. PKPD model comparison

A total of seven different PKPD models were modeled, and the best PKPD model was selected by Sycomore software based on Corrected Bayesian Information Criteria (BICc) criteria. The stochastic estimation method was used to estimate the standard error and likelihood estimates. In this PKPD model, Fisher's matrix correlation estimations results were used to select the best PKPD model in addition to BICc criteria. The BICc of the PKPD6 and PKPD7 models were 169.88 and 173.06, respectively, but the selected best model was PKPD7(Figure 3.22). The BICc of the PKPD6 model was smaller than the PKPD7 model, but the correlation matrix of the estimates was not estimated correctly. The correlation matrix was one of the inputs for Simulix software for simulations of PKPD(Table 3.4).

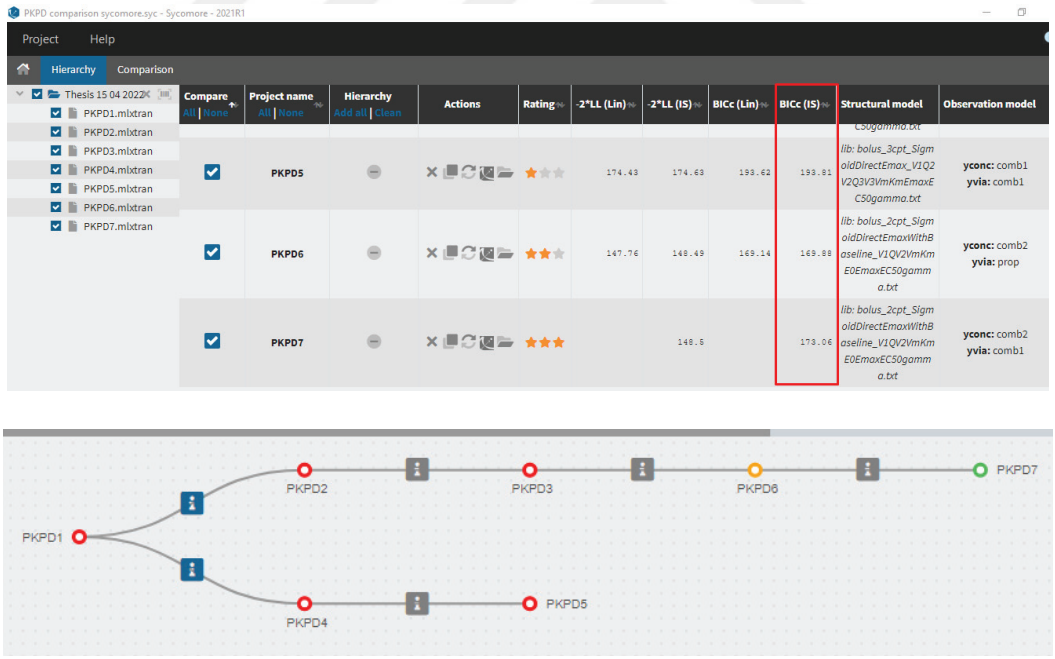

Figure 3. 23. PKPD model comparison in Sycomore software

Convergence indicator assessment was another important criterion for selecting the best PKPD model. PKPD7 had an excellent convergence indicator than the other PKPD models(Figure 3.23).

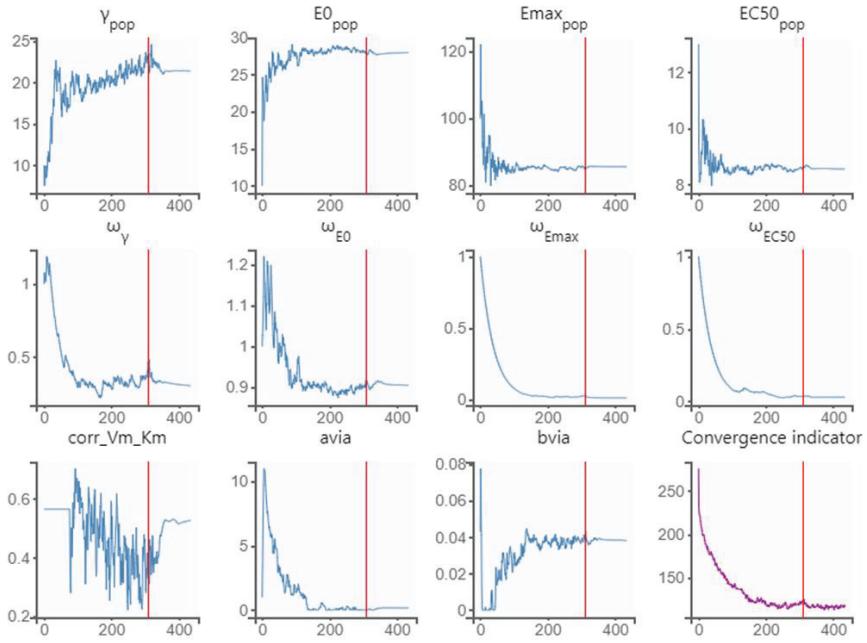

Figure 3. 24. PKPD model convergence indicator

Table 3.4 showed that the correlation matrix of the estimates of the PKPD7 model.İn model PKPD6 the model the correlation matrix was not estimated corrctlly, is showd error during estimation. In the PKPD7 model, the correlation matrix of the estimates was correctly estimated. The correlation matrix impacted the PKPD simulations, and a model with the correct correlation matrix was necessary, and the PKPD7 model was selected.

Table 3. 4. Correlation matrix of the estimates of PKPD7 model

	R.S.E.(%)										
gamma_pop	36.0	1									
E0_pop	52.9	0.04954	1								
Emax_pop	5.41	-0.2003	-0.1								
EC50_pop	14.9	-0.1474	-0.093	0.5609	1						
corr_Vm_Km	168	0.03349	0.07602	-0.4125	-0.7428	1					
omega_gamma	234	0.3244	0.0889	-0.5393	-0.4344	0.3376	1				
omega_E0	42.5	-0.0546	-0.05538	0.1339	0.1025	-0.08255	-0.09807	1			
omega_Emax	362	-0.1365	-0.09483	0.7598	0.4175	-0.2666	-0.5942	0.107	1		
omega_EC50	92.4	-0.03723	0.01736	-0.06334	-0.256	0.1816	0.1299	-0.01764	0.0115	1	
avia	1.63e+3	-0.1982	-0.06655	0.6038	0.6078	-0.407	-0.293	0.07807	0.2999	-0.1042	1
bvia	72.4	0.1469	0.02887	-0.2939	-0.4256	0.293	0.1296	-0.03513	-0.01042	0.05414	-0.8432

	MIN	MAX	MAX/MIN
Eigen values	0.08	3.85	47.88

3.8. PKPD model assessment

The PKPD7 model was selected as the best model for the presented PK and PD data using the Sycomore comparison method and other criteria. In the PKPD7 model, the population parameter estimates, individual estimates, estimated log-likelihood and information criteria, and distribution of the random effects were calculated by the PKPD model. The estimated standard error (RSE) was good in most population parameters. Omega indicated the fixed effects. The population parameter estimates of this experiment were V1(0.8 ml), V2(0.8 ml), Q(0.2 ml/h), Vm(0.4 ng/h), Km(10 ng/ml), Emax(85.74) and EC_{50}(8.56)(Table 3.5). Population PK analyses were done in plasm collected from human cancer patients, and the estimated human population PK parameters were 61.8 L/h, 112 L/h, 23.3 L, 1130 L for clearance, intercompartmental clearance, the volume of distribution in the main compartment, and volume of distribution in the peripheral compartment respectively[95].

Table 3. 5. Population parameter estimates of the PKPD7 model

	VALUE	STOCH. APPROX. S.E.	R.S.E. (%)
Fixed Effects			
V1_pop	0.8		
Q_pop	0.2		
V2_pop	0.8		
Vm_pop	0.4		
Km_pop	10		
gamma_pop	21.4	7.71	36
E0_pop	27.95	14.79	52.9
Emax_pop	85.54	4.62	5.41
EC50_pop	8.56	1.27	14.9
Standard Deviation of the Random Effects			
omega_V1	1		
omega_Q	1		
omega_V2	1		
omega_Vm	1		
omega_Km	1		
omega_gamma	0.3	0.71	234
omega_E0	0.9	0.38	42.5
omega_Emax	0.011	0.041	362
omega_EC50	0.029	0.027	92.4
Correlations			
corr_Vm_Km	0.53	0.89	168

Table 3.6 showed that the individual estimates for each dose in this experiment

Monolix uses population estimation, and the Emax and EC50 of the estimates of the three doses look similar.

Table 3. 6. Individual estimates of the PKPD7 model

id	V1	Q	V2	Vm	Km	gamma	E0	Emax	EC50
1	1.01	0.2	0.78	0.31	12.63	21.4	99.62	85.54	8.56
2	0.87	0.22	0.36	0.14	9.93	23.62	14.49	85.57	8.56
3	1.02	0.2	0.99	0.23	10.34	20.49	15.81	85.46	8.53

One of the criteria for selecting the best model that predicts the observed data in Monolix was the estimated log-likelihood and information criteria. Table 3.7 showed the estimated log-likelihood and information criteria of the PKPD7 model. The Sycomore result presented the other results in figure 3.22.

Table 3. 7. Estimated log-likelihood and info criteria of PKPD7 model

"-2 x log-likelihood (OFV)	148.5
Akaike Information Criteria (AIC)	170.5
Bayesian Information Criteria (BIC)	160.58
Corrected Bayesian Information Criteria (BICc)	173.06"

The Shapiro Wilk test tested the inter-individual and intra-individual and residual variability, and eta_E0 was statistical significance.

Table 3. 8. Distribution of the random effects of the PKPD7 model

	STATISTICS	P-VALUE
eta_V1	0.96	9.97E-01
eta_Q	0.97	9.56E-01
eta_V2	0.94	8.79E-01

eta_Vm	0.9	6.35E-01
eta_Km	0.94	8.67E-01
eta_gamma	0.89	3.33E-01
eta_E0	0.78	7.25E-02
eta_Emax	0.92	7.48E-01
eta_EC50	0.89	3.75E-01

3.9. Definition and exploration of PKPD in Simulix

The PKPD population simulations were done by Simulix software. The Monolix data was directly exported to Simulix software. The first step in the simulation was to define the treatment, the route of administration, the duration of treatment, and the amount of the drug. Defining the dosing time as a stat, regular, or loading dose before maintenance should be described as needed. In this simulation, the amount of the drug was defined as 10, 25, 35, and 100 ng/ml a single of each drug.

The second step in PKPD simulation was to explore individual parameters, outputs, and adjustments of the duration of the treatment based on the achievement of the steady-state for PK and PD. When the different times were used, the PK and PD graph changed. In the exploration step, the parameters and treatments could be replaced by other values, and we could see the change in the PK and PD graph change interactively. Before changing values, the reference mark was clicked to create broken lines to compare to the newly created diagram. In parameter exploration, the intercompartmental clearance(Q) value changed from 0.2 to 0.09, and the change in steady-state was observed in both PK and PD. The broken line indicated the reference value in the steady-state, but when the clearance decreased, the concentration of the drug increased, and the steady-state of PD was achieved in a short period (Figure 3.24). The data for this simulation was directly imported from Monolix PKPD modeling.

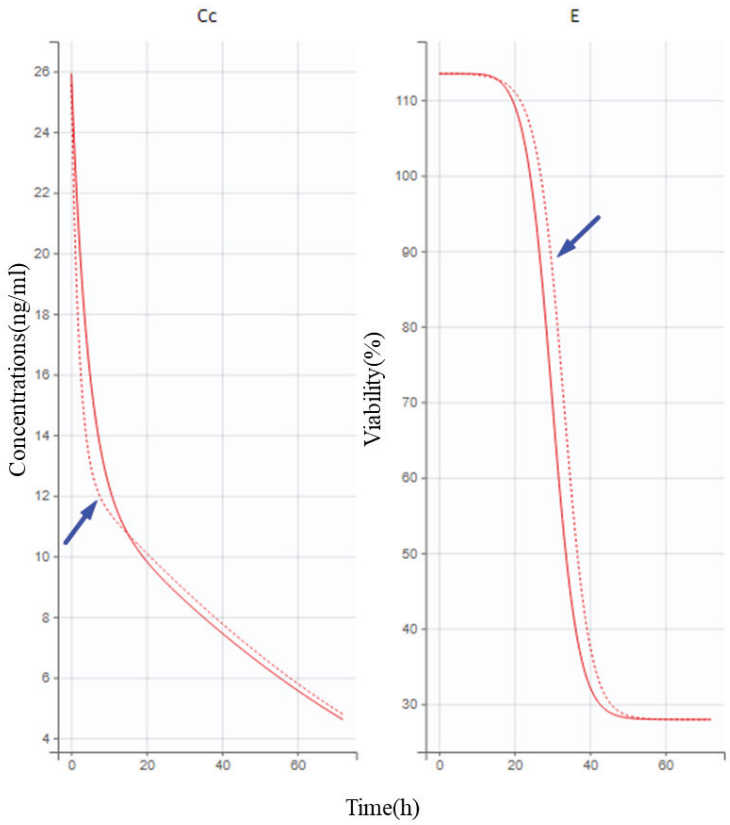

Figure 3. 25. Clearance parameter exploration of PKPD7 model

In this step, the defined treatments in the first step were selected, the time changed to 240 hours, and the steady state of the PD was significantly affected. The PD needs more time to reach a steady state. As shown in figure 3.25, the PK was not affected a lot, but the PD was affected a lot and needed more time to reach a steady state. When the time was changed, the effect was visible in the graph.

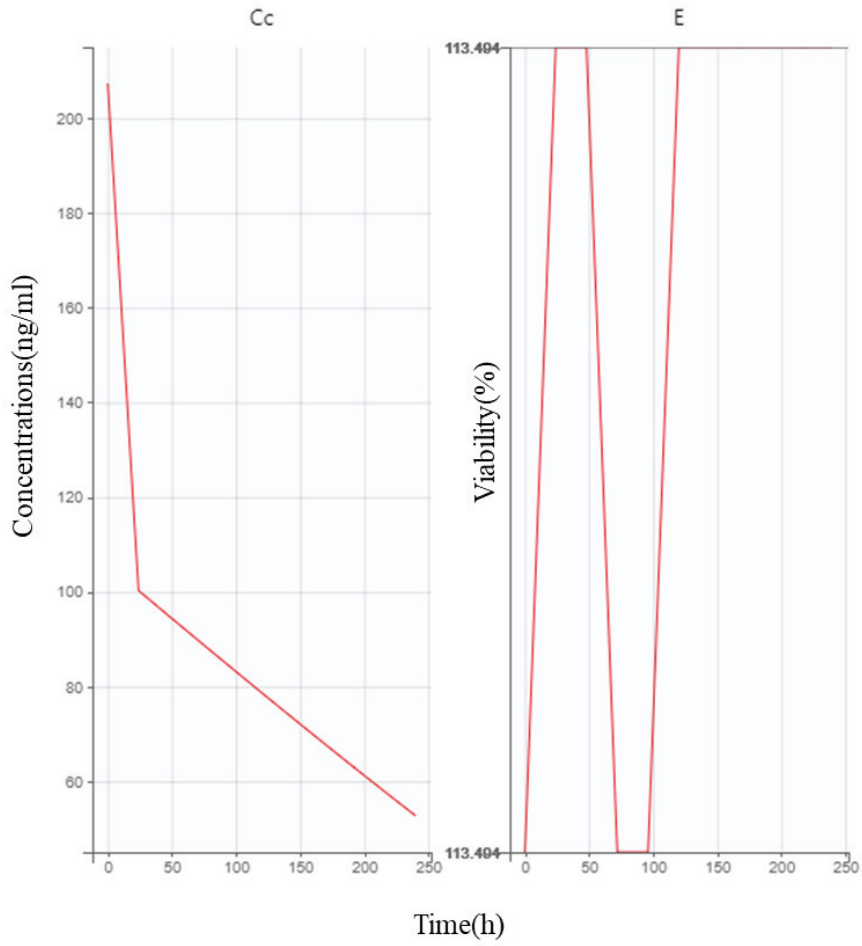

Figure 3. 26. PK and PD parameter explorations at 240 hours.

The 240 hours were not enough to reach a steady state for the PD concentration. The time increased to 360 hours, and both the PD and PK reached to steady state (Figure 3.26).

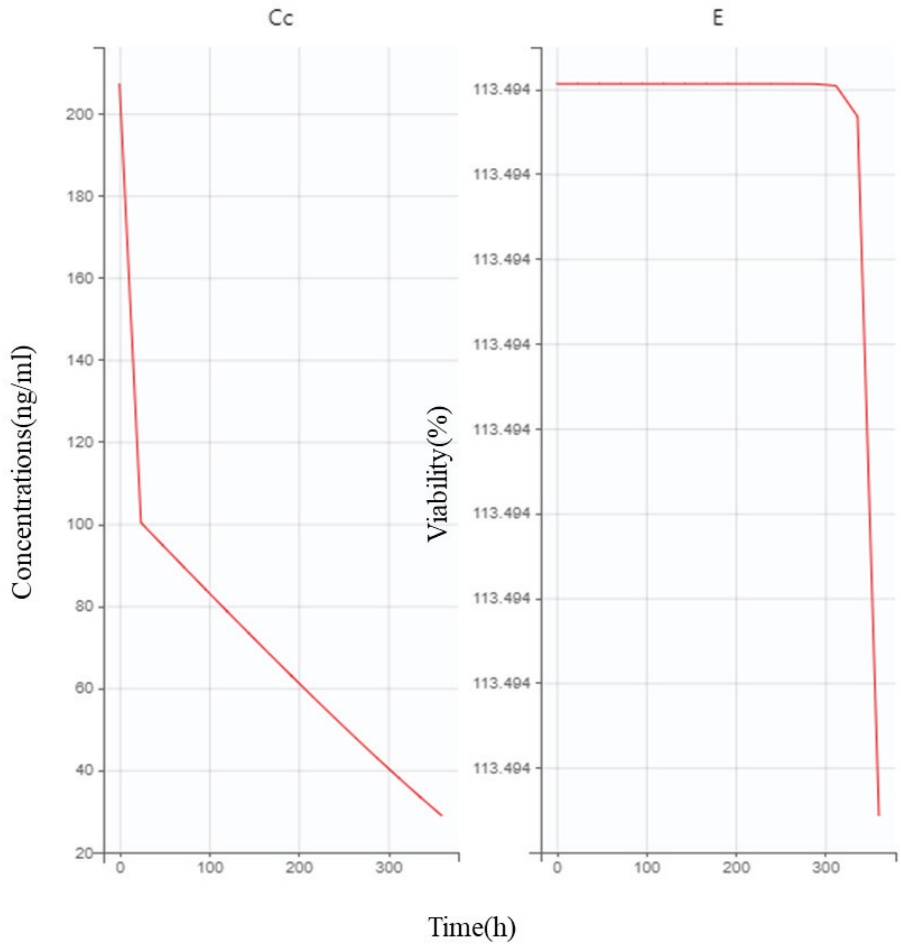

Figure 3. 27. PK and PD parameter explorations at 360 hours.

3.10. PKPD simulations

The third step in Simulix was simulations of PKPD parameters based on the inputs. In the simulation step, the new treatments and new outputs were selected, and the simulation was run. The simulation outputs were individual outputs and distributions for PK(Cc) and PD(E) as Cc versus time and E versus time. The Cc vs. time graph shows the decrease of the drug in a time-dependent manner. The 100 ng/ml dose had the highest drug concentration, and the 10 ng/ml dose had the lowest. The black line is the arithmetic mean, and the blue dots are the observed data.

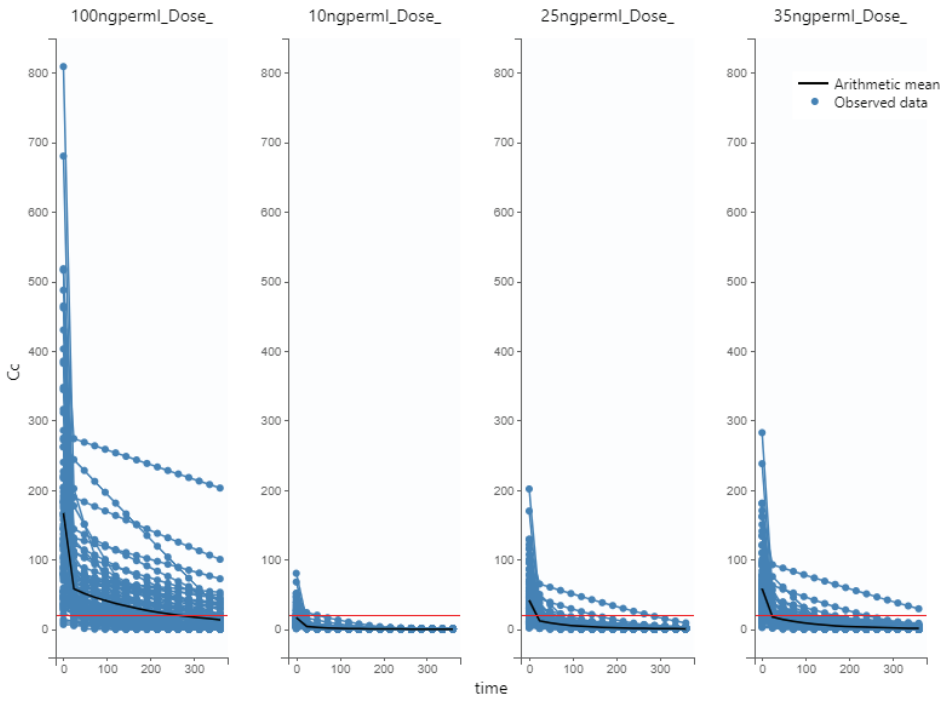

Figure 3. 28. Comparison of the PK of doses in simulations.

Figures 3.27 and 3.28 compared the PK of the four doses by the median value. The red line is the 80% cell death indicator mark that was pre-set during simulation definitions.

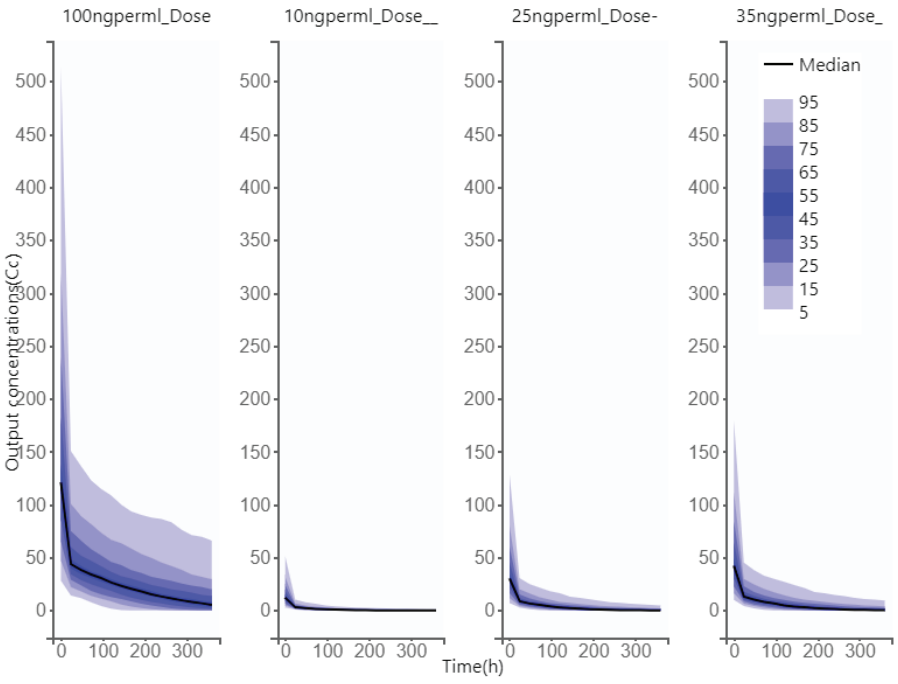

Figure 3. 29. Comparison of the PK of doses in simulations.

The spaghetti graph showed that most doses were enough to create good efficacy but not based on the set criteria. The red line indicates 80% efficacy of the drug.

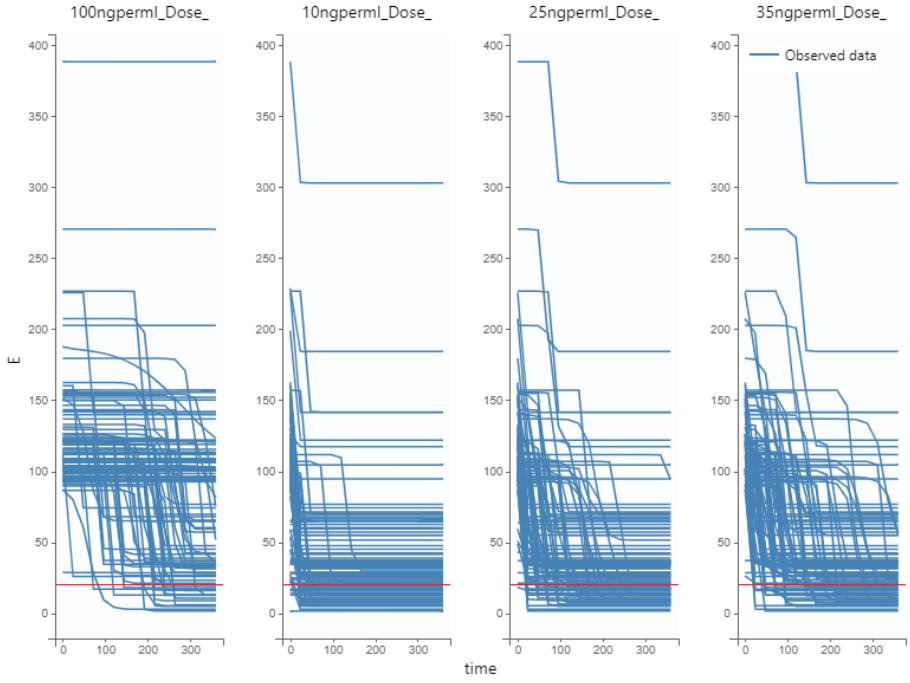

Figure 3. 30. The effect of the drug in a time-dependent manner.

In figure 3.30, the median of each dose was compared.

The 100 ng/ml dose had the highest median, followed by the 35 ng per ml dose.

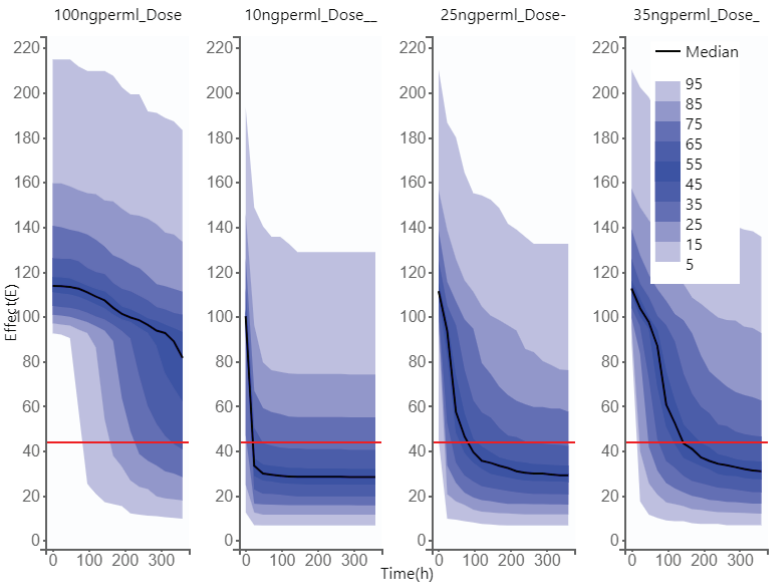

Figure 3. 31. Drug median comparison in the simulated drugs

In the simulation process, the population parameters(V1, V2, Km, Vm, Emax, and EC_{50}) of the PKPD model were simulated for each drug used in the simulation and presented in the following tables. The parameter simulation outputs were similar for all doses; the simulation outputs were used to calculate outcomes and endpoints (Table 3.9).

Table 3. 9. Parameter simulation output for each drug in Simulix

	10 NG/ML_DOSE				
	MIN	Q1	MEDIAN	Q3	MAX
V1	0.019	0.39	0.8	1.52	14.77
Q	0.013	0.11	0.2	0.39	2.28
V2	0.049	0.41	0.8	1.58	17.84
Vm	0.021	0.19	0.38	0.83	5.42
Km	0.34	5.35	10.69	20.67	253.06
gamma	8.82	17.3	21.64	26.08	48.66
E0	1.65	15.75	28.37	55.04	398.04
Emax	81.57	84.87	85.53	86.22	88.45
EC50	7.95	8.39	8.56	8.73	9.35

The end part of the simulation was investigating outcomes and endpoints. In this step, the drug's efficacy and safety were assessed. The best efficacy and safety drug was selected based on the defined criteria. Achievement of 80% of efficacy was the criteria for efficacy selection just for the predefined doses (10, 25, 35, and 100 ng/ml). For safety selection, the Cmax values of each drug were compared. The efficacy output was set to E, and Cc was set as output for the safety. For efficacy, percent true was assessed by an odds ratio greater than one, and for safety, the arithmetic means with a difference less than zero was used because the median of the drug had a significant difference.

The target was to achieve at least 80% drug efficacy. The 25 ng/ml dose was used as a reference in the efficacy and safety comparison procedure. The 10 ng/ml drug dose archived more true than the other doses(Figure 3.31).

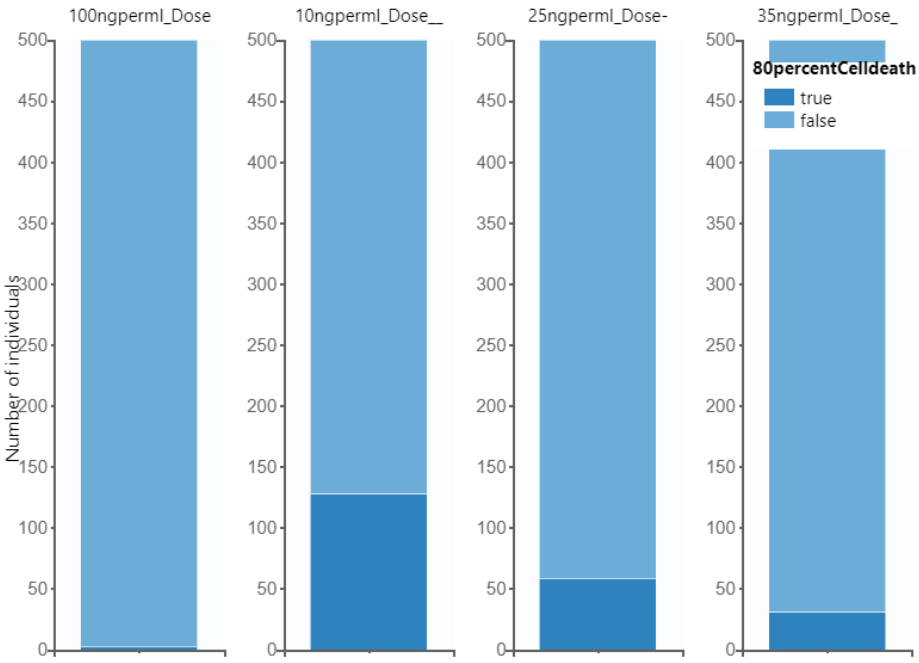

Figure 3. 32. Efficacy assessment in the PKPD7 model simulations

The 100 ng/ml drug dose had the highest Cmax, followed by 35 and 25 ng/ml doses. The drug dose with the highest Cmax might cause toxicity(figure 3.32).

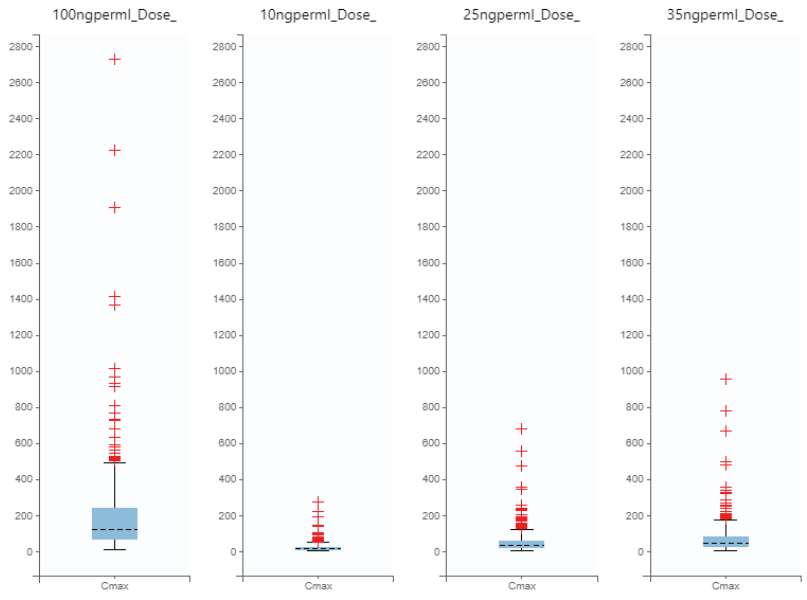

Figure 3. 33. Cmax assessment in PKPD7 model simulations

Additionally, in the 80% drug efficacy assessment 10 ng/ml drug dose had the highest percentage in target than other dose regiments. The 100 ng/ml dose had the lowest percentage on target. It does not mean the 100 ng/ml dose lost efficacy but is not the best dose based on the predefined criteria (Figure 3.33).

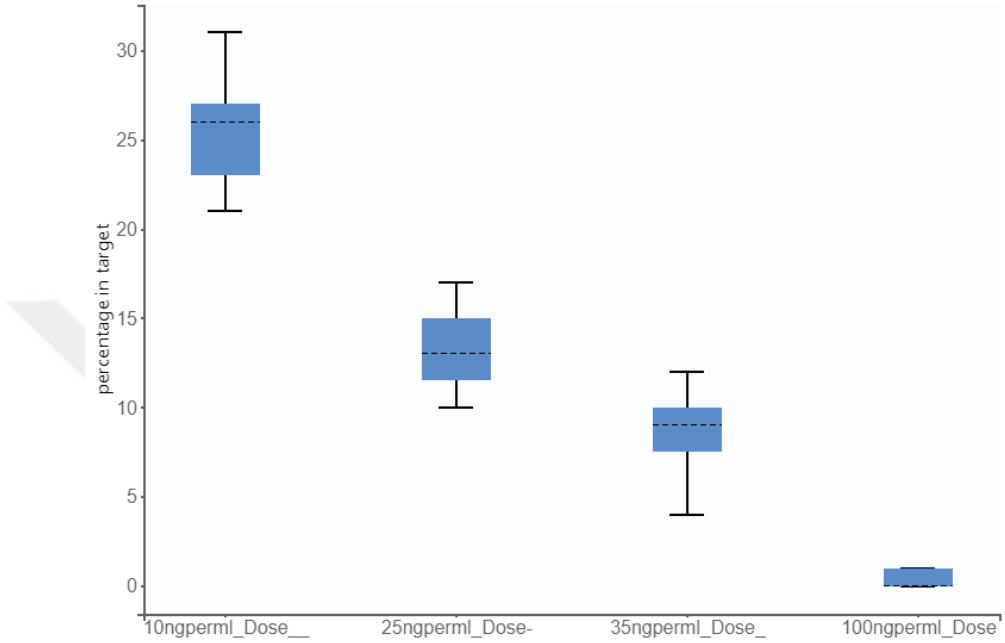

Figure 3. 34. Percentage in target for the selected doses in the PKPD7 model simulations

3.11. The outcome and endpoint results

The 10 ng /ml dose had the highest percent true(replicate three = 30) of all other doses in assessing efficacy based on the predefined criteria after five replicates run. The 100 ng/ml dose had the lowest percent true. Our target in this simulatiıon was to achieve 80% of efficacy. The 100 ng/ml dose showed almost 100% efficacy. Having 100% drug efficacy was good, but it was not selected as the best dose in this simulation based on our criteria. During efficacy assessment safety of the drug also should be in consideration. The drug with the highest dose might create toxicity, and the drug's safety would be in question. In dose selection, the drug's efficacy and safety had to be achieved[96].

Table 3. 10. The efficacy outcome in the PKPD7 simulations

Efficacy

10 ng/ml_Dose			25 ng/ml_Dose		
rep	percent True	Total True	rep	percent True	total true
1	26	26	1	10	10
2	26	26	2	12	12
3	30	30	3	15	15
4	22	22	4	10	10
5	24	24	5	11	11

35 ng/ml_Dose			100 ng/ml_Dose		
rep	percent True	totalTrue	rep	percent True	totalTrue
1	3	3	1	1	1
2	3	3	2	0	0
3	9	9	3	0	0
4	8	8	4	0	0
5	8	8	5	1	1

Table 3. 11. Safety out come in the PKPD7 simulations

Safety

10 ng/ml_Dose			25 ng/ml_Dose		
rep	arithmetic Mean	standard Deviation	arithmetic Mean	standard Deviation	
1	16.63	14.79	41.64	37.06	
2	20.6	25.57	51.62	64.26	
3	22.76	29.52	57.04	74.21	
4	17.04	15.91	42.67	39.87	
5	17.89	28.95	44.85	72.89	

35 ng/ml_Dose			100 ng/ml_Dose		
rep	arithmetic Mean	standard Deviation	arithmetic Mean	standard Deviation	
1	58.32	51.91	166.78	148.47	
2	72.3	90.06	206.8	257.8	
3	79.9	104.01	228.51	297.69	
4	59.77	55.85	170.93	159.75	
5	62.83	102.18	179.73	292.62	

In assessing the safety of the doses in the five replicates, the Cmax of 10 ng/ml was 228.51, and the Cmax of 100 ng/ml was 2729.75 ng/ml. The 10 ng/dose achieved 80% efficacy with low drug concentration. At the same time, if the dose is small and archives the target efficacy, the drug's safety might be excellent. The choice of dose in this simulation was 10 ng/ml dose. The Cmax of 100 ng/ml dose was 2729.75 ng/ml was too high compared with the Cmax of 10 ng/ml dose(270.22 ng/ml).

Table 3. 12. Cmax in the PKPD7 model simulations

Cmax

	MIN	P05	MEDIAN	P95	MAX
10ngperml_Dose_	0.67	2.82	12.05	50.7	270.22
25ngperml_Dose_	1.68	7.05	30.16	127.66	680.11
35ngperml_Dose_	2.36	9.88	42.24	179.01	953.39
100ngperml_Dose_	6.74	28.23	120.86	512.8	2729.75

The final result output in this simulation was group comparison. The efficacy and safety of the administered drug doses were evaluated statistically, and the final result was expressed as success and failure. This result confirms that the 10 ng/ml drug dose was the treatment choice in this simulation(Tables 3.13 and 3.14).

Table 3. 13. Efficacy group comparison in PKPD7 model simulations.

Efficacy

REP	10NGPERML_DOSE_			35NGPERML_DOSE_			100NGPERML_DOSE_		
	ODDSRATIO	P-VALUE	SUCCESS	ODDSRATIO	P-VALUE	SUCCESS	ODDSRATIO	P-VALUE	SUCCESS
1	Inf	1.53e-5	✓	0	1e+0	✗	0	1e+0	✗
2	Inf	6.1e-5	✓	0	1e+0	✗	0	1e+0	✗
3	Inf	3.05e-5	✓	0	1e+0	✗	0	1e+0	✗
4	Inf	2.44e-4	✓	0	1e+0	✗	0	1e+0	✗
5	Inf	1.22e-4	✓	0	1e+0	✗	0	1e+0	✗

Table 3. 14. Safety group comparison in PKPD7 model simulations.

Safety

REP	10NGPERML_DOSE_			35NGPERML_DOSE_			100NGPERML_DOSE_		
	DIFFERENCE	P-VALUE	SUCCESS	DIFFERENCE	P-VALUE	SUCCESS	DIFFERENCE	P-VALUE	SUCCESS
1	-25.01	<2.2e-16	✓	16.68	1e+0	✗	125.14	1e+0	✗
2	-31.02	1.1e-12	✓	20.69	1e+0	✗	155.18	1e+0	✗
3	-34.28	6.02e-12	✓	22.86	1e+0	✗	171.47	1e+0	✗
4	-25.64	<2.2e-16	✓	17.1	1e+0	✗	128.26	1e+0	✗
5	-26.96	8.72e-9	✓	17.98	1e+0	✗	134.88	1e+0	✗

CHAPTER 4

CONCLUSION

Cancer is a significant public health problem and a devastating disease; it kills millions of people each year around the globe. Despite the advanced science and technology in the modern era, cancer incidence, morbidity, and mortality are increasing exponentially[97, 98]. One of the main reasons for cancer death is cancer metastasis. There is no hundred percent effective drug for metastasized cancer. There are many treatment options for most cancer types, but for triple-negative breast cancer(TNBC), the choice of treatment is chemotherapy[22]. Drug resistance is one of the other problems that make most cancer chemotherapies useless[25].

The success rate of compounds for regulatory approval of oncology drugs is 5%[99]. One of the reasons for less success rate is an unforeseen lack of efficacy or toxicity, which is not recognized until the late stage of clinical trials[30]. In the current drug discovery and development process, the efficacy and toxicity of the drug are evaluated in 2D and animal testing.

The complex internal microenvironment of animals seems suitable for efficacy and toxicity assessment of drugs in the drug discovery and development process. Animal testing has many limitations despite the complex internal microenvironment; for instance, the tumor cell interaction with the immune system in animals and humans is not the same[32, 34]. The most common method used in the drug discovery and development process for efficacy and toxicity assessment is the 2D cell culture technique. Despite this, the 2D cell culturing technique does not simulate most of the internal biological systems of living things[35].

The other technique emerging currently for assessing drug efficacy and toxicity is organs-on-a-chip. "Organs-on-chip is microfluidic cell culture systems with controlled, dynamic conditions that directly emulate the physicochemical microenvironment of tissues in the human body[28]". In the organs-on-a-chip, different compartments are connected to allow the movement of molecules and chemicals from one compartment to the other and vice versa, allowing paracrine signaling and cell to cell communication[29].

In the 2D cell culture technique, there is no paracrine signaling, cell to cell communication, and extracellular matrix. After the drug administration, there are multiorgan interactions in the human body such as absorption, distribution, metabolism, and excretion (ADME) in a time-dependent manner[40, 41]. Unfortunately, there are no multiorgan interactions in the 2D cell culture technique, and the drug developed with this method shows a lack of efficacy and toxicity at the final stage of the clinical trial[30]. This research designed used multiorgan-on-a-chip (MOC) to assess the doxorubicin efficacy and toxicity in MDA-MB-231, HePG2, and MCF-10A cells, PKPD modeling, and simulations.

In this research, different organs-on-a-chip were designed and tested. Two organ-on-a-chips and one multiorgan-on-a-chip were designed and optimized. The organ-on-a-chip bonded with a microscopic slide had diffusion limitations and was excluded from the research. The diffusion limitation was confirmed by confocal imaging and Vcell simulation. In addition, the top-open organ-on-a-chip had diffusion limitations confirmed by experiment and Vcell simulation. The final chip design was multiorgan-on-a-chip with liver (HePG2) and breast (MDA-MB-231/MCF-10A) compartments with the same matrix thickness.

One of the objectives of this research was PKPD modeling. The data for PD modeling was obtained from viability experiments. The cells were stained with different dyes and imaged with confocal microscopy. Due to diffusion limitation on the chips, non-specific staining of cells by Nucred Dead 647 and NucGreen dye interaction with doxorubicin forced us to choose Alamar blue cell viability assay to get PD data.

The data for PK modeling was obtained from HPLC analysis of media samples collected during cell viability experiments. HPLC analysis was optimized with different mobile phase conditions, detectors, and amounts of samples. The retention time for all drugs and metabolites was identified, and different concentrations of the same drug were analyzed to see the method's reproducibility. The standard of the drugs was analyzed, and calibration curves were prepared for all the drugs and metabolites.

After having the PK and PD data, PKPD modeling was done by Monolix software. In PKPD modeling, the population parameter estimates, individual estimates, correlation matrix of the estimates, information criteria, and tests for distribution of the random effects were analyzed. Different PKPD models were modeled, and the best model was selected by Sycomore software.

After PKPD modeling was done in Monolix, the data was exported to Simulix software for drug simulations. In Simulix software, new treatment doses were defined, parameter and treatment exploration were done, and drug regimen comparisons were made. The best dose was selected based on the preset efficacy and safety criteria. This experiment's PK and PD data were generated from human cell lines cultured in 3D microenvironments. The Doxorubicin metabolism pathway needs distribution, metabolism, and excretion organs. In our experiment, the function of HePG2 cells is metabolism and excretion of doxorubicin. The mixture of cells and Matrigel in the liver and breast compartment is used to distribute doxorubicin. Moreover, we evaluated the pharmacological effect of doxorubicin by assessing the cells' viability at different time points. We can conclude that the data generated in this research are representative of the in vivo microenvironment.

To conclude, we developed a new multiorgan-on-a-chip (MOC) platform used for PKPD modeling and PKPD simulations that would be helpful in the preclinical trial to evaluate the efficacy and safety of drugs. In this research, the viability of each cell type was not evaluated because of the lack of a specific death indicator dye. Identifying the death ratio of each cell might help to understand the drug effect correctly in each cell line. In the future, using calceinAM, a fluorescent cell viability dye, generating PD data for each cell type and determining side effects of doxorubicin in each cell line is essential. Adding more organs to the MOC, such as heart tissue, to study the cytotoxicity of doxorubicin in different organs gives more efficient data for PKPD modeling.

REFERENCES

1. World Health Organization Cancer. https://www.who.int/news-room/fact-sheets/detail/cancer.

2. National Cancer İnstitute Understanding Cancer. https://www.cancer.gov/about-cancer/understanding (accessed March 26).

3. Nie, S.; Xing, Y.; Kim, G. J.; Simons, J. W., Nanotechnology Applications in Cancer. *Annual Review of Biomedical Engineering* **2007,** *9* (1), 257-288.

4. Hanahan, D.; Weinberg, R. A., Biological Hallmarks of Cancer. In *Holland-Frei Cancer Medicine*, 2017; pp 1-10.

5. Patel, A., Benign vs Malignant Tumors. *Jama Oncology* **2020,** *6* (9), 1488-1488.

6. Seyfried, T. N.; Huysentruyt, L. C., On the origin of cancer metastasis. *Critical reviews in oncogenesis* **2013,** *18* (1-2), 43-73.

7. Guan, X. M., Cancer metastases: challenges and opportunities. *Acta Pharmaceutica Sinica B* **2015,** *5* (5), 402-418.

8. Patanaphan, V.; Salazar, O. M.; Risco, R., Breast cancer: metastatic patterns and their prognosis. *South Med J* **1988,** *81* (9), 1109-12.

9. Community, C. S., Metastatic Breast Cancer. *Web Page* **2022**.

10. International Agency for Research on Cancer Cancer Fact Sheets. https://gco.iarc.fr/today/fact-sheets-cancers (accessed March 28,).

11. Torre, L. A.; Siegel, R. L.; Ward, E. M.; Jemal, A., Global Cancer Incidence and Mortality Rates and Trends-An Update. *Cancer Epidemiology Biomarkers & Prevention* **2016,** *25* (1), 16-27.

12. Sung, H.; Ferlay, J.; Siegel, R. L.; Laversanne, M.; Soerjomataram, I.; Jemal, A.; Bray, F., Global Cancer Statistics 2020: GLOBOCAN Estimates of Incidence and Mortality Worldwide for 36 Cancers in 185 Countries. *CA: A Cancer Journal for Clinicians* **2021,** *71* (3), 209-249.

13. Department of Economic and Social Affairs World Population Prospects 2019: Highlights. https://www.un.org/development/desa/publications/world-population-prospects-2019-highlights.html (accessed March 31,).

14. Bray, F.; Jemal, A.; Grey, N.; Ferlay, J.; Forman, D., Global cancer transitions according to the Human Development Index (2008-2030): a population-based study. *Lancet Oncology* **2012,** *13* (8), 790-801.

15. World Health Organization Breast cancer,. https://www.who.int/news-room/fact-sheets/detail/breast-cancer (accessed April 2,).

16. Libson, S.; Lippman, M., A review of clinical aspects of breast cancer. *International Review of Psychiatry* **2014,** *26* (1), 4-15.

17. Prager, G. W.; Braga, S.; Bystricky, B.; Qvortrup, C.; Criscitiello, C.; Esin, E.; Sonke, G. S.; Martínez, G. A.; Frenel, J.-S.; Karamouzis, M.; Strijbos, M.; Yazici, O.; Bossi, P.; Banerjee, S.; Troiani, T.; Eniu, A.; Ciardiello, F.; Tabernero, J.; Zielinski, C. C.; Casali, P. G.; Cardoso, F.; Douillard, J.-Y.; Jezdic, S.; McGregor, K.; Bricalli, G.; Vyas, M.; Ilbawi, A., Global cancer control: responding to the growing burden, rising costs and inequalities in access. *ESMO open* **2018,** *3* (2), e000285-e000285.

18. Vos, T.; Lim, S. S.; Abbafati, C.; L., C. J., Global burden of 369 diseases and injuries in 204 countries and territories, 1990&x2013;2019: a systematic analysis for the Global Burden of Disease Study 2019. *The Lancet* **2020,** *396* (10258), 1204-1222.

19. Alok, A. a. P., Sunil and Aggarwal, Ashish and Upadhyay, Nitin and Agarwal, Nupur and Kishore, Mallika, Nanotechnology: A boon in oral cancer diagnosis and therapeutics. *SRM Journal of Research in Dental Sciences* **2013,** *4* (4).

20. Gmeiner, W. H.; Ghosh, S., Nanotechnology for cancer treatment. *Nanotechnology Reviews* **2014,** *3* (2), 111-122.

21. Mansoori, B.; Mohammadi, A.; Davudian, S.; Shirjang, S.; Baradaran, B., The Different Mechanisms of Cancer Drug Resistance: A Brief Review. *Advanced Pharmaceutical Bulletin* **2017,** *7* (3), 339-348.

22. Welsh, J., Chapter 40 - Animal Models for Studying Prevention and Treatment of Breast Cancer. In *Animal Models for the Study of Human Disease*, Conn, P. M., Ed. Academic Press: Boston, 2013; pp 997-1018.

23. Lanz, H. L.; Saleh, A.; Kramer, B.; Cairns, J.; Ng, C. P.; Yu, J.; Trietsch, S. J.; Hankemeier, T.; Joore, J.; Vulto, P.; Weinshilboum, R.; Wang, L., Therapy response testing of breast cancer in a 3D high-throughput perfused microfluidic platform. *BMC Cancer* **2017,** *17* (1), 709-709.

24. American Cancer Society Chemotherapy for Breast Cancer. https://www.cancer.org/cancer/breast-cancer/treatment/chemotherapy-for-breast-cancer.html (accessed March 26,).

25. Holohan, C.; Van Schaeybroeck, S.; Longley, D. B.; Johnston, P. G., Cancer drug resistance: an evolving paradigm. *Nature Reviews Cancer* **2013,** *13* (10), 714-726.

26. Gottesman, M. M., Mechanisms of cancer drug resistance. *Annual Review of Medicine* **2002,** *53*, 615-627.

27. Housman, G.; Byler, S.; Heerboth, S.; Lapinska, K.; Longacre, M.; Snyder, N.; Sarkar, S., Drug Resistance in Cancer: An Overview. *Cancers* **2014,** *6* (3), 1769-1792.

28. van den Berg, A.; Mummery, C. L.; Passier, R.; van der Meer, A. D., Personalised organs-on-chips: functional testing for precision medicine. *Lab on a Chip* **2019,** *19* (2), 198-205.

29. Lee, H.; Kim, D. S.; Ha, S. K.; Choi, I.; Lee, J. M.; Sung, J. H., A pumpless multi-organ-on-a-chip (MOC) combined with a pharmacokinetic-pharmacodynamic (PK-PD) model. *Biotechnology and Bioengineering* **2017,** *114* (2), 432-443.

30. Lin, J. H.; Lu, A. Y. H., Role of pharmacokinetics and metabolism in drug discovery and development. *Pharmacological Reviews* **1997,** *49* (4), 403-449.

31. Hingorani, A. D.; Kuan, V.; Finan, C.; Kruger, F. A.; Gaulton, A.; Chopade, S.; Sofat, R.; MacAllister, R. J.; Overington, J. P.; Hemingway, H.; Denaxas, S.; Prieto, D.; Casas, J. P., Improving the odds of drug development success through human genomics: modelling study. *Scientific Reports* **2019,** *9* (1), 18911.

32. Dickson, M.; Gagnon, J. P., Key factors in the rising cost of new drug discovery and development. *Nature Reviews Drug Discovery* **2004,** *3* (5), 417-429.

33. Ferdowsian, H. R.; Beck, N., Ethical and Scientific Considerations Regarding Animal Testing and Research. *Plos One* **2011,** *6* (9), 4.

34. Lanz, H. L.; Saleh, A.; Kramer, B.; Cairns, J.; Ng, C. P.; Yu, J.; Trietsch, S. J.; Hankemeier, T.; Joore, J.; Vulto, P.; Weinshilboum, R.; Wang, L., Therapy response testing of breast cancer in a 3D high-throughput perfused microfluidic platform. *Bmc Cancer* **2017,** *17*.

35. Meyvantsson, I.; Beebe, D. J., Cell Culture Models in Microfluidic Systems. *Annual Review of Analytical Chemistry* **2008,** *1*, 423-449.

36. Abbott, A., Cell culture: Biology's new dimension. *Nature* **2003,** *424* (6951), 870-872.

37. Lee, G. Y.; Kenny, P. A.; Lee, E. H.; Bissell, M. J., Three-dimensional culture models of normal and malignant breast epithelial cells. *Nature Methods* **2007,** *4* (4), 359-365.

38. Matsusaki, M.; Case, C. P.; Akashi, M., Three-dimensional cell culture technique and pathophysiology. *Advanced Drug Delivery Reviews* **2014,** *74*, 95-103.

39. Tsai, H.-F.; Trubelja, A.; Shen, A. Q.; Bao, G., Tumour-on-a-chip: microfluidic models of tumour morphology, growth and microenvironment. *Journal of the Royal Society Interface* **2017,** *14* (131).

40. Sung, J. H.; Dhiman, A.; Shuler, M. L., A Combined Pharmacokinetic-Pharmacodynamic (PK-PD) Model for Tumor Growth in the Rat with UFT Administration. *Journal of Pharmaceutical Sciences* **2009,** *98* (5), 1885-1904.

41. Lee, S. Y.; Lee, B. R.; Lee, J.; Kim, S.; Kim, J. K.; Jeong, Y. H.; Jin, S., Microscale Diffusion Measurements and Simulation of a Scaffold with a Permeable Strut. *International Journal of Molecular Sciences* **2013,** *14* (10), 20157-20170.

42. Hwang, H.; Park, J.; Shin, C.; Do, Y.; Cho, Y.-K., Three dimensional multicellular co-cultures and anti-cancer drug assays in rapid prototyped multilevel microfluidic devices. *Biomedical Microdevices* **2013,** *15* (4), 627-634.

43. Zervantonakis, I. K.; Kothapalli, C. R.; Chung, S.; Sudo, R.; Kamm, R. D., Microfluidic devices for studying heterotypic cell-cell interactions and tissue specimen cultures under controlled microenvironments. *Biomicrofluidics* **2011,** *5* (1).

44. Zhao, Y.; Kankala, R. K.; Wang, S. B.; Chen, A. Z., Multi-Organs-on-Chips: Towards Long-Term Biomedical Investigations. *Molecules* **2019,** *24* (4), 22.

45. FDA The Drug Development Process. https://www.fda.gov/patients/learn-about-drug-and-device-approvals/drug-development-process (accessed March 27,).

46. Matthews, H.; Hanison, J.; Nirmalan, N., "Omics"-Informed Drug and Biomarker Discovery: Opportunities, Challenges and Future Perspectives. *Proteomes* **2016,** *4* (3), 28.

47. Wysowski, D. K.; Swartz, L., Adverse drug event surveillance and drug withdrawals in the United States, 1969-2002 - The importance of reporting suspected reactions. *Archives of Internal Medicine* **2005,** *165* (12), 1363-1369.

48. Hay, M.; Thomas, D. W.; Craighead, J. L.; Economides, C.; Rosenthal, J., Clinical development success rates for investigational drugs. *Nature Biotechnology* **2014,** *32* (1), 40-51.

49. Lynch, S.; Pridgeon, C. S.; Duckworth, C. A.; Sharma, P.; Park, B. K.; Goldring, C. E. P., Stem cell models as an in vitro model for predictive toxicology. *Biochemical Journal* **2019,** *476*, 1149-1158.

50. Prasad, V.; Mailankody, S., Research and Development Spending to Bring a Single Cancer Drug to Market and Revenues After Approval. *JAMA Internal Medicine* **2017,** *177* (11), 1569-1575.

51. Oleaga, C.; Bernabini, C.; Smith, A. S. T.; Srinivasan, B.; Jackson, M.; McLamb, W.; Platt, V.; Bridges, R.; Cai, Y.; Santhanam, N.; Berry, B.; Najjar, S.; Akanda, N.; Guo, X.; Martin, C.; Ekman, G.; Esch, M. B.; Langer, J.; Ouedraogo, G.; Cotovio, J.; Breton, L.; Shuler, M. L.; Hickman, J. J., Multi-Organ toxicity demonstration in a functional human in vitro system composed of four organs. *Scientific Reports* **2016,** *6*.

52. Sung, J. H.; Kam, C.; Shuler, M. L., A microfluidic device for a pharmacokinetic-pharmacodynamic (PK-PD) model on a chip. *Lab on a Chip* **2010,** *10* (4), 446-455.

53. Meibohm, B.; Derendorf, H., Basic concepts of pharmacokinetic/pharmacodynamic (PK/PD) modelling. *International Journal of Clinical Pharmacology and Therapeutics* **1997,** *35* (10), 401-413.

54. Sung, J. H.; Shuler, M. L., A micro cell culture analog (μCCA) with 3-D hydrogel culture of multiple cell lines to assess metabolism-dependent cytotoxicity of anti-cancer drugs. *Lab on a Chip* **2009,** *9* (10), 1385-1394.

55. Sung, J. H.; Esch, M. B.; Shuler, M. L., Integration of in silico and in vitro platforms for pharmacokinetic–pharmacodynamic modeling. *Expert Opinion on Drug Metabolism & Toxicology* **2010,** *6* (9), 1063-1081.

56. National Center for Biotechnology Information, PubChem Compound Summary for CID 31703, Doxorubicin. **2021**.

57. Guo, Y.; Lee, H.; Jeong, H., Gut microbiota in reductive drug metabolism. *Prog Mol Biol Transl Sci* **2020,** *171*, 61-93.

58. Ferreira, L. L.; Oliveira, P. J.; Cunha-Oliveira, T., Chapter 33 - Epigenetics in Doxorubicin Cardiotoxicity. In *Pharmacoepigenetics*, Cacabelos, R., Ed. Academic Press: 2019; Vol. 10, pp 837-846.

59. Thorn, C. F.; Oshiro, C.; Marsh, S.; Hernandez-Boussard, T.; McLeod, H.; Klein, T. E.; Altman, R. B., Doxorubicin pathways: pharmacodynamics and adverse effects. *Pharmacogenetics and Genomics* **2011,** *21* (7).

60. Zhao, L.; Zhang, B., Doxorubicin induces cardiotoxicity through upregulation of death receptors mediated apoptosis in cardiomyocytes. *Scientific Reports* **2017,** *7* (1), 44735.

61. Shen, F.; Chu, S.; Bence, A. K.; Bailey, B.; Xue, X.; Erickson, P. A.; Montrose, M. H.; Beck, W. T.; Erickson, L. C., Quantitation of Doxorubicin Uptake, Efflux, and Modulation of Multidrug Resistance (MDR) in MDR Human Cancer Cells. *Journal of Pharmacology and Experimental Therapeutics* **2008,** *324* (1), 95.

62. Whirl-Carrillo, M.; Huddart, R.; Gong, L.; Sangkuhl, K.; Thorn, C. F.; Whaley, R.; Klein, T. E., An Evidence-Based Framework for Evaluating Pharmacogenomics Knowledge for Personalized Medicine. *Clin Pharmacol Ther* **2021,** *110* (3), 563-572.

63. Esch, M. B.; Mahler, G. J.; Stokor, T.; Shuler, M. L., Body-on-a-chip simulation with gastrointestinal tract and liver tissues suggests that ingested nanoparticles have the potential to cause liver injury. *Lab on a Chip* **2014,** *14* (16), 3081-3092.

64. Iori, E.; Vinci, B.; Murphy, E.; Marescotti, M. C.; Avogaro, A.; Ahluwalia, A., Glucose and Fatty Acid Metabolism in a 3 Tissue In-Vitro Model Challenged with Normo- and Hyperglycaemia. *Plos one* **2012,** *7* (4), e34704.

65. Viravaidya, K.; Sin, A.; Shuler, M. L., Development of a microscale cell culture analog to probe naphthalene toxicity. *Biotechnology Progress* **2004,** *20* (1), 316-323.

66. Wagner, I.; Materne, E.-M.; Brincker, S.; Süßbier, U.; Frädrich, C.; Busek, M.; Sonntag, F.; Sakharov, D. A.; Trushkin, E. V.; Tonevitsky, A. G.; Lauster, R.; Marx, U., A dynamic multi-organ-chip for long-term cultivation and substance testing proven by 3D human liver and skin tissue co-culture. *Lab on a Chip* **2013,** *13* (18), 3538-3547.

67. Moller, S.; Bernardi, M., Interactions of the heart and the liver. *European Heart Journal* **2013,** *34* (36), 2804.

68. Lautt, W. W., Colloquium Series on Integrated Systems Physiology: From Molecule to Function to Disease. In *Hepatic Circulation: Physiology and Pathophysiology*, Morgan & Claypool Life Sciences.

69. Price, P. S.; Conolly, R. B.; Chaisson, C. F.; Gross, E. A.; Young, J. S.; Mathis, E. T.; Tedder, D. R., Modeling Interindividual Variation in Physiological Factors Used in PBPK Models of Humans. *Critical Reviews in Toxicology* **2003,** *33* (5), 469-503.

70. Abaci, H. E.; Shuler, M. L., Human-on-a-chip design strategies and principles for physiologically based pharmacokinetics/pharmacodynamics modeling. *Integrative Biology* **2015,** *7* (4), 383-391.

71. Xu, H.; Wu, J.; Chu, C.-C.; Shuler, M. L., Development of disposable PDMS micro cell culture analog devices with photopolymerizable hydrogel encapsulating living cells. *Biomedical Microdevices* **2012,** *14* (2), 409-418.

72. Andersen, V.; Sonne, J.; Sletting, S.; Prip, A., The volume of the liver in patients correlates to body weight and alcohol consumption. *Alcohol and alcoholism* **2000,** *35* (5), 531-532.

73. McGhee, D. E.; Steele, J. R., Breast volume and bra size. *International Journal of Clothing Science and Technology* **2011,** *23* (5), 351-360.

74. Mankoff, D. A.; Dunnwald, L. K.; Gralow, J. R.; Ellis, G. K.; Charlop, A.; Lawton, T. J.; Schubert, E. K.; Tseng, J.; Livingston, R. B., Blood flow and metabolism in locally advanced breast cancer: Relationship to response to therapy. *Journal of Nuclear Medicine* **2002,** *43* (4), 500-509.

75. Faermann, R.; Sperber, F.; Schneebaum, S.; Barsuk, D., Tumor-to-Breast Volume Ratio as Measured on MRI: A Possible Predictor of Breast-Conserving Surgery versus Mastectomy. *Israel Medical Association Journal* **2014,** *16* (2), 101-105.

76. Biosciences, A. Cell Viability Assay based on Metabolic Activity. https://www.abpbio.com/product/cell-viability-assay-based-on-metabolic-activity/ (accessed 23).

77. JoVE Science Education Database, Analytical Chemistry. High-Performance Liquid Chromatography (HPLC). JoVE, Cambridge, MA: 2021.

78. Weston, A.; Brown, P. R., Chapter 1 - High-Performance Liquid Chromatography. In *HPLC and CE*, Weston, A.; Brown, P. R., Eds. Academic Press: San Diego, 1997; pp 1-23.

79. Daeihamed, M.; Haeri, A.; Dadashzadeh, S., A Simple and Sensitive HPLC Method for Fluorescence Quantitation of Doxorubicin in Micro-volume Plasma: Applications to Pharmacokinetic Studies in Rats. *Iran J Pharm Res* **2015,** *14* (Suppl), 33-42.

80. Arnold, R. D.; Slack, J. E.; Straubinger, R. M., Quantification of doxorubicin and metabolites in rat plasma and small volume tissue samples by liquid chromatography/electrospray tandem mass spectroscopy. *Journal of chromatography b-analytical technologies in the biomedical and life sciences* **2004,** *808* (2), 141-152.

81. Daeihamed, M.; Haeri, A.; Ostad, S. N.; Akhlaghi, M. F.; Dadashzadeh, S., Doxorubicin-loaded liposomes: enhancing the oral bioavailability by modulation of physicochemical characteristics. *Nanomedicine* **2017,** *12* (10), 1187-1202.

82. Al-Abd, A. M.; Kim, N. H.; Song, S. C.; Lee, S. J.; Kuh, H. J., A simple HPLC method for doxorubicin in plasma and tissues of nude mice. *Archives of pharmacal research* **2009,** *32* (4), 605-611.

83. van Asperen, J.; van Tellingen, O.; Beijnen, J. H., Determination of doxorubicin and metabolites in murine specimens by high-performance liquid chromatography. *Journal of chromatography b-analytical technologies in the biomedical and life sciences* **1998,** *712* (1-2), 129-143.

84. Alvarez-Cedron, L.; Sayalero, M. L.; Lanao, J. M., High-performance liquid chromatographic validated assay of doxorubicin in rat plasma and tissues. *Journal of chromatography b-analytical technologies in the biomedical and life sciences* **1999,** *721* (2), 271-278.

85. Kummerle, A.; Krueger, T.; Dusmet, M.; Vallet, C.; Pan, Y.; Ris, H. B.; Decosterd, L. A., A validated assay for measuring doxorubicin in biological fluids and tissues in an isolated lung perfusion model: matrix effect and heparin interference strongly influence doxorubicin measurements. *Journal of pharmaceutical and biomedical analysis* **2003,** *33* (3), 475-494.

86. Shah, M.; Bourner, L.; Ali, S.; Al-Enazy, S.; Youssef, M. M.; Fisler, M.; Rytting, E., HPLC Method Development for Quantification of Doxorubicin in Cell Culture and Placental Perfusion Media. *Separations* **2018,** *5* (1).

87. Ricciarello, R.; Pichini, S.; Pacifici, R.; Altieri, I.; Pellegrini, M.; Fattorossi, A.; Zuccaro, P., Simultaneous determination of epirubicin, doxorubicin and their principal metabolites in human plasma by high-performance liquid chromatography and electrochemical detection. *Journal of chromatography B* **1998,** *707* (1-2), 219-225.

88. Chang, H. P.; Cheung, Y. K.; Shah, D. K., Whole-Body Pharmacokinetics and Physiologically Based Pharmacokinetic Model for Monomethyl Auristatin E (MMAE). *J Clin Med* **2021,** *10* (6), 1332.

89. Wang, Y. I.; Carmona, C.; Hickman, J. J.; Shuler, M. L., Multiorgan Microphysiological Systems for Drug Development: Strategies, Advances, and Challenges. *Adv Healthc Mater* **2018,** *7* (2), 10.1002/adhm.201701000.

90. B. Heymsfield, S.; Wang, Z.; Baumgartner, R. N.; Ross, R., Human Body Composition: Advances in Models and Methods. *Annual Review of Nutrition* **1997,** *17* (1), 527-558.

91. Lixoft Monolix version 2021R1. Antony, France: Lixoft SAS, 2021. http://lixoft.com/products/monolix/ (accessed 20 May 2022).

92. Choi, C.-H., ABC transporters as multidrug resistance mechanisms and the development of chemosensitizers for their reversal. *Cancer Cell Int* **2005,** *5*, 30-30.

93. Benet, L. Z.; Zia-Amirhosseini, P., Basic principles of pharmacokinetics. *Toxicol Pathol* **1995,** *23* (2), 115-23.

94. Barreto, E. F.; Larson, T. R.; Koubek, E. J., Drug Excretion. In *Reference Module in Biomedical Sciences*, Elsevier: 2021.

95. Joerger, M.; Huitema, A. D. R.; Meenhorst, P. L.; Schellens, J. H. M.; Beijnen, J. H., Pharmacokinetics of low-dose doxorubicin and metabolites in patients with AIDS-related Kaposi sarcoma. *Cancer Chemotherapy and Pharmacology* **2005,** *55* (5), 488-496.

96. Brown, M. J., A rational basis for selection among drugs of the same class. *Heart* **2003,** *89* (6), 687-694.

97. Zhang, Y.; Bai, Y.; Yan, B., Functionalized carbon nanotubes for potential medicinal applications. *Drug Discovery Today* **2010,** *15* (11-12), 428-435.

98. Sutradhar, K. B.; Amin, M. L., Nanotechnology in Cancer Drug Delivery and Selective Targeting. *ISRN Nanotechnology* **2014,** *2014*, 939378.

99. De Mello, C. P. F.; Carmona-Moran, C.; McAleer, C. W.; Perez, J.; Coln, E. A.; Long, C. J.; Oleaga, C.; Riu, A.; Note, R.; Teissier, S.; Langer, J.; Hickman, J. J., Microphysiological heart-liver body-on-a-chip system with a skin mimic for evaluating topical drug delivery. *Lab on a Chip* **2020,** *20* (4), 749-759.

VITA

Educational

2017-2022 Ph.D. in Bioengineering, Department of Biotechnology and Bioengineering, Izmir Institute of Technology, Turkey

Dissertation "Multi-organ-on-a-chip (MOC) for cancer drug testing" (Patent on progress).

Advisors: Prof. Dr. Devrim Pesen OKVUR & Prof. Dr. Esra Erdal Bağrıyanık

2012-2014 MSc. In Clinical Laboratory Science (Specialty in Clinical Chemistry), Department of Medical Laboratory Sciences & Pathology, Jimma University, Ethiopia

Thesis "Diabetes mellitus and risk factors in human immunodeficiency virus-infected individuals at Jimma University Specialized Hospital, Southwest Ethiopia."

Advisors: Tilahun Yemane Shenkute (MD, Associate professor), Waqtola Cheneke Gebisa (Associate professor)

2006-2010 BSc. In Medical Laboratory Technology (MLT), Department of Medical Laboratory Sciences & Pathology, Jimma University, Ethiopia

The research project "Mycobacterium tuberculosis in Lymph Node Biopsy Paraffin-Embedded Sections." Supervisor: Mona Mohammed (M.D., Professor)

Work Experience

11/2014-2016 Lecturer and Researcher, Department of Medical Laboratory Sciences & Pathology, Jimma University, Ethiopia

06/2010-2012 Graduate assistant II & Senior Medical Laboratory Technologist, Department of Medical Laboratory Sciences & Pathology and Jimma University Hospital Laboratory, Jimma University, Ethiopia

Laboratory Skills

- Lab-on-a-chip (Multiorgan-on-a-chip (MOC) design with AutoCAD software, MOC mold printing by Formlabs 3D printer Form 2, molds processing after printed, chips fabrication and bonding, and setting up in vitro controlled experiment on Multiorgan-on-a-chip).
- Cell culture (Two-dimensional (2D) and Three-dimensional (3D) Cell culture of MDA-MB-231, HePG2, and MCF-10A cell lines.
- Confocal microscopy (Live cell imaging, Time-lapse imaging, Z-stack imaging)
- Image analysis (separating image channels with python code, Macro code writing for automatic image analysis, Image analysis by İmage J/Fiji).
- Drug analysis with High-performance liquid chromatography (HPLC) (mobile phase preparation, stationary phase adjustment, Chromatogram interpretation).
- Virtual cell (Vcell) simulations (AutoCAD designed biochips simulation of fluid flow from one compartment in the Multiorgan-on-a-chip).
- Analysis of Clinical Chemistry tests from patient samples by different Clinical chemistry automation (Liver function test, Kidney function test, cardiac function test, Urinalysis, Hormone analysis, Thyroid function tests, Serum glucose analysis, and Lipid profile analysis, and Electrolyte analysis).
- Therapeutic drug monitoring tests from blood and urine samples
- Tumor marker analysis (PSA, CA-125, CA-15, CA-27…)
- Histopathological tissue biopsy preparation (processing, trimming, sectioning, staining, and microscopy).
- PCR
- Microbiological cell culture

Teaching Experience

11/2014-07/2016 MELT 215 Clinical Chemistry I

MELT 406 Clinical Chemistry III

MeLS 430 Urinalysis and Body fluid analysis,

MELT 102 Introduction to Medical Laboratory Science

Clinical Experience

- Giving Clinical service at Jimma University Specialized Hospital Laboratory
- Preparation of different clinical specimens, reagents, and chemicals
- Participating in clinical trial research

Computer Skills

- Microsoft office
- Image J/Fiji
- R Programming
- SPSS
- MATLAB(SimBiology)
- Vcell simulation
- Python Programming
- AutoCAD
- Monolix suite (PKPD Modeling, PKPD Simulation)

Awards

- Turkish government scholarship (2016/17)
- Keystone symposia global health travel award, funded by bill & Melinda Gates Foundation, Emerging Technologies in Vaccine Discovery, and Development,

joint with Progress and Pathways Toward an Effective HIV Vaccine, Date: January 28 - February 01, 2018, Location: Fairmont Banff Springs, Banff, AB, Canada

Languages

- Amharic (Native)
- English (All of my undergraduate, Master's, and Ph.D. education medium of instruction is English)
- Turkish (C1)

Peer-reviewed journal articles

1. Bekele S, Yohannes T, Mohammed AE. Dyslipidemia and associated factors among Diabetic patients attending Durame General Hospital in Southern Nations, Nationalities, and People's Region. Diabetes, Metabolic Syndrome and Obesity: Targets and Therapy. 2017; 10:265—271DOI https://doi.org/10.2147/DMSO.S135064
2. Abdurehman Eshete Mohammed, Tilahun Yemane Shenkute, Waqtola Cheneke Gebisa. Diabetes mellitus and risk factors in human immunodeficiency virus-infected individuals at Jimma University Specialized Hospital, Southwest Ethiopia. Diabetes, Metabolic Syndrome and Obesity: Targets and Therapy .2015, Volume 8:197-206. DOI http://dx.doi.org/10.2147/DMSO.S80084
3. Bahiru Terefe, Endalew Zemene and Abdurehman E. Mohammed. Intestinal helminth Infections among inmates in Bedele prison with emphasis on soil-transmitted helminths. BMC Research Notes 2015 8:779
4. Abdurehman Eshete, Zeleke Mekonnen, and Ahmed Zeynudin, "Trichomonas vaginalis Infection among Pregnant Women in Jimma University Specialized Hospital, Southwest Ethiopia," ISRN Infectious Diseases, vol. 2013, Article ID 485439, 5 pages,2013. doi:10.5402/2013/485439
5. Abdurehman Eshete, Ahmed Zeyinudin, Solomon Ali, Solomon Abera, and Mona Mohammed. M. tuberculosis in Lymph Node Biopsy Paraffin-Embedded

Sections. Tuberculosis Research and Treatment, vol. 2011, Article ID 127817, 5 pages, 2011. doi:10.1155/2011/127817

6. Bula Boru Winsa, Abdurehman Eshete Mohammed. Investigation on Pulmonary Tuberculosis among Bedele Woreda Prisoners, Southwest Ethiopia. International Journal of Biomedical Science and Engineering.Vol.3, No. 6, 2015, pp. 69-73. doi: 10.11648/j.ijbse.20150306.11